Study of pre-evaporation and matrix effects on multi-elemental analysis by ICP-TOFMS

by

Shulan Liu

A thesis submitted to the Department of Chemistry

in conformity with the requirements for

the degree of Doctor of Philosophy

Queen's University

Kingston, Ontario, Canada

July, 2007

Abstract

The ultimate goal of this project was to improve the sensitivity and detection limits of inductively coupled plasma time-of-flight mass spectrometry (ICP-TOFMS) and then apply it to the speciation analysis of As. To this end, two approaches were taken: the use of organic modifiers and that of a pre-evaporation interface between the spray chamber and the plasma torch.

The radial profiles of some background ions and analytes in three different matrices (1% HNO3, 1% HNO3 with 2% v/v methanol, 1% HNO3 with 0.2% m/v sodium dodecylsulfate (SDS)) were investigated in ICP-TOFMS. Although these concentrations of methanol and SDS induced the same increase (37%) in sample introduction efficiency, the change in analyte signal as a function of m/z followed opposite trends in these two matrices. The results show that matrix effects arising from different organic modifiers affected the distribution of ions in the plasma differently as a result of changes induced in the predominant ionisation mechanisms in the plasma.

The effect of a pre-evaporation interface on the distribution of ions in ICP-TOFMS was also investigated by spatial profiling, which showed that the optimal axial position of all elements shifted closer to the load coil. Furthermore, the radial profiles became significantly narrower and Gaussian.

The decrease of droplet size thus improved the sensitivity and detection limits for multi-elemental analysis.

A further investigation of the effect of the pre-evaporation interface revealed that, for cationic analytes, the signal enhancement had an inverse dependency on analyte mass upon heating the interface. In the case of As, a signal enhancement upon heating the interface only resulted when concomitant ionic analytes were present or with a 0.01 M NaOH matrix. All these observations could be rationalised by changes in the number of Coulomb fission events occurring during pre-evaporation, which depend on the size and charge of droplets, as well as the identity and concentration of the matrix.

Finally, the baseline separation of four As species by ion exchange liquid chromatography with detection by ICP-TOFMS and application of the pre-evaporation interface tube to As speciation were achieved using a mobile phase of NH_4NO_3, following an investigation of its matrix effects.

Co-Authorship

All work contained in this thesis was completed by the author in the department of Chemistry at Queen's University under the guidance of Dr. Diane Beauchemin. Sections of this thesis have been published in refereed journals as the following papers:

1. S. Liu, and D. Beauchemin, The effect of pre-evaporation on ion distribution in inductively coupled plasma mass spectrometry, Spectrochim. Acta B, 61 (2006) 157-163.

2. S. Liu and D. Beauchemin, Effect of methanol and sodium dodecylsulfate on radial profiles of ion abundance in inductively coupled plasma mass spectrometry, Spectrochim. Acta B, 61 (2006) 319-325.

3. S. Liu and D. Beauchemin, Effect of concomitant analytes on As signal during pre-evaporation of the solvent prior to introduction into inductively coupled plasma mass spectrometry, Spectrochim. Acta B, 61 (2006) 965-970.

Acknowledgements

I would like to express my sincere gratitude to Dr. Beauchemin for her guidance, expertise and encouragement. Her patience, understanding and help made my years of study enjoyable.

I would also like to thank my supervisory committee members, Dr. R. Stephen Brown and Dr. Richard Oleschuk, for their helpful suggestions, and April Vuletich for her assistance with the ICP-TOFMS instrument.

R. S. McLaughlin Fellowships and the financial support from the School of Graduate Studies and Research of Queen's University are also gratefully acknowledged.

Special thanks go to Dr. Beauchemin's group for the discussion and friendship and to my family for their support and patience during my four years of study.

Statement of Originality

This thesis reports the first spatial profiling of analyte ion distribution in inductively coupled plasma time of flight mass spectrometry (ICP-TOFMS) with and without a pre-evaporation interface installed between the spray chamber and torch. It also includes the first known characterisation of the effect of concomitant analytes on the As signal with a pre-evaporation interface. Finally, for the first time, a characterization of the radial distribution of analytes and background ions was carried out in the presence of organic modifiers.

Table of Contents

List of Tables

List of Figures

List of abbreviations

AC	Alternating current
AIR	Aerosol ionic re-distribution
As(III)	As_2O_3
As(V)	As_2O_5
BP	Boiling point
CMC	Critical micelle concentration
DC	Direct current
DIHEN	Direct injection high efficiency nebulizer
DIN	Direct injection nebulizer
DMA	Dimethylarsinic acid
ESI	Electrospray ionisation
ETV	Electrothermal vaporization
FI	Flow injection
FWHM	Full width at half maximum
GC	Gas chromatography
HEN	High efficiency nebulizer
HR	High resolution
HPLC	High-performance liquid chromatography
ICP	Inductively coupled plasma
IEC	Ion-exchange chromatography
IP	Ionization potential
MMA	Monomethylarsonic acid
MS	Mass spectrometry

OES	Optical emission spectrometry
PTFE	Polytetrafluoroethylene
RF	Radio-frequency
SDS	Sodium dodecylsulfate
TOF	Time-of-flight
USN	Ultrasonic nebulizer

Chapter 1 Introduction

The inductively coupled plasma (ICP) was originally developed for optical emission spectroscopy (OES). ICP-OES became a very useful technique for trace level multi-elemental analysis by the end of the 1960's [1]. In 1980, Houk [2] first reported combining an ICP source and a mass spectrometer. Soon thereafter, the first commercially available ICP mass spectrometry (MS) instrument was introduced in 1983 by Sciex Ltd, and shortly afterwards by V.G. Isotopes Ltd. [3]. Different types of ICP-MS instruments have since been developed, such as high resolution (HR) double-focusing magnetic sector ICP-MS [4], which can resolve many spectroscopic interferences or improve the detection limits in low resolution [5], and time-of-flight (TOF) ICP-MS for high precision isotope ratio determination and simultaneous multi-elemental measurements [6]. As a result, ICP-MS has been used in many areas of science, from geological, environmental, and industrial applications to clinical studies [7].

ICP-MS has thus been accepted as an extremely sensitive and powerful analytical technique for multi-elements analysis [8], as it offers very low detection limits for many elements of the periodic table (down to the ng/L) [9,10], a wide linear dynamic range(nine orders magnitude), and simple mass spectra compared to those of ICP-OES. However, as in other analytical techniques, there are problems with ICP-MS, such as matrix effects (non-spectroscopic interferences) arising from matrix elements and spectroscopic

interferences originating from either the plasma or the matrix [1]. These limitations, in addition to approaches used to overcome them, will be discussed in detail in sections 1.1.5 and 1.2.

1.1 Description of ICP-MS

All ICP-MS instruments consist of at least four basic components: the sample introduction system, the ICP generation system (which is circled in Figure 1.1), the sampling interface between the plasma and a mass analyzer, and a mass spectrometer with ions lenses and an ion detector (Figure 1.1) [11]. Samples undergo nebulisation, desolvation, vaporization, atomization and ionization before entering the mass spectrometer for separation and detection.

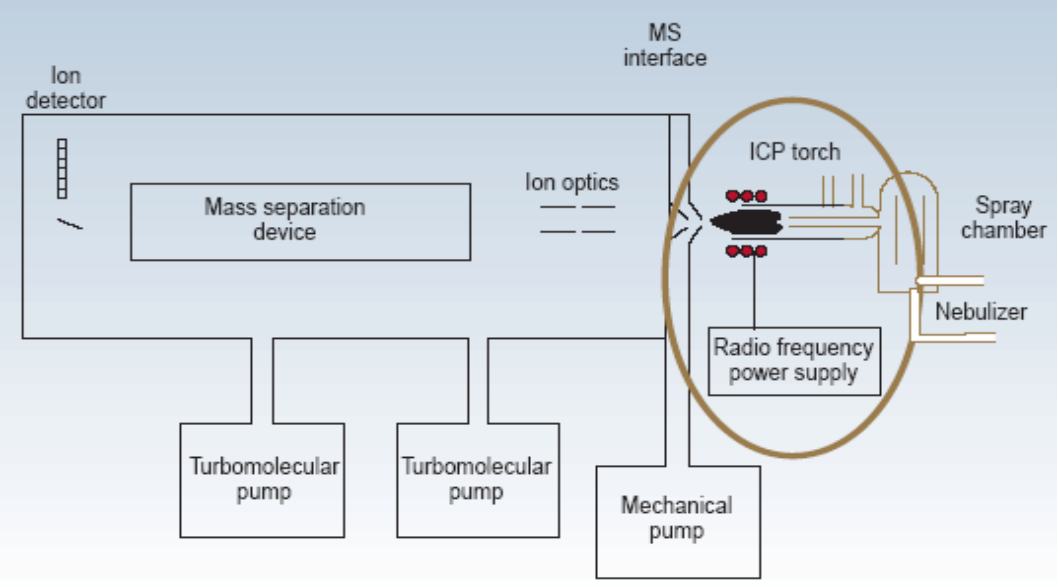

Figure 1.1 ICP-MS system diagram (from ref. [11])

1.1.1 The sample introduction system

In most cases, the samples analyzed by ICP-MS are aqueous solutions, although a variety of different methods have been used for the direct introduction of solids, such as electrothermal vaporization (ETV) [12] and laser ablation [13]. Gas chromatography (GC) has been most frequently used for the introduction of gaseous samples into ICP-MS [14]. However, since only aqueous solutions were used in this thesis, the remainder of this section will focus on the sample introduction of solutions.

Aqueous solution samples are usually pumped by a peristaltic pump, at a delivery rate of 0.5-2 mL/min, to a nebulizer, which transforms the liquid solution into aerosol droplets that then pass through a spray chamber for droplet selection [1]. A nebulizer is normally used to convert the analyte solution to fine aerosol droplets in a pneumatic nebulizer. Different nebulizer geometries are available, including a concentric (Meinhard) type, which is the most widely used (and was used in this project), and cross flow, or a Babington-type (V-groove) [1]. The design of the nebulizer is critical in producing aerosol droplets along with the nebulizer gas flow, which also affects the droplet size distribution.

The primary aerosol produced by a nebulizer has a range of droplet sizes, which are differentiated by the spray chamber, such as double-pass or cyclonic spray chambers (the latter was used in this project), when the

droplets pass through it. The spray chamber only allows fine droplets to pass into the plasma by removing the coarsest aerosol droplets. This is essential for ICP-MS detection limits, as droplets with a diameter greater than 12 μm can pass through the plasma without being completely desolvated [15]. Large droplets degrade signal stability by cooling the plasma region near analyte clouds from small droplets that are then undergoing ionisation [1]. Typically, only 2% of the original sample will reach the plasma. Large droplets hit the surface of the spray chamber, which are finally drained to waste. The low percentage of total sample reaching the detector limits sensitivity. On the other hand, it prevents overloading and cooling of the plasma, which can either induce a reduction in the degree of ionization of analytes or even extinguish the plasma altogether [15].

Different approaches have been used to overcome the low sample introduction efficiency of the conventional nebulizer/spray chamber setup, including a direct injection nebulizer (DIN) [16], an ultrasonic nebulizer (USN) [17,18] and a high efficiency nebulizer (HEN) [19]. A USN produces very fine droplets, which increases the proportion of aerosol reaching the plasma [17, 18]. It can be used with lower gas flow rate compared to that with a pneumatic nebulizer, resulting in a longer residence time of analytes in the plasma [1], which causes a considerable increase in sensitivity and improvement in detection limits. However, the increase in nebulization efficiency also increases the solvent (mostly water) load in the plasma, which can cool the

plasma, reduce the degree of ionisation of analyte and increase spectroscopic and non-spectroscopic interferences [17]. Furthermore, recombination of droplets can occur, because of the high density of aerosol, on the way to the torch resulting in big droplets that are drained off. Other systems, such as hydraulic high pressure nebulization [20,21] and thermospray nebulization [18,22] also have the same trouble of solvent overloading, which ultimately reduces the degree of ionisation of analyte although the sample introduction efficiency can be improved to up to 50%.

To avoid solvent overloading of the plasma, desolvation systems, consisting of a heated spray chamber and a condenser or a membrane desolvation system, were applied to remove the solvent [23]. However, problems of sample loss through the permeable membrane material (of porous membrane dryer) and build-up of electrostatic charge on the transfer line (of non-porous membrane dryer) occurred.

A reduction in the critical dimensions of a pneumatic concentric nebulizer (similar to the Meinhard type) gave the HEN [19]. The aerosol going to the plasma produced by this nebulizer is smaller than that from a conventional pneumatic concentric nebulizer. Indeed, 90-95% of the droplets are under 8 μm in diameter [24] (as opposed to a wide range of droplet size of up to 100 μm for a conventional pneumatic nebulizer [1], see Figure 2.3), and reach the plasma with high efficiency. However, the reduced inner diameter of the

capillary and low cross-sectional area of the gas exit results in higher gas pressure and easy blockage of the tip [25].

A DIN, which replaces the torch injector and injects the sample directly into the plasma without using a spray chamber, is another suitable alternative for small-volume sample or very low concentration sample since 100% of the sample reaches the plasma [26]. Unfortunately, solvent load also increases [26]. Moreover, very large droplets, and droplets with a greater range of size are injected into the plasma since no spray chamber is present, which increases plasma instability, i.e. the noise level in the plasma. Furthermore, a DIN is not easy to install and is prone to blockage and melting. Nonetheless, both the HEN and DIN can be effectively used for microsample introduction when the sample volume is limited (<1 mL) [25].

A direct injection, high efficiency nebulizer (DIHEN) that is demountable and less expensive than a DIN has also been designed [27]. The risk of melting is decreased since the optimum position of the DIHEN is farther below the torch intermediate tube than that for the DIN, while other operating conditions (aerosol carrier gas flow rate, RF power and sample uptake rate) are similar to those for a DIN. The sensitivity for 16 analytes with different masses has been reported to increase because of the lower mean velocity of the analyte droplets [27].

Regardless of the type of the nebulizer, the dissolved solids content of aqueous solutions should, in general, be kept under 0.2%, since more concentrated solutions cause deposition of solids on the torch and cones during continuous sample introduction, and this can lead to the plugging of the cone's orifice [1]. For concentrated solutions, either dilution or flow injection (FI) is usually necessary to reduce non-spectroscopic interferences.

The ICP-MS sample introduction system can readily be coupled to other techniques. In particular, the coupling of a separation system to ICP-MS (as detector) has opened the route to elemental speciation developments. Chromatography (including GC and high-performance liquid chromatography (HPLC) is the most widely used in combination with ICP-MS [28]. Capillary electrophoresis, another important separation technique, can also be coupled to ICP-MS [29, 30]. Finally, hydride generation can be useful for metal speciation of some inorganic species [31,32]. In any case, HPLC is most often used for speciation analysis, as it is easily connected to the regular nebulization system [21,33-35].

1.1.2 The plasma

A plasma is a partially ionized gas at high temperature. The ICP is a flame-like electrodeless discharge produced by inductive coupling in a gas at atmospheric pressure. This makes it very suitable as an ion source for mass spectrometric detection. Argon gas is most often used in ICP-MS, although

other gases, such as helium [36] and nitrogen mixed with argon [37,38] have been employed to reduce argon-based spectroscopic interferences [36] (discussed further in section 1.1.5.1).

An Ar plasma is initially ignited within a quartz torch by a high voltage electrical discharge while Ar is flowing through the torch. This Tesla discharge generates seed electrons that are then accelerated by the RF (Radio frequency) field of a water-cooled load coil that surrounds the end of the torch [39] (Figure 1.2). A high-frequency current (usually 27 or 40 MHz) from a RF generator passes through the load coil, producing a magnetic field of rapidly changing direction. The moving direction of the highly mobile light electrons thus changes very quickly because of the alternating current, resulting in collisions between electrons and slower moving neutral argon atoms. These, in turn, produce more electrons and heat. When a dynamic equilibrium is established between the production of new free electrons plus ions and their recombination, the plasma is stable and self-sustaining at the top end of the torch [1].

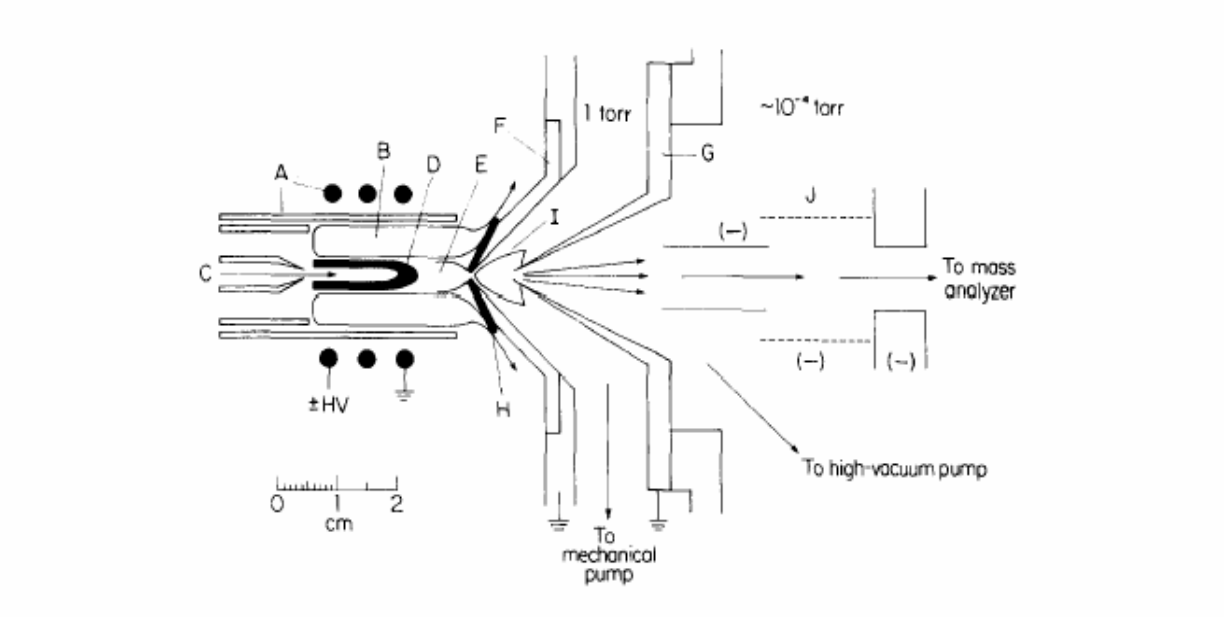

Figure 1.2 Schematic diagram of ICP and ion extraction device. A, torch and load coil; B, hot outer torus of ICP; C, sample flowing into axial channel of ICP; D, initial radiation zone (IRZ) showing emission from oxides and neutral atoms; E, normal analytical zone showing emission from ions; F, sampler with 1 mm hole in tip; G, skimmer; H, boundary layer of cold gas outside sampler; I, supersonic jet between sampler and skimmer; J, ion lenses. HV, high voltage. (from Ref.39)

The torch consists of three concentric quartz tubes. The sample aerosol passes through the central tube (called injector) into the plasma where it physically punches a hole in the centre of the plasma (called the central channel). The aerosol carrier gas flow rate (often equivalent to the nebulizer gas flow rate when a nebulizer is used) is typically of the order of 1 L/min. The middle tube is for an auxiliary gas, which is used to position the plasma above the inner tubes and prevent melting the central sample injector tube. This gas flow rate is in the range of 0-1 L/min [1]. The outermost tube provides the main plasma support gas, which tangentially flows through the

torch at a flow rate of typically around 15 L/min, and serves as a coolant flow as well to protect the tube wall from melting [1].

The sample injector tube in the middle of the torch allows a cool gas flow, carrying the sample aerosol, to punch a channel through the centre of the plasma. This central channel is heated to 6000-7500 K by radiation from the outer induction region (where the temperature is of the order of 10000 K) of the plasma (Figure 1.3). At this temperature, many elements are ionized to singly positively charged ions with high ionization efficiency in what is referred to as the normal analytical zone. Only elements with a first ionization potential in the range of 9-11 eV will have a lower degree of ionization efficiency, and thus a reduced sensitivity compared to that achieved for elements that are essentially 100% ionized in the plasma.

The plasma therefore functions as an ion source. The sample aerosol needs much of the plasma energy for the processes of desolvation, vaporization, atomization and ionization. Desolvation, where the solvent (such as water) is evaporated from the sample aerosol droplets, significantly affects the plasma temperature although the energy used for this process does not represent a large portion of the total plasma energy. A big droplet will have a local cooling effect in the plasma since more energy is needed to evaporate a large amount of water. This in turn will reduce the energy that is available for subsequent processes such as vaporization, atomization and ionization, and

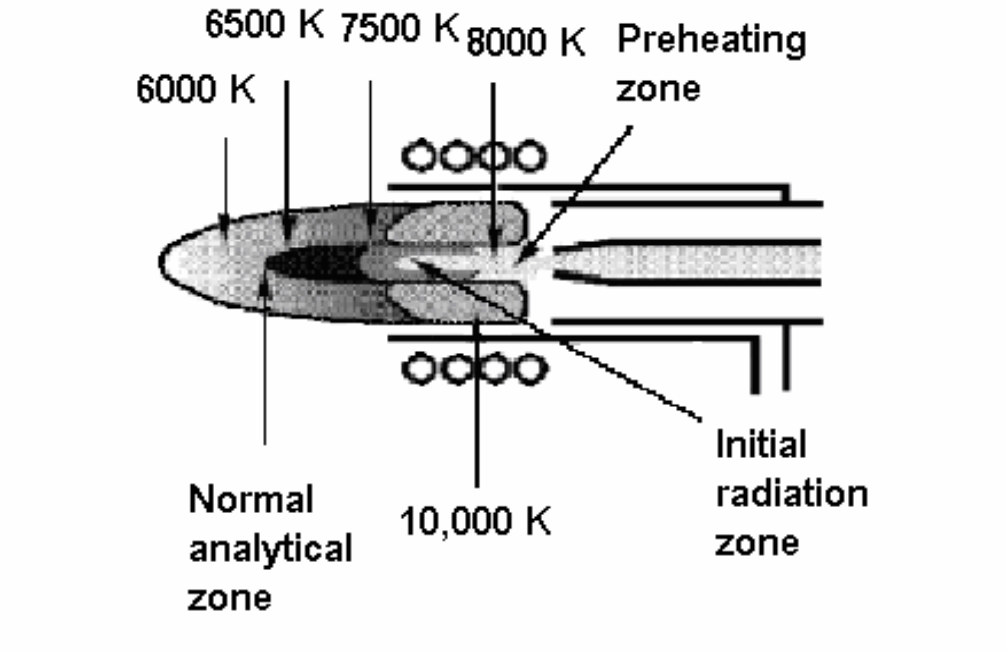

Figure 1.3 Different temperature zones in the plasma (from Ref. [11])

may also lead to unstable plasma conditions or lower sensitivity [40]. Following desolvation, the aerosol droplet becomes a solid particle, which is then vaporized and atomized, before being finally ionized mainly through collisions with energetic electrons.

The ionization process of the analytes in the plasma is complicated and has not been fully characterized. Different mechanisms may be involved in the ionization process at the same time. Three possible major ionization mechanisms have been proposed: electron impact ionization, charge transfer ionization and Penning ionization [39].

The electron impact ionization mechanism is considered to be the most dominant mechanism because of the high abundance of electrons resulting from the ionisation of argon [39]. This mechanism involves collisions between free electrons and analyte atoms, where electrons should have a greater kinetic energy than the ionization potential of the analyte atoms in order to make the analyte (X) lose a valence electron and become a positive ion (Equation 1.1). ΔE is the access energy. This ionization process is non-selective [39].

$$X + e^- \rightarrow X^+ + 2e^- + \Delta E \qquad (1.1)$$

On the other hand, a charge transfer mechanism can also happen in the plasma, which involves charge transfer from positive ions (normally Ar^+) to neutral analyte, where the positive ion takes an electron from the neutral analyte (X) (Equation 1. 2).

$$Ar^+ + X \rightarrow Ar + X^+ + \Delta E \qquad (1.2)$$

This process can occur easily because many analytes have a first ionization potential that is less than that of argon (15.76 eV). Furthermore, Ar^+ is in high abundance in the plasma. A charge transfer mechanism has been described for non-argon reactant ions as well in some cases. For example, charge

transfer may occur from carbon ions to analyte atoms in the plasma when organic solvents are present in the sample solution [41].

The third proposed mechanism is Penning ionization, which involves a collision between a metastable argon atom (Ar^m) and an analyte atom (X), resulting in the analyte atom losing an electron to become a positively charge ion (Equation 1.3).This was thought to be an important mechanism for a while until further research showed that the density of Ar^m in the plasma was too low to have a significant effect on the degree of ionization of the analyte [42].

$$Ar^m + X \rightarrow Ar + X^+ + e^- + \Delta E \qquad (1.3)$$

Any excess energy remaining after the collision with the analyte in the three proposed mechanisms can generate an analyte ion in an excited state, which may then emit light to return to its ground state. This light is monitored in optical emission spectrometry.

Because of the rapid changes in temperature and particle density, the plasma is not in thermodynamic equilibrium. However, around an individual droplet or particle in the process of atomization, excitation and dissociation, a local thermodynamic equilibrium can be assumed [43]. Hence, the ionization process of an element in a localized area can be simplified by the following equilibrium:

$$X \leftrightarrows X^+ + e^- \qquad (1.4)$$

Therefore, the temperature can be measured for the local, instantaneous environment. The temperatures measured in different regions or using different species are different and follow the trend of $T_{Ar\ ion} > T_e > T_{ion} > T_{exc} > T_g > T_{rot}$ [43], where $T_{Ar\ ion}$ is the argon ionization temperature, T_e is the electron temperature, T_{ion} is the analyte ionization temperature, T_{exc} is the analyte excitation temperature, T_g is the gas or heavy particle temperature, and T_{rot} is the rotational temperature.

Then, using any of above temperatures (although normally T_{ion} is used), the degree of ionization for any given element can be calculated by using the Saha equation [44], regardless of ionization mechanisms:

$$\frac{[X^+]}{[X]} = \frac{2}{n_e}\frac{Q_i^+}{Q_a}\left\{\frac{2\pi m_e kT_{ion}}{h^2}\right\}^{3/2}\exp\left\{-\frac{IP}{kT_{ion}}\right\} \qquad (1.5)$$

Where n_e is the number density of the free electrons, Q_i^+ and Q_a are the electronic partition function of the two levels (ion and atom), m_e is the electron mass, k is Boltzmann's constant, T_{ion} is the analyte ionization temperature, h is Plank's constant, and IP is the first ionization potential energy of the analyte [44].

Assuming that the temperatures of the electrons and analyte ions are equal (which correspond to 7500 K), most elements (52 elements) have a degree of ionization of 90% or better at this plasma temperature, as predicted by the Saha equation [44]. Only a few elements (e.g. La) can be doubly charged because their second ionization potential is lower than the first ionization potential of Ar.

Local thermodynamic equilibrium however, does not really exist in the plasma since the temperatures of argon ionization, analyte ionization, analyte excitation, of the electron, of the gas and of rotation are not equal [43]. The plasma temperature also varies with the sampling depth (the axial distance from the RF coil) and radially across the plasma [11] (Figure 1.3). The desolvation, evaporation of droplets and fluctuations in atom density affect plasma temperature, and therefore, there is both disagreement and difficulty in using the Saha equation [40].

1.1.3 The interface

The interface between the plasma and mass analyzer is probably the most critical component to link the high temperature, atmospheric pressure plasma to the high vacuum region of the mass spectrometer where the ions can be detected. Its main purpose is to representatively extract ions from the ICP. This is achieved by using a sampler cone with a suitable sampling orifice size. The sampler cones that were initially used on early ICP-MS had a small-

diameter orifice (70 μm) that caused the formation of a boundary layer in front of the sampler cone [3]. Ions then dwelled in this region and underwent many collisions leading to the formation of oxides and other polyatomic ions [3]. Therefore, two metallic cones (sampler and skimmer cones normally made of Ni or Pt) were developed instead to form an intermediate vacuum stage that removes a considerable portion of the plasma gas and brings the pressure down to about 1 torr.

A central portion of the plasma gas first passes through the sampler cone (which normally has an orifice of 0.8-1.2 mm in diameter). It then expands supersonically through the intermediate stage before passing through a sharp skimmer cone (with an orifice diameter of 0.4-0.8 mm). Since this supersonic expansion is rapid, diffusion and mixing of the sampled gas is minimized in this region [45]. Furthermore, only the central line flow passes through the aperture of the steeper-sides skimmer cone, reducing the amount of plasma species transported into the mass spectrometer. The whole interface is water-cooled, as the sampler is in direct contact with the high temperature plasma.

If the difference in potential between the plasma and the interface cones is high enough, a secondary discharge or pinch effect occurs, which results in further ionization of analyte and plasma species and, in turn, increases the percentage of doubly charged ions. The secondary discharge broadens the distribution of kinetic energy of ions and, as a result, lowers the resolution of

the instrument. The additional etching reduces the lifetime of the sampler cone. Positioning a grounded shield between the coil and the torch [46], grounding on the central turn of the load coil (instead of grounding at the end of the coil), or using interlaced RF coils can significantly reduce or even eliminate secondary discharge [47].

Downstream from the skimmer cone lies an ion focusing system that consists of a series of lenses with applied voltages. It is used to focus and accelerate the ions, repel electrons, finally separate ions (normally cations in ICP-MS) from the neutral species so that the ions may reach the mass spectrometer for detection (photon-stop blocks photons). This ensures a low background level and, thus, good detection limits. The potential voltage applied on the ion lenses can be adjusted in most ICP-MS systems to an optimum setting for multi-elemental analysis. Higher sensitivity of an individual ion of interest can be achieved by optimizing the lens potential voltage specifically for this ion. However, one phenomenon, called the space charge effect, arises in this region, which is caused by the forced close proximity of a positively charged ion current [48]. This space charge effect causes light mass ions with high charge to be deflected most easily off the pathway to the mass analyzer compared to heavier mass and lower charged ions that are more difficult to deflect off the pathway. As a result, the radial distribution of lighter analyte ions is usually broader than that of heavier analyte ions [49].

1.1.4 The mass spectrometer

Once the ions have been produced and separated from the neutral species, photons and electrons, they need to be further separated and detected according to their mass-to-charge ratio. This is the function of a mass spectrometer: to separate and measure the ion flux at a given m/z. There are several types of mass spectrometer. The most commonly used type in ICP-MS is a quadrupole because of its lower cost, and the fact that it is more compact and more robust than other types of mass spectrometers. The time-of-flight (TOF) mass spectrometer that allows the quasi-simultaneous transmission of all ions is very suitable for multielemental analysis and isotope ratio analysis. It was therefore used throughout this project. However, in order to facilitate the comparison, a brief description of a quadrupole mass spectrometer is given followed by a more thorough description of a TOF mass spectrometer.

1.1.4.1 Quadrupole mass analyzer

The quadrupole analyzer is the most commonly used detector in ICP-MS, which can monitor only one m/z at a given time. A quadrupole mass filter consists of four metal rods that serve as electrodes. Opposite pairs are connected together, one pair being positive, and the other pair being negative. A DC source and a radio-frequency (RF) AC source are connected to these pairs of rods. By varying the DC potential and the AC amplitude, the quadrupole can select specific ions passing through it to the detector at any

given time. All other ions hit the rods and are not transmitted to the detector. The voltage required for each specific m/z is determined empirically by mass calibration during instrument optimization. Since only one single m/z can be transmitted at a given time, in order to perform multi-elemental analysis, the quadrupole mass spectrometer allows the detection of ions in a rapid sequence (a full mass scan can require around 100 ms) [1], limiting precision (particularly for isotope ratios) and limiting elemental coverage when measuring rapid transient signal [50]. The scanning analyzer transmits ions of different masses sequentially, preventing its use for truly simultaneous multi-elemental analysis. This may lead to serious problems when measuring isotope ratios. As the isotopes being measured can not be detected simultaneously, fluctuations of the plasma may influence the precision and accuracy of the results [51]. In order to apply the quadrupole analyzer to isotope ratio measurement, low integration times are required so that the spectrometer can “peak hop” (requiring adjustment of RF and DC voltage) between isotopes. When only selected ions are monitored, it can also be used for transient signal analysis without curtailing the transient peak since the dwell time at each m/z can then be reduced to the low millisecond range, which can accommodate coupling to liquid chromatography or FI.

1.1.4.2 Time-of-flight mass analyzer

A TOF mass analyzer is a simple type of mass spectrometer that allows the separation of ions with different m/z according to their different flight times

through a fixed field-free region. This technique offers simultaneous ion extraction, quasi-simultaneous measurement (nanosecond regime) of ions from the ion source and high data acquisition speed [52].

Ions of different m/z are extracted from the ion source through a sampler and a skimmer cone. As shown in Figure 2.1, they are then guided into an acceleration region where a high voltage is imposed. In this region, all ions are accelerated to the same kinetic energy ($E=1/2mv^2$) and cut into ion packets. These discrete ion packets are then introduced into a field-free region under high vacuum, called a flight tube, where the separation of ions with different m/z occurs due to the different times they take to flight through the fixed pathway.

Since the ion velocity is inversely proportional to the square root of m/z, ions with different masses reach the detector at different times after they all travel through the fixed flight tube (0.5 m). Normally, the light mass ions (small m/z) travel fast and reach the detector first. The heavy mass ions (big m/z) move slowly and reach the detector later (see figure 1.4). A mass spectrum is a plot of ion signal versus time calibrated to m/z.

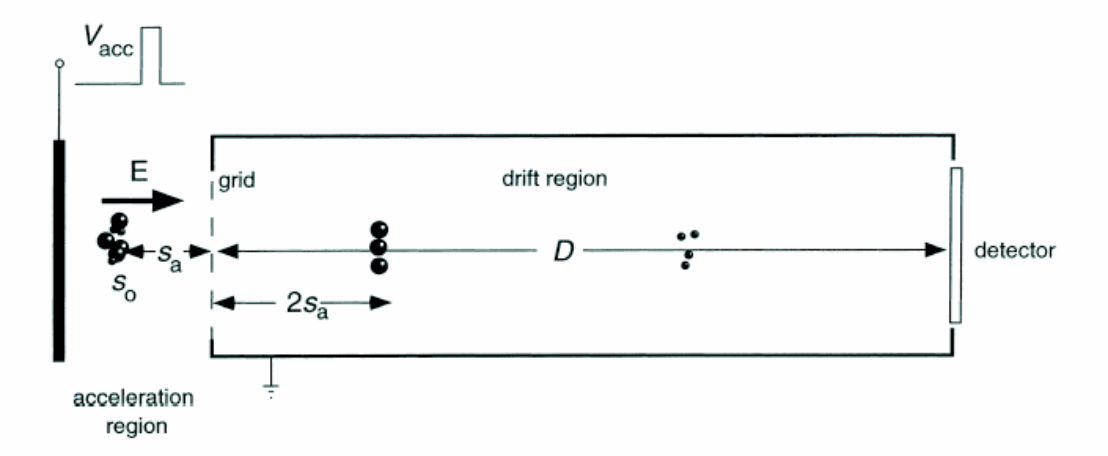

Figure 1.4 TOF principles for a simple linear TOF instrument. The packet of ions formed or sampled in the acceleration region is seen to separate in the drift region with the lighter ions (small spheres) traveling faster and reaching the detector first. E is the electric field strength in the accelerator, s_0 is the average initial position of the ions, s_a is the average distance traveled by ions in the accelerator, D is the field-free drift distance, V_{acc} is the pulsed acceleration voltage.(from Ref. 53).

In order to reduce small variations in the kinetic energy possessed by the ions with the same mass and thus improve mass resolution, most TOF instruments use an additional device called a reflectron (also called electrostatic reflector, see Figure 2.1), which is a series of grids and ring electrodes. It creates a retarding field that acts as an ion mirror by deflecting the ions and sending them back through the flight tube. The reflectron device effectively doubles the flight tube length without lengthening the instrument since the detector is usually located near the ion acceleration region (Figure 2.1). The ions originating from a fixed point that have the same m/z but a small difference in velocity can then arrive at the detector at the same time. This is because the faster ions (with more energy) penetrate deeper into the ion mirror and take

more time to emerge compared to the slower ions (with less energy), which take less time to emerge from the mirror. As a result, the ion mirror corrects spatial spread and energy dispersion of ions with the same m/z, and hence increases mass resolution [53,54]. The reflectron decreases the noise level as the majority of background ions do not have enough energy to traverse the flight tube [55].

There are two types of commercially-available ICP-TOFMS systems used in atomic spectroscopy: axial acceleration and orthogonal acceleration ICP-TOFMS instruments. The axial ICP-TOFMS was commercialized by LECO in 1998, and was used in this thesis. Compared to the scanning mode analyzers that are equipped with a single detector, such as quadrupole and magnetic analyzer, which can only detect one mass at a given time, some important advantages of TOF appear. Foremost is the simultaneous multielemental detection as all ions of different *m/z* are sent into the TOF mass spectrometer at the same time. The simultaneous ion extraction and quasi-simultaneous measurement of the whole mass spectrum from each packet of ions extracted from the ion source provide an extremely high speed of data acquisition. The repetition rate of TOFMS is determined by the flight time of the heaviest ion through the field-free region, which is normally less than 40 μs for atomic species, thereby allowing the generation of thousands of mass spectra per second in ICP-TOFMS [56].

ICP-TOFMS reduces analysis time, which is independent of the number of isotopes being measured, and is an ideal choice for multi-elemental analysis, rapid transient signal analysis, and isotope ratio measurement. The simultaneous extraction of ions from the plasma eliminates flicker noise, which improves the performance compared to quadrupole ICP-MS for multielemental analysis [56]. Quasi-simultaneous detection of all masses is also possible due to the extremely short time difference between adjacent masses [57]. A TOF mass analyzer substantially improves the detection of rapid transient signals as well as isotope ratio precision as a result of this simultaneous sampling [58]. The spectral acquisition speed of a TOF-MS analyzer surpasses that of a quadrupole by at least two orders of magnitude [9, 56]. In addition, the entire spectrum can be measured from small sample volumes. Another practical advantage of TOF is the absence of spectral skew during the measurement of transient signals.

ICP-TOFMS has several disadvantages, including the low mass resolution (defined in 1.1.5), which is similar to that observed on quadrupole instruments, a lower sensitivity (an order of magnitude lower) and poorer detection limits compared to quadrupole-based instruments [52,56,58], as a result of the lower duty factor (the fraction of ions measured relative to the total number available for analysis). Indeed, for the continuous monitoring of a single ion, the duty factor is only 10% as opposed to 100% for quadrupole instruments [57]. Thus, single-ion monitoring is clearly not advantageous by TOFMS [56,

58]. Because the detection limits depend on the background noise level and signal strength, and that the background levels are higher with TOFMS than with a quadrupole, the detection limits of ICP-TOFMS are usually higher than those of quadrupole instruments even at high signal strength (up to 10^7 counts per second per mg/L). Therefore, for the measurement of a single ion or less than 7 isotopes, quadrupole ICP-MS is a better choice [55].

The resolution of TOF-MS is affected by the flight time of the ions. Thus, all the factors that influence the flight time will then affect mass resolution. These factors include the length of the ion extraction pulse (time distribution), the volume where the ions are formed (spatial distribution), and variation of the initial kinetic energy of the ions (kinetic energy distribution) [59]. Increasing the length of the flight tube or decreasing the acceleration voltage can increase the mass resolution, but the latter reduces the sensitivity as well. Therefore, the best compromise in mass resolution and sensitivity is achieved by using a flight path of 1-2 m and an acceleration voltage of at least 2 kV.

All ions coming from the acceleration region can reach the detector whether they are analytes of interest or background ions, which causes a problem of overloading the detector of a TOF-ICPMS instrument. In contrast, quadrupole ICP-MS eliminates the background ions by skipping over certain DC/RF settings that would otherwise allow them to pass through and reach the detector). In order to avoid this situation, a “Transverse Rejection Ion Pulse”

is applied to deflect unwanted ions. This is achieved by applying a high voltage pulse on the ion beam passing through the ion gate, so as to deflect matrix ions such as O^+, OH^+, NO^+, Ar^+ ArO^+ and Ar_2^+. Additional deflection windows are also needed to eliminate concomitant and background ions from the sample matrix to avoid overloading the detector [60]. They must be set carefully since they may affect analyte ions in the same mass region.

1.1.5 Limitations of Inductively coupled plasma mass spectrometry

ICP-MS suffers from several limitations although it has many advantages for multi-elemental analysis. Helium, neon and fluorine, with higher first ionization potential than argon, cannot be efficiently ionized and determined using an argon-based plasma. Hydrogen, nitrogen and oxygen cannot be determined because of the large background arising from water and nitric acid in the samples and entrained air. Some elements have poor detection limits because of serious spectroscopic interferences arising from the plasma itself. In general, the detection limits of heavier mass elements are better than those of lighter mass elements since there is less spectroscopic interference at higher m/z. Detection limits in ICP-MS also suffer from the noise in signal caused by the aerosol generation process and transportation [61], as well as the vaporization of aerosol droplets [40]. Moreover, the long-term precision can be affected by deposition of solids onto the interface and ion lenses [62].

Interferences in ICP-MS have been divided into two main categories in Evans and Giglio's review of 1993 [63]: spectroscopic interferences and non-spectroscopic interferences (which will be discussed in 1.2).

1.1.5.1 Spectroscopic interferences in ICP-MS

A spectroscopic interference, also called an isobaric interference, is a signal overlap from atomic or polyatomic ions with similar m/z as the analyte ion, which the mass spectrometer cannot discriminate and therefore results in a positively biased signal for the analyte ion. Spectroscopic interferences come from different sources: 1) ions of other elements; 2) multiply-charged ions of heavier elements; 3) polyatomic species originating from the plasma and other elements from the sample, whose exact origin is still largely unknown [64].

Plasma gas is one of the most important sources of interferences. Ar is the most widely used plasma gases, and the presence of interferences involving Ar-containing ions can be predicted; only a limited number of possible polyatomic ions containing Ar have been identified. The use of a mixed-gas plasma typically increases the number of background ions and polyatomic ions originating from the gas that is added to Ar, while simultaneously decreasing argon-based interferences [63].

The decomposition of water, which is omnipresent in aqueous solutions, releases oxygen atoms in the plasma, which can then form oxide ions with the analyte (MO^+). This leads to spectroscopic interferences at M+16, M+17 and M+18 nominal values of m/z. Although oxygen can also come from entrained air, this contribution is usually negligible compared to that originating from water. In any case, monitoring of oxide interferences is required. In problematic cases, either hydride generation or desolvation of the sample aerosol prior to its introduction into the plasma is very often used to minimise oxide interferences [64].

Matrix elements from the sample and the reagents used for sample preparation (such as to digest or dissolve the sample) can also cause spectroscopic interferences. Nitric acid is most commonly used in ICP-MS since it does not result in additional interference to those arising from water and entrained air). In fact, not only does nitric acid not cause additional spectroscopic interference but it may even lower some polyatomic interferences arising from matrix ions through competitive formation of nitrides. For samples with unknown complex matrices, prediction of all polyatomic interferences is often not trivial, if at all possible, although those arising from some common matrix elements, such as Na, K and Cl, are known. Several of these matrix elements not only cause spectroscopic interferences, but they induce non-spectroscopic interferences as well.

Spectroscopic interferences contribute to the overall signal at the analyte's m/z, resulting in an apparent enhancement of the analyte signal intensity in the absence of a suitable correction. The simplest way around this problem is to choose an alternative isotope of the analyte for the determination if possible (i.e. if the analyte is not monoisotopic and if there is a sufficiently abundant isotope that is free of spectroscopic interference). If available, an ICP-HRMS instrument can often distinguish between the analyte of interest and the isobaric interferences. The mass resolution is generally calculated as:

$$R=m/\Delta m \qquad (1.6)$$

where R is the resolution, m is the nominal mass of the first peak, and Δm is the mass difference between the two peaks (for singly charged species, m is m/z). For TOFMS, the resolution can also be defined as:

$$R=t/2\Delta t \qquad (1.7)$$

where t is the analyte flight time through the flight tube, Δt is the finite time interval of the full width at half maximum (HWHM) of the peak. This definition gives almost double the value of resolution than the result calculated using equation 1.6 [65].

In general, TOF and quadrupole mass spectrometers have unit mass resolution, which means that ions having a mass difference less than one unit can not be detected separately. On average, this corresponds to R=300 (i.e. the low resolution setting of HR instruments) to give a 10% valley between the two peaks to be resolved. ICP-HRMS can operate at a resolution up to R=10,000, which can resolve many interferences. For example, a resolution of 7500 can resolve $^{75}As^{+}$ from $^{40}Ar^{35}Cl^{+}$. However, the sensitivity of the instrument concurrently decreases, as the increase in resolution is achieved by narrowing the entrance slit, which results in a smaller portion of the analyte being detected [66].

The review by Evans and Giglio [63] provides a thorough description of methods used for overcoming spectroscopic and non-spectroscopic interferences (see matrix effects, in section 1.2), which includes various separation methods that can be used to isolate the analyte from the troublesome matrix. Beauchemin's reviews in 2004 [8] and 2006 [67] provide more thorough and up-to-date information on the methodology available for overcoming these interferences as well as on the related fundamental studies. For example, collision and reaction cells before the mass analyzer, or ETV have been used for eliminating the spectroscopic interferences and non-spectroscopic interferences. The collision cell or dynamic reaction cell is the most recent method that has been implemented on quadrupole-based instruments to reduce spectroscopic interferences [67, 68].

The use of a correction equation to correct the data of the analyte isotope of interest after determining the concentration of the interfering element is simple and common practice. This method requires that the interfering element has more than one isotope and that the isotopic distribution does not vary in nature. Correction equations are usually part of the ICP-MS data reduction software and performed automatically. A representative correction equation is [69]:

$$^{X}A_{signal} = \text{total signal at } x - [(^{x}B_{abundance}/^{y}B_{abundance}) \times {}^{y}B_{signal}] \qquad (1.8)$$

where $^{X}A_{signal}$ is the real signal of analyte A at m/z=x, ^{x}B is the isotope that will interfere with the determination of the analyte. $^{x}B_{abundance}$ and $^{y}B_{abundance}$ are the natural abundance of the two isotopes of B, where ^{y}B is free of spectroscopic interference.

When correction equations cannot be used, ICP-HRMS is the most straightforward method to resolve many spectroscopic interferences without potential contamination resulting from the sample pre-treatment step that may otherwise be required to remove the source of the interference [70]. Removing the solvent using a desolvation system can eliminate spectroscopic interferences arising mainly from the solvent [71]. For example, cryogenic cooling [72] or the sequential use of a heater-condenser and membrane desolvation with an USN [73] can effectively reduce this kind of interference.

Solvent-free sample introduction, such as laser ablation [13,74] and ETV [67,75], which are the most common methods for direct solid sample introduction, can completely solve problems of spectroscopic interferences arising from the solvent. Hydride generation [76] can be applied to selected elements by converting analytes into gaseous hydrides, to get rid of spectroscopic interferences and non-spectroscopic interferences.

If none of the above methods are applicable then removal of the matrix or chromatographically separating the analyte from the interfering matrix species can effectively eliminate the spectroscopic interferences, in addition to non-spectroscopic interferences arising from these sources [77,78]. However, such separation cannot eliminate spectroscopic interferences arising from the plasma itself. In the latter case, a mixed-gas plasma may be used (where, for example, nitrogen is introduced into the nebulizer gas flow of an Ar-based plasma) to reduce argon-based polyatomic interferences, such as $^{40}Ar^{35}Cl^{+}$ on $^{75}As^{+}$, $^{40}Ar^{37}Cl^{+}$ on $^{77}Se^{+}$, $^{40}Ar^{36}Ar^{+}$ on $^{76}Se^{+}$, $^{40}Ar^{38}Ar^{+}$ on $^{78}Se^{+}$ and $^{40}Ar^{40}Ar^{+}$ on $^{80}Se^{+}$ [79,80].

1.2 Non-spectroscopic interferences (matrix effects)

A non-spectroscopic interference is characterized by a suppression or enhancement of the analyte signal due to various factors exerting influences on the whole process, from the sample introduction to analyte ionization and detection. The nature and concentration of the sample matrix have a direct

influence on matrix effects [63]. These effects can be divided in two categories: 1) effects from dissolved and undissolved solids in sample solution (such as clogging of the injector and cones through deposition of salts); 2) other effects resulting in suppression or enhancement of the analyte signal.

1.2.1 Observed effects (enhancement and suppression)

The continuous nebulization of solutions containing more than 0.2% m/v or 2 mg/mL of dissolved solids can be problematic since they may deposit on the sampling cone orifice, thereby causing signal drift and signal suppression over a short time period [81]. This signal suppression is not simply a result of the reduction in the number of ions entering the ICP-MS detection system, but also of a modification of the ion extraction process due to the reduction in orifice diameter [82]. The degree of suppression or enhancement is influenced by the identity and absolute amount of matrix element, rather than by the relative amount of matrix to analyte. Therefore, the sample introduction system may also exacerbate these effects because it determines the amount of sample, and thus, matrix going into the plasma. For instance, a DIN or a HEN that greatly increases the sample transport efficiency compared to a conventional system, but concurrently worsens non-spectroscopic interferences as the absolute amount of matrix going to the plasma is thereby increased.

Sample introduction and transport processes are also affected by physical properties of the solution, including its viscosity, surface tension, density, evaporation rate and vapour pressure. Hence, any change in these factors will change the primary droplet size distribution and consequently the aerosol droplet size distribution doing to the plasma, which can in turn change in the analyte signal intensity. In addition, matrix effects are also strongly dependent on the nebulizer gas flow rate [83] because it affects the residence time in the plasma and the position of the initial radiation zone (see Figure 1.3)where maximum sensitivity is generally observed.

The most frequently observed matrix effect is analyte signal suppression [63, 84-86]. However, matrices containing concomitant elements with different mass may cause different levels of matrix effects. In general, heavier matrix elements cause greater matrix effects, resulting in greater signal suppression on lighter analytes [83, 85]. When the matrix includes a significant amount of organic solvent, a severe suppression of analyte signal can result as the organic solvent decreases the plasma temperature and electron density. It also causes soot deposition on the sampler and skimmer cones and the ion lenses, which can also significantly suppress the analyte signal intensity.

Matrix effects can also result in signal enhancement [63, 86, 87]. For example, the addition of small amount of organic solvents or compounds as modifiers to sample solutions can have a significant effect on the behaviors of analytes in

ICP-MS. They can affect ionisation conditions in the plasma, the aerosol mass transport rate, the vapour mass load, or nebulisation [88]. Although, as mentioned above, a significant amount of organic solvent causes suppression, a small amount of organic additives often induce a signal enhancement of elements, such as As [89-91], Se [86, 89, 92-96], Hg [97] and Zn [98], with ionisation potentials in the range of 9-11 eV [99]. This enhancement cannot be ascribed to space charge effects (which will be discussed in section 1.2.2), as space-charge effects only induce signal suppression, but has been attributed to an improvement in the degree of ionization of these elements through a modification of the ionization mechanisms in the plasma when organic solvents are present [99]. This is in contrast to matrix effects caused by matrix elements (such as Na and Ca) that mostly induce space-charge effects and cause signal suppression.

Literature indicates that the carbon source need not be an organic solvent, which often has the drawback of increasing the solvent load in the plasma. In particular, analyte signal enhancement was observed in presence of a surfactant [91]. A source of carbon may also change the physical properties (density, viscosity, surface tension) of liquid samples, resulting in improved nebulisation efficiency and, hence, improved signals for all analytes (see Chapter 3). Surfactants can be used during sample preparation to improve leaching efficiency [100], for cloud point extraction [101, 102], and as emulsifiers for the determination of metals in organic matrices [103]. They are

also useful for the generation of volatile analyte species, such as hydride and alkylcompounds of metals [104-106], because the self-aggregation of surfactant molecules creates a different microenvironment in comparison to the bulk solution. Compared to the addition of organic solvents, which induces enhancement effects only for the elements with a high ionization potential, an addition of surfactant may enhance the signal intensity not only for the elements with higher ionization potential, but also for the elements with lower ionization potential as well.

1.2.2 Proposed mechanisms of matrix effects

1.2.2.1 Space charge effect

As mentioned in section 1.1.3, when a portion of ions and electrons leaves the skimmer, the lenses downstream of the skimmer collect positive ions and repel electrons. The mutual repulsion of ions in the ion beam occurs through a space-charge effect, which causes a broadening of the ion beam; ultimately resulting in a loss of ions because the collection of all ions leaving the skimmer then becomes more difficult [48]. When the same space charge force acts on all ions, the light ions are affected and deflected most extensively, resulting in poorer sensitivity compared to that of heavy ions [48]. This space-charge effect is the major cause of signal suppression. As the concentration of the matrix elements increases, a greater matrix effect (suppression) is expected. Similarly, the greater the mass of the matrix

elements, the more severe will the matrix effect be on light analytes [83, 85,107]. Space-charge effects cannot be investigated by spatial profiling of ion distribution in the plasma because they occur in the mass spectrometer (not in the ion source). Thus, they can only explain a signal suppression effect.

1.2.2.2 Shift in atom-ion equilibrium

Elements with low ionization potential in the matrix can increase the electron density in the plasma [43]. This increase in electron density may in turn cause a shift in the atom-ion equilibrium (forcing the equilibrium back toward the atom) and induce signal suppression, which should be most noticeable for analytes with high IP [85]. On the other hand, an increase in electron density may favour the electron impact ionization of analyte, resulting in signal enhancement [108].

1.2.2.3 Ambipolar diffusion

In the plasma, electrons and ions tend to diffuse away from the source to the lower charge density areas. The diffusion rate of electrons is much faster than that of ions because of their much lighter mass. At a given non-boundary point, the number of charge density of electrons must be approximately equal to that of cations in order to keep electrical neutrality. As a result, ions speed up and keep the same diffusion rate as electrons (called ambipolar diffusion).

If the density of electrons increases, for example, by adding easily ionized elements, the rate of ambipolar diffusion would then increase and the radial profile of analyte ions would expand and broaden at a given axial position. This would be observed as a suppression of analyte signal in the central channel [107]. Ambipolar diffusion is not mass dependent [109].

1.2.2.4 Matrix effects on aerosol droplet formation

Matrix properties (density, viscosity and surface tension) affect the aerosol droplet distribution during the whole nebulisation process, i.e. from the primary aerosol to tertiary aerosol formation, and, as a result, the sample transport efficiency [110, 111]. Most of the previous work on this aspect has focused on a study of the addition of a small amount of organic solvents and surfactant [91, 99]. The presence of organic solvents and surfactants changes the physical properties of the solution and, therefore, affects the nebulization process, ideally resulting in a smaller droplet size distribution and an increase in sample mass transport efficiency [63, 112,113]. Although organic solvents [89, 92] and surfactants [91] can be used to improve the sensitivity of high IP elements, the situation is often complicated by matrix effects from carbon that is concurrently introduced in the plasma, as well as from changes in the nebulisation and sample transportation processes. Xu *et al.* [114] reported that a higher ionic strength matrix increased the abundance of small droplets in the tertiary aerosol because of an increased incidence of

Coulomb fission events during the desolvation occurring through the spray chamber, which ultimately enhanced the analyte signal.

The enhancement observed in presence of 5% Triton X-100 [91] and 3% v/v methanol [89] was greater than what could be ascribed solely to an increase in nebulisation efficiency. Furthermore, a similar signal enhancement was also observed with an equivalent amount of ammonium carbonate [89], which does not affect the nebulisation efficiency, clearly indicated the existence of at least one other mechanism that contributed to signal enhancement.

1.2.2.5 Carbon charge transfer

The addition of organic compounds to the analyte solution in combination with the use of a higher RF power enhances the signal of the analytes with a relatively high ionization potential (As, Se, Hg, Zn) [89-98]. This enhancement cannot be attributed solely to sample transport phenomena. An increase in their degree of ionisation may thus result from different ionisation processes in the plasma when organic compounds are present. Carbon-containing compounds lead to an increased ion population of carbon (IP 11.26 eV) and carbon-containing ions (14.01 eV and 13.77 eV for CO^+ and CO_2^+, respectively) [98], which in turn undergo charge transfer with analyte elements [89] with IP between 9-11eV [98, 99] by stripping an electron from these analytes; a process which is well known from chemical ionization in organic MS [89]. This mechanism can only explain enhancement effects on

analytes with higher IP since they are not completely ionized under normal plasma operating conditions [115]. The competitive formation of CO^+ also reduces the formation of refractory oxides and thus contributes to the enhancement [99]. Organic solvents can also suppress ionisation and increase the breakdown of polyatomic ions through competitive formation of ArC^+ from altered plasma conditions [79].

1.2.3 Spatial profiling for investigating matrix effects

Fundamental studies in ICP-MS are very important for understanding how the plasma works and to decipher some of its persistent problems. One simple way of characterizing the plasma and investigating spectroscopic and non-spectroscopic interferences (matrix effects) is spatial profiling. By simply changing the relative axial position of the torch with respect to the sampler cone (i.e. move the torch away or toward the interface), defined as axial Z position (also called sampling depth), an axial profile is obtained. Similarly, by changing the radial X or Y direction, radial profiling is accomplished. With recent instrumentation, a full spatial profile can be readily obtained using a computer-controlled three-dimensional translation stage under the plasma torch.

Spatial profiling has played an important role in the development of ICP-MS, from the determination of optimum sampling position as a function of plasma parameters, to allowing a theoretical framework for proposed ionization

mechanisms [116]. Early studies on spatial profiling focused on the inter-relationships between parameters of the nebulizer gas flow rate, the RF power, and the sampling depth. Any change in one of these parameters caused changes in the optimal value of the other parameters because they all influence ion distribution in the plasma. For example, an increase in the nebulizer gas flow rate will increase the amount of sample aerosol introduced into the ICP, and more RF power will be needed to cope with the increased solvent load at a given Z position. Similarly, at a given RF power, an increase in nebulizer gas flow rate will increase the sampling depth (Z position) because a longer residence time is then needed to compensate for the increased amount of aerosol being introduced, which needs more time for its complete desolvation, vaporization, atomization and ionization [117-119]. Under fixed plasma operating conditions (i.e. constant gas flow rates and RF power), a profile of ion distribution in the plasma can be obtained by changing the sampling position, and the optimum position can be determined.

Investigation of the ion distribution in the plasma, including analytes and background ions, can provide very useful information on spectroscopic and non-spectroscopic interferences and thus, uncover possible sources of interferences. Axial profiling can provide information about the energy and time needed to form ions [120], whereas radial profiles can provide insight on ionization mechanisms in the plasma [117]. For example, by investigating the spatial distribution of analyte and background ions in the plasma, a charge

transfer ionization mechanism could be proposed for a mixed-gas (Ar-N_2) plasma, which reduced matrix effects [69]. Other studies involving radial profiling of analytes ion distribution, revealed that matrix effects decreased at greater sampling depth [85, 107].

1.2.4 Means to alleviate matrix effects

Three important reviews [8, 63, 67] thoroughly covered both the methodology that is currently available to alleviate matrix effects in addition to fundamental studies on non-spectroscopic interferences. Sometimes, a single method, such as selective separation of the analyte from the matrix, or a use of collision and reaction cell, can efficiently eliminate both spectroscopic and non-spectroscopic interferences. However, most often, two or more different methods are used together to enable the accurate analysis of different samples [38, 121].

1.2.4.1 Most common methods for eliminating matrix effects

The simplest way of reducing or eliminating matrix effects is sample dilution since the matrix effect is dependent on the absolute concentration of the matrix. Both analyte and matrix are diluted at the same time until an acceptable interference level (i.e. less than 5% of signal suppression or enhancement) is obtained. An obvious requirement of this approach is that the detection limit for the analyte should be low enough and the analyte

concentration should be high enough to still enable analyte detection following dilution. Thus, dilution cannot be applied to samples with a very low analyte concentration.

Separation of the matrix from the analyte is another very common choice to avoid matrix effects (as well as spectroscopic interferences arising from the matrix), which can be performed either off- or on-line to ICP-MS. Off-line separation includes solvent extraction [122] and selective precipitation of the analyte [123]. The precipitation approach has also been implemented for on-line separation [123], particularly in combination with FI (as discussed in section 1.2.4.3). A chromatographic separation can also be used for on-line separation of the matrix as well as for speciation analysis [34, 124]. However, the main limitations of these techniques are that they are often time-consuming and involve a significant risk of sample contamination.

An instrument modification was proposed to eliminate space charge effects, which, as discussed earlier, are the main sources of analyte signal suppression. It involved the introduction of electrons between the skimmer cone and the extraction lens to balance the excess positive charge in the ion beam [125, 126]. Matrix effects arising from space-charge effects may also be alleviated through adjustment of the ion lens potentials [127].

1.2.4.2 Calibration strategies that compensate for matrix effects

Some calibration strategies are used to compensate for matrix effects, such as matrix-matched standardisation, standard additions, internal standardization and isotope dilution analysis. If the matrices of the standard solutions and samples are exactly matched, quantification by external calibration should be possible because the same non-spectroscopic interferences should affect all of these solutions. In practice, matrix-matching is often difficult for real samples whose matrix is complex or unknown.

By adding an appropriate internal standard to the sample and standard solutions, matrix effects can be corrected [41], as well as short term and long term signal drifts since the analyte and the internal standard are then subjected to the same matrix effects. In order for the correction to be successful, the internal standard should have a similar mass and first ionization potential as the analyte. It should not be present in the samples, and should be affected in a similar manner as the analyte by the matrix. In this case, knowledge of the matrix composition of samples is not necessary. In some cases, a plasma ion (such as Ar_2^+) has also been successfully used as an internal standard [108,128], which has the advantage of eliminating a possible source of sample contamination since nothing then needs to be added to the samples. If the internal standard is added during the sample preparation step, analyte loss during this step may be compensated [129]. By plotting the ratio of analyte signal to internal standard signal as a function of

analyte concentration, a calibration curve is obtained that is not affected by matrix effects, enabling accurate quantitative analysis. Internal standardization is the most widely used means of compensating for matrix effects. It is also recommended for routine analysis, even for samples with simple matrices, in order to compensate for signal drift [1].

Isotope dilution involves a measurement of the change in the signal ratio for two selected isotopes of interest after adding a known quantity of a spike containing one enriched isotope of the analyte (it is often considered as the ideal internal standard). As the two isotopes have a very small mass difference and are subject to the same matrix, isotope dilution is ideal for overcoming matrix effects [130, 131] and is considered as an absolute quantification method providing results with high precision and accuracy. However, because a ratio of the levels of the two analyte isotopes in the spiked sample is usually desired to be near unity, a preliminary estimation of the analyte concentration is required in order to calculate the mass of isotopic spike [132]. Also, the analyte to be determined by this method must have at least two isotopes that are free of spectroscopic interference.

If the matrix is too complicated for matrix-matching, and isotope dilution analysis is not possible, than the method of standard addition is the best choice. This method involves the addition of known quantities of analyte to aliquots of the sample while keeping the sample matrix constant. In this way,

the analyte in the unspiked and spiked samples is subject to the same matrix, and any matrix effect will be effectively corrected. However, it is time-consuming as a preliminary estimation of the analyte concentration is required in order to obtain a moderate slope in the resulting calibration curve. It also increase the sample load by at least 3 times

1.2.4.3 Flow injection analysis

FI analysis was first introduced by Ruzicka and Hansen in 1975 [133]. It involves the injection of a discrete volume of sample solution into a rapidly flowing unsegmented carrier stream, which results in lower sample consumption and higher sample throughout. The resulting FI signal is transient, in contrast to the steady-state signal that is obtained by direct continuous nebulization of the sample solution. Nonetheless, this transient signal is very reproducible since the sample injection volume and the dispersion of the sample plug in the carrier stream are reproducible. It makes numerous on-line techniques possible, such as on-line matrix separation/preconcentration when the sample contains high level of dissolved solids or has a very low analyte concentration [123,134,135] as well as on-line calibration strategies e.g. on-line isotope dilution [131,135,136]. Because the dispersion in FI resulted in dilution of the sample, FI has been used as an efficient method to reduce matrix effects [137].

As mentioned earlier, on-line separation/preconcentration can be used to remove the matrix elements [134,138], which effectively reduces both spectroscopic and non-spectroscopic interferences. For instance, on-line precipitation combined with FI has the distinct advantage of pre-concentrating the analyte while the matrix is removed [134,139,140], making possible the analysis of samples with very low analyte concentration. Similarly, chelating resins are often used for on-line separation in combination with FI [130]. FI also has the important advantage of preventing clogging of the sampler cone orifice because of the washing effect of the carrier stream [130].

1.3 Pre-evaporation interface

Although ICP-MS is recognized as an extremely sensitive and powerful technique for multi-elemental analysis [8], the optimum plasma operating conditions vary from element to element and, as a result, compromise operating conditions must be selected for multi-elemental analysis. For example, the optimal axial sampling position of elements forming refractory oxides is farther above the load coil than that of other elements, when a conventional sample introduction is used [85], i.e. a pneumatic nebulizer with a spray chamber. This difference in optimal sampling position should be less important when desolvation is performed prior to introducing the sample in the plasma since desolvation drastically reduces the formation of oxides [72]. Conversely, it is worse with a DIN [26] or a DIHEN [16] since the sample is nebulized directly into the plasma with sampling efficiency up to 100%.

Although the sensitivity is improved, it exacerbates non-spectroscopic interferences as well because both the analytes and the matrix are efficiently introduced into the plasma [26]. Desolvation in combination with a HEN significantly improves the sample introduction efficiency, compared to the typical 1–2% of the conventional concentric nebulizer/spray chamber approach, when the sample uptake rate is around 1 mL/ min. However, it also increases the total amount of dissolved solids entering the plasma, which exacerbates non-spectroscopic interferences. Furthermore, the complete removal of water is not advisable since the presence of a small amount of water vapour may improve sensitivity as well as the stability of the analyte signal [141]. In fact, Long and Browner [142] reported that there was a difference between the interaction of water vapour and water aerosol with the ICP. Water introduced into the plasma as an aerosol greatly increased the noise level of the background and decreased both the ionisation temperature and the electron density of the ICP. In contrast, when water was introduced in the form of vapour, little effect was observed [142].

In an attempt to examine the effect of pre-evaporation, Peters and Beauchemin [143] inserted a heated tube between the spray chamber and the torch. They noticed improved sensitivity for many analytes in addition to a reduction of noise since the detection limits improved more than the sensitivity. This was attributed to a reduction in the average droplet size entering the plasma. The desolvation and vaporisation of droplets has indeed been

demonstrated to be a significant source of noise since incompletely desolvated droplets or vaporising particles can lower the ion formation efficiency near them [144].

The study by Peters and Beauchemin [143] also showed that the same optimum nebulizer gas flow rate was found for a greater number of elements than without pre-evaporation; the change being most noticeable for elements forming refractory oxides. However, changing the nebulizer gas flow rate changed more than the sampling position. It also affected the residence time of analytes in the plasma, changing the location of the sharp temperature gradient (from less than 100 ºC to around 5000 ºC) in the plasma without changing the gas velocities in the center of the plasma downstream of the load coil. Most importantly, it significantly changed the sample introduction efficiency. For example, increasing the nebulizer gas flow rate from 0.82 to 1.02 L/min (i.e., by 200 mL/min difference), increased the amount of aerosol entering the torch by 60% [84]. This not only increases the analyte load but also the solvent load in the plasma. Nonetheless, inserting a pre-evaporation interface did not significantly change the plasma ionisation temperature since the greatest improvement was not systematically observed for elements with a high first ionisation potential, such as As, which should be more susceptible to these effects since they are not completely ionised in the ICP. Indeed, anything affecting the ionisation temperature and electron density of the latter should change their degree of ionisation and, hence, the sensitivity of ICP-MS

for these analytes. A more thorough study of the effect of a pre-evaporation interface, including its dimensions and position in the ICP-MS instrument is thus warranted, under constant plasma operating conditions.

Although organic solvents [89, 92] and surfactants [91] can be used to improve the sensitivity of high IP elements, the situation is often complicated by matrix effects from the carbon that is concurrently introduced in the plasma, as well as from changes in the nebulisation and sample transportation processes. For example, the amount and droplet size distribution of the aerosol exiting the spray chamber and solvent vapour loading, which are affected by the volatility of the solvent, influenced analyte signal [111]. Furthermore, Xu *et al.* [114] reported that a higher ionic strength matrix increased the abundance of small droplets in the tertiary aerosol because of Coulomb fission events during the desolvation occurring through the spray chamber, which ultimately enhanced the analyte signal. This effect would likely be exacerbated by the pre-evaporation tube through evaporation and desolvation of the solvent from analytes, which in turn would increase the charge density of droplets.

1.4 Thesis objectives

The ultimate goal of this project was to develop methods to improve the sensitivity and detection limits of ICP-TOFMS and then apply the methods to As speciation analysis.

To this end, an investigation of matrix effects (as well as their mechanisms) induced by organic solvents and surfactants was conducted, using radial profiling of analytes and background ions distribution. The effect of pre-evaporation on ion distributions (including different analytes and some background ions) under otherwise constant plasma operating conditions (nebulizer gas flow, RF power, etc.) was also investigated by spatial profiling of ion signals in the plasma, with and without a pre-evaporation tube. Different sizes of pre-evaporation tubes were used and installed in different positions in order to establish which provided the best results. ICP-TOFMS facilitated the multi-elemental determination of ions distributions in the plasma through axial and radial profiling, with and without heating the connecting tube between the spray chamber and the torch.

Axial profiling was also used to further investigate how the pre-evaporation tube affects As and other analyte signals. This investigation was prompted by an attempt to use the pre-evaporation tube as an interface between HPLC and ICP-MS for the speciation of As, where the reproducible enhancement observed with a multi-elemental solution was not observed with a mono-elemental solution of As. Yet, pre-evaporation was expected to increase the frequency of Coulomb fission events, thereby reducing the droplet size distribution of the aerosol and thus enhancing sensitivity. After elucidating the reason for this discrepancy, consideration was given to the selection of a

suitable mobile phase for the separation of As species and application of the pre-evaporation interface on arsenic speciation analysis by HPLC-ICP-TOFMS.

Chapter 2 Experimental

2.1 Instrumentation

2.1.1 ICP-TOFMS

An axial ICP-TOFMS (Renaissance, LECO Corp., St. Joseph, MI., USA) instrument was used throughout this work, whose schematic diagram is shown in Figure 2.1. The plasma generation portion of this instrument includes a dual frequency RF generator that can operate at either 27.12 or 40.68 MHz. In this work, 40.68 MHz was systematically used. The standard Fassel-type ICP torch (shown in Figure 2.2) is mounted horizontally in the torch box. Its radial (X and Y) or axial (Z) position is controlled precisely by computer software. An external circulating chiller (model CFT-75, Neslab Instruments Inc., Newington, NH, USA) is used to supply cooling water to both the cones and the plasma load coil.

Sample introduction into the plasma is done using a system that is external to the torch box. It consists of a Meinhard concentric nebulizer (type C, model # TR-30-C3, Figure. 2.3) and a Smith-Hieftje cyclonic spray chamber (Figure 2.4), both made of glass, which is connected to the torch by a piece of plastic tubing.

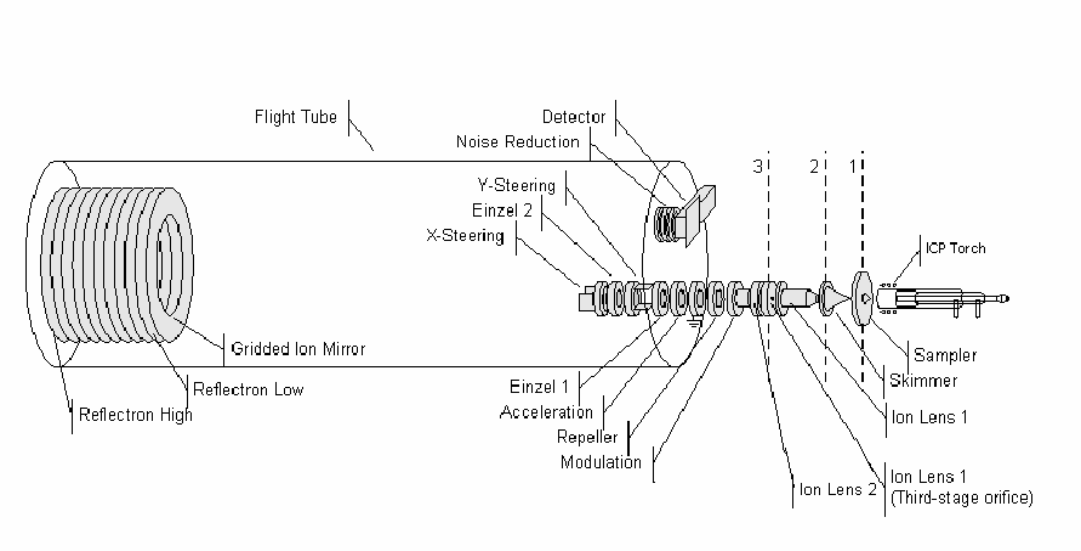

Figure 2.1 Schematic diagram of LECO Renaissance axial ICP-TOFMS system used in this work. The function and operation of the various components are described in the text (from ref. 56).

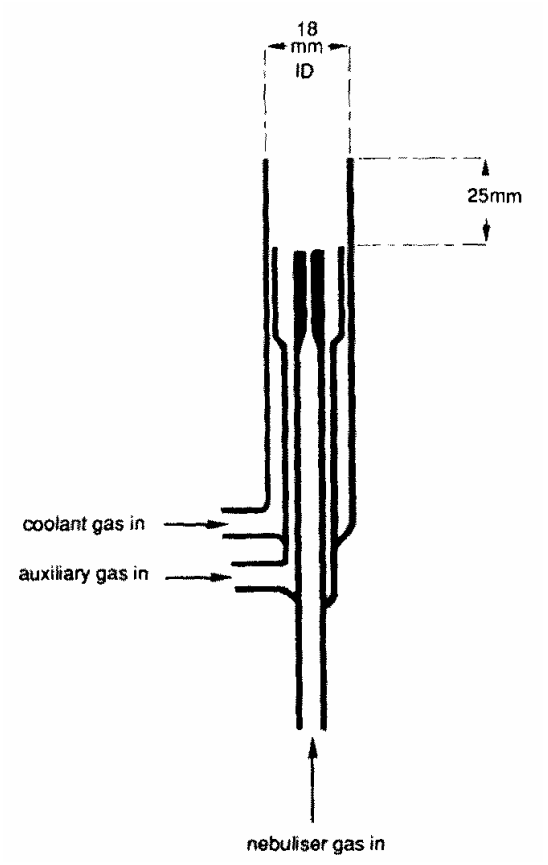

Figure 2.2 Schematic of a Fassel-type ICP torch (from Ref. 1)

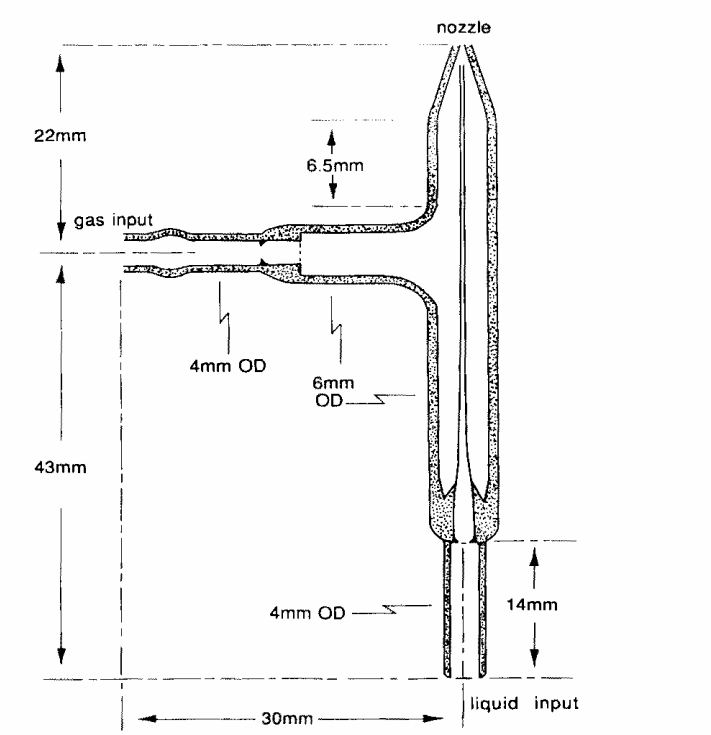

Figure 2.3 Meinhard concentric glass nebulizer (from Ref.1)

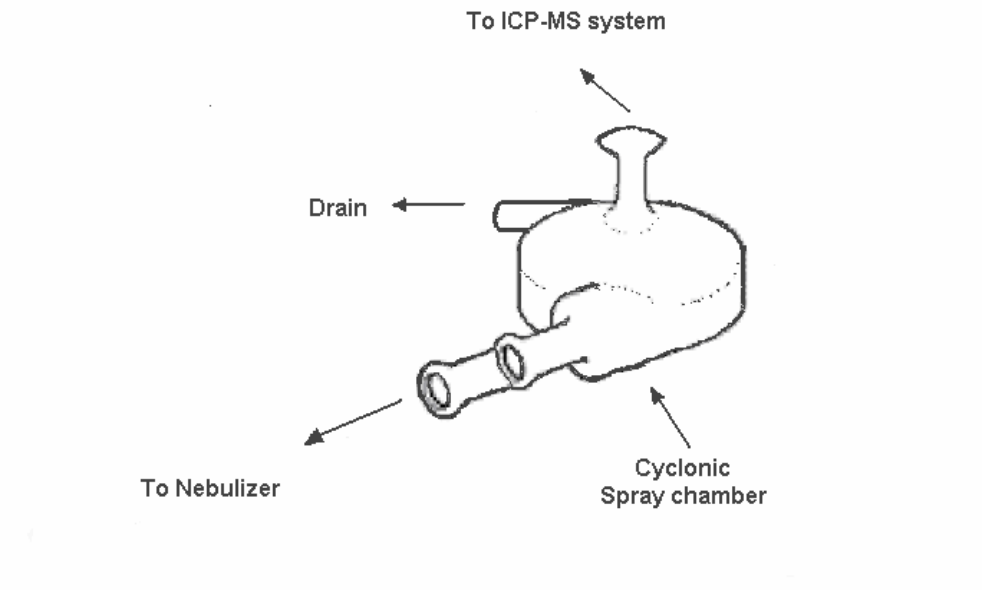

Figure 2.4 Schematic of a cyclonic spray chamber (modified from Ref. 145)

A sample of the plasma is extracted through a differentially pumped interface (between grounded sampler and skimmer cones) where the pressure is maintained at 2-3 Torr (using a rotary vane pump). Ions are then extracted using ion lenses 1 and 2, whose recommended potential is in the range of -500 V to -1000 V, under a vacuum of 10^{-3} Torr (maintained by a turbo molecular pump). These ion lenses focus the positive ion beam and direct it to a modulation and acceleration region. Their potential needs to be optimized according to the m/z of the analyte. For multi-elemental analysis, compromised potentials must thus be selected for these two lenses, which, in this work, were adjusted so as to get an optimum signal for a middle mass element (normally ^{115}In).

Switching the potential of the modulation cylinder from a negative value (in the range of -80 to -150 V) to a positive fixed value of 100 V results in ion packets (1.5-cm long segments). The repeller electrode (with a 1000 V positive potential pulse for 1 μs) pushes each ion packet into the acceleration region, so that all ions enter at the same time and with the same kinetic energy. The negative voltage on the steering optics and Einzel lenses in the flight tube increases the ions transmission to the ion mirror. The latter contains two electrodes with positive potential: reflectron low with a fixed value of 200 V and reflectron high with the optimum potential of 1537 V (which should be in the range of 1500 to 1600 V). A discrete dynode electron multiplier detector, which allows simultaneous counting and analog mode

detection, is located above the ion optics. A positive voltage (500 V) is used on the middle grid of the detector to reduce noise from low energy background ions. The optimal potentials of the lenses, X- and Y- steering, and reflectron, which can have a significant effect on sensitivity, do not change much from day to day, and need not be adjusted frequently. The operating conditions used during the course of this work are summarized in table 2.1. Analytes were selected that covered the mass range as well as a range of IP. In general, the most abundant isotope of each analyte was monitored, except for Se where m/z 78 was used instead because of the high background and, thus, required deflection at m/z 80 of the most abundant argon dimer.

2.1.2 Pre-evaporation tube

Three glass tubes were fabricated (in house) and tested. One 11-cm long extension had a 5-mm i.d., which matched exactly the i.d. of the spray chamber exit and the entrance to the plasma torch. The other two tubes had a 2-mm i.d. over the majority of their length, with a 5-mm i.d. entrance and exit, and a length of 11 and 22 cm, respectively. All three tubes ended with 12-mm/5-mm ground glass ball joints, which exactly matched the joints of the spray chamber and the torch. Heating was done using OMEGALUX flexible heating tape (120 V, 0.437 x 8 inch, 35 W; OMEGA Engineering Inc., Stamford Connecticut, USA) and controlled by a Mantle-Minder temperature controller PL512 (GLAS-COL apparatus company), with a temperature probe inserted between the tube and the heating tape. Because the extension tubes

Table 2.1 The instrument operating conditions

ICP source	RF power (kW)	1.25-1.5*
	RF frequency (MHz)	40.68
	Ar plasma gas flow rate (L/min)	15
	Ar auxiliary gas flow rate (L/min)	0.85
	Ar nebulizer gas flow (L/min)	0.85-0.98
	Sample uptake rate (mL/min)	0.6-0.88
Interface	Ni sampler cone orifice diameter (mm)	0.9
	Ni skimmer cone orifice (mm)	0.5
Mass	Flight tube (V)	-1500
spectrometer	Reflectron low (V)	200
	Reflectron high (V)	1537
	X steering (V)	(-1503) - (-1537)
	Y steering (V)	(-1560) - (-1575)
	Einzel lens1 (V)	(-1220) - (-1400)
	Einzel lens2 (V)	(-925) -(-1005)
	Ion lens 1 (V)	(-550) - (-600)
	Ion lens 2 (V)	(-425) - (-475)
	Modulation negative (V)	(-100) – (-115)
	Detector (V)	(-1900) – (-2700)
	Integration time (second)	1-5
	Ions monitored	$^{27}Al^{+}$, $^{51}V^{+}$, $^{52}Cr^{+}$, $^{60}Ni^{+}$, $^{63}Cu^{+}$, $^{55}Mn^{+}$, $^{64}Zn^{+}$, $^{66}Zn^{+}$ $^{75}As^{+}$, $^{78}Se^{+}$, $^{98}Mo^{+}$, $^{114}Cd^{+}$, $^{121}Sb^{+}$, $^{127}I^{+}$, $^{139}La^{+}$, $^{208}Pb^{+}$, $^{139}La^{16}O^{+}$, $^{139}La^{2+}$ $^{36}Ar^{+}$ $^{40}Ar^{12}C^{+}$, $^{12}C^{16}O^{+}$,

* 1.5 kW with organic solvents.

were made of Pyrex® glass, the maximum temperature that could be used was 400°C.

2.2 Reagents

Several 20 µg/L multi-elemental solutions of Al, Co, Ni, Zn, Cu, As, Se, Mo, Cd, Sb, La, Pb and their corresponding blanks were prepared in different matrices for Chapter 3. Multi-elemental solutions containing 20 and 40 µg/L each of Al, V, Cr, Ni, Zn, Mn, As, Se, Mo, Cd, Sb, La and Pb and mono-elemental solutions of each of the above analytes were also prepared for Chapters 4 and 5. Similarly, solutions containing 20 µg/L of these 13 analytes was prepared in 0.025 M NH_4NO_3 for Chapter 6. Mono-elemental stock standard solutions (SPEX Industries Inc. Edision, N.J. and SCP Science, Champlain NY, USA), purified water (18Ω cm^{-1} Milli-Q, Millipore, Harrick Scientific Corporation, Ossining N.Y., USA) and either high purity nitric acid (trace metal grade, Fisher Scientific, Ontario, Canada) or ammonium nitrate (98+%, A.C.S. reagent, and 99.999%, Aldrich Chemical Company Inc. Milwaukee, USA) were used for this purpose. Except for the solutions in NH_4NO_3, all the prepared solutions contained 1% HNO_3.

For Chapter 3, some sets of standards and blank also contained (i.e. in addition to 1% HNO_3) 0.2% (m/m) sodium dodecyl sulfate (SDS, GC grade Sigma-Aldrich Canada Ltd., Oakville, ON., Canada), 2% (v/v) methanol (HPLC grade, BDH Inc., Gibbstown, N.J., U.S.A), 1-2% (v/v) acetone (HPLC

grade, Sigma-Aldrich Canada Ltd., Oakville, ON., Canada) or 2% (v/v) ethylene glycol (Sigma-Aldrich Canada Ltd., Oakville, ON., Canada). The surfactants methoxypolyethylene glycol (Sigma-Aldrich Canada Ltd., Oakville, ON., Canada) and Triton X-100 (electrophoresis grade, Fisher Scientific Corporation, Fair Lawn, N.J., U.S.A) were also used to investigate matrix effects. Solutions of 0.007 M $NaNO_3$ (analytical reagent 99.5%, BDH Inc., Toronto, ON, Canada) in 1% HNO_3, with and without 20 µg/L of all the analytes, were also prepared to check if Na was the source of the enhancement effect observed with 0.2% SDS.

For chapter 5, a 20 µg/L As solution was prepared in 0.01 M NaOH by diluting the 1000 mg/L standard solution with 0.01 M NaOH prepared by dissolving NaOH (NF/FCC pellets, Fisher Scientific, Fair Lawn, NJ, USA) in high purity water. Sodium iodide (analytical reagent, BDH chemical, Toronto, ON, Canada) was used to prepare a 20 µg/L iodine solution in 0.01 M NaOH by first preparing a 1000 mg/L NaI solution and then diluting it with 0.01 M NaOH. For Chapter 6, the pH of 0.00625 to 0.025 M NH_4NO_3 solutions (used as mobile phase for As speciation) was adjusted to 8.6 by adding ammonia solution (EM Science, A division of EM Industries, Inc., Gibbstown, NJ 08027, USA) and using an Accumet® Basic AB 15 pH meter (Fisher Scientific limited, Canada).

Four arsenic species standard solutions of As(III) (As_2O_3, 99.999%, metal basis, ALFA AESAR, Johnson Matthey Company, Ward Hill, MA); As(V) (As_2O_5, 99.9%, metals basis, ALFA AESAR, Johnson Matthey Company, Ward Hill, MA); DMA (dimethylarsinic acid (or cacodylic acid), supplied as sodium salt trihydrate, 98%, ACROS Organics, New Jersey, USA); MMA (monomethylarsonic acid, supplied as disodium methylarsonate, Chem.. Service Inc., West Chester, PA, USA) were prepared by dissolving their salts and diluting them to 50 µg/L and 25 µg/L with high purity water.

2.3 Procedures

2.3.1 ICP-TOFMS instrument optimisation

Mass calibration was performed each day before data collection in order to achieve maximum sensitivity and precision. This step is absolutely required whenever parameters of the mass spectrometer have significantly changed (such as after cleaning lenses). To this purpose, a multi-elemental solution in 1% HNO_3 containing 5 µg/L Ba, Bi, Co, In, Pb, Li, Mg, Sc and Y (prepared from a 10 µg/mL stock solution supplied by LECO) was used that covered a wide mass range. The $^{115}In^+$ signal was then maximized, without compromizing the signals of the other analytes, by adjusting the vertical (X) and horizontal (Y) positions, as well as the sampling depth (Z, a measure of the relative distance between the load coil and sampler) and nebulizer gas flow rate. This mass calibration established the best compromise of radial X, Y, Z positions and nebulizer gas flow rate.

To protect the detector, which is continuously exposed to all ions (unlike scanning types ICP-MS instruments), deflection windows were carefully set to reduce the background from major ions (O^+, OH^+, NO^+, Ar^+, ArO^+ and Ar_2^+) at m/z 12-23, 28, 30-40, 56, 80. These deflection windows are selected by applying timed voltage pulses to the X-steering plate. Unfortunately, they also affect the signal intensity of analyte ions at nearby m/z (such as m/z 55). Additional deflection windows were also required, according to the matrix composition (for example, to deflect Na^+ when aspirating saline solutions). Typical deflection windows are summarized in table 2.2.

Table 2.2 Ion deflection window of ICP-TOFMS

Start time(μs)	Width (μs)	Deflected ions
0.924	0.150	12-16 amu: C^+, N^+, O^+,
1.097	0.078	17-23 amu: Na^+, H_2O^+, H_3O^+
1.320	0.136	28-36 amu: N_2^+, NO^+, O_2^+, O_2H^+, Si^+, $^{36}Ar^+$
1.497	0.078	36-40 amu: $^{40}Ar^+$, $^{40}Ca^+$
1.580	0.030	40-42 amu: $^{40}ArH^+$, $^{40}ArH_2^+$,
1.776	0.030	56 amu: $^{40}ArO^+$, $^{40}CaO^+$, $^{38}Ar^{18}O^+$
2.084	0.030	80 amu: $^{40}Ar_2^+$

Finally, the optimum RF power was determined for each matrix with the 20 μg/L analyte solutions in that matrix while keeping other parameters constant. In particular, the aerosol carrier gas flow rate was deliberately kept constant to ensure that the nebulisation efficiency would remain constant.

2.3.2 Measurement of the sample transport efficiency

Self-indicating silica gel (BDH Inc., Toronto, ON, Canada) was used to measure the sample transport efficiency, as described before [84]. Briefly, it was ground and dried in the oven at 100-120°C. The dried silica gel (about 0.9 g) was placed in a 1000 µL plastic pipette tip (Fisher Scientific limited), between two pieces of glass wool. The pipette tip was cut so that its exit diameter would match that of the tube connecting the torch to the spray chamber. It was then attached to the end of this connection tube (instead of the torch). Nebulisation was done during 3 minutes and the silica gel weighed. Sample transport efficiency was determined 5 times for each matrix.

2.3.3 Measurement of analyte transport efficiency

The same procedure as in 2.3.2 was followed, except that, after nebulising a solution for 3 min, the analytes were eluted from the silica gel using 1% HNO_3 at the same sample uptake rate. The eluted sample solution was collected and diluted for subsequent analysis by ICP-MS.

2.3.4 Evaluation of the secondary discharge

In order to ascertain to which extent spatial profiles are representative of ions distribution in the plasma, the extent of any secondary discharge had to be assessed as it is known to increase the level of doubly-charged elements while concurrently reducing their oxide level [1,146]. Increasing the moisture

in the plasma (through, for instance, increasing the nebulizer gas flow rate) has also been demonstrated to exacerbate the secondary discharge. The extent of such discharge was thus assessed by measuring the ratio of La^{2+} and LaO^{+} to the total La signal as a function of an increase in nebulizer gas flow rate or a change in sampling depth (Z position).

2.3.5 Spatial profiling

Unless otherwise specified, spatial profiling was carried out under the best compromise multi-elemental conditions, both with and without the heated tube (standard configuration). Axial profiling was done, using the computer-controlled translation stage of the instrument, by moving the torch with respect to the sampling interface while keeping the vertical radial position fixed once optimized. Increments of 0.5 mm were used in an attempt to compensate for fluctuations and heterogeneity in the sampled volume [116].

Radial profiles were obtained while keeping all the other parameters (X position, Z position, RF power, etc.) constant, except for the horizontal radial position (Y), which was varied by 0.2 mm increment (or 0.1 mm near the centre of the central channel). In each case, a blank was aspirated for 3 minutes followed by 20 and 40 µg/L standard solutions. Studies with the tube heated or not were always carried out on the same day whenever the results were to be compared with each other.

2.3.6 Study of the effect of a pre-evaporation tube

2.3.6.1 Heated tube outside the torch box

Experiments were first done, as this was most easily implemented on this instrument, with the heated tube located outside the torch box, between the spray chamber outlet and the connection plastic tube that normally links the spray chamber directly to the torch (see figure 2.5). A wrapping with teflon tape and Tygon tubing was used to insulate the plastic connection tubing located in the torch box to somewhat prevent cooling in this region. The whole tube was wrapped with heating tape when it was positioned outside the torch box.

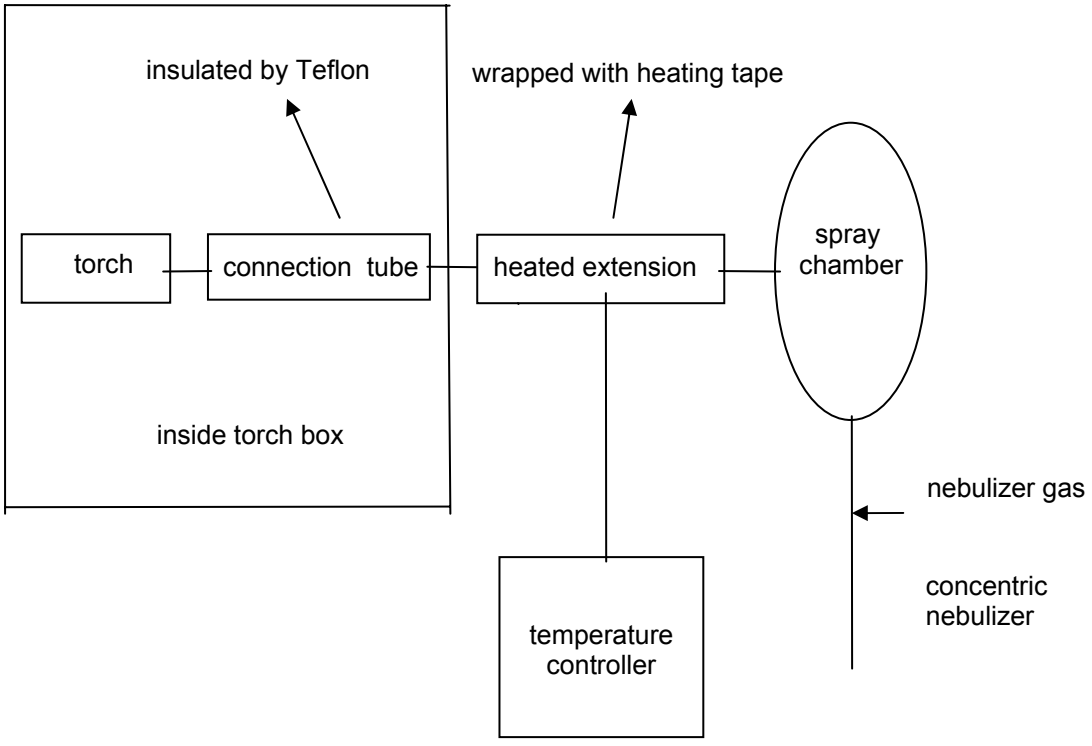

Figure 2.5 Schematic diagram of heated tube outside the torch box

2.3.6.2 Heated tube inside the torch box

Most of the experiments were carried out with the heated tube inserted in place of the plastic connection tubing (which is exactly 11 cm long) inside the torch box, as this configuration did not lengthen the transport line. However, only a 7-mm length could be wrapped with heating tape because of physical constraints (i.e. to prevent melting of electrical wires hanging near the entrance of the torch box). The setup also provided at least 2 cm of clearance between the heating tape and the igniter clip. No interference effects between the heating system and the plasma generation process were observed with heating tape wrapped right up to the base of the torch inside the torch box.

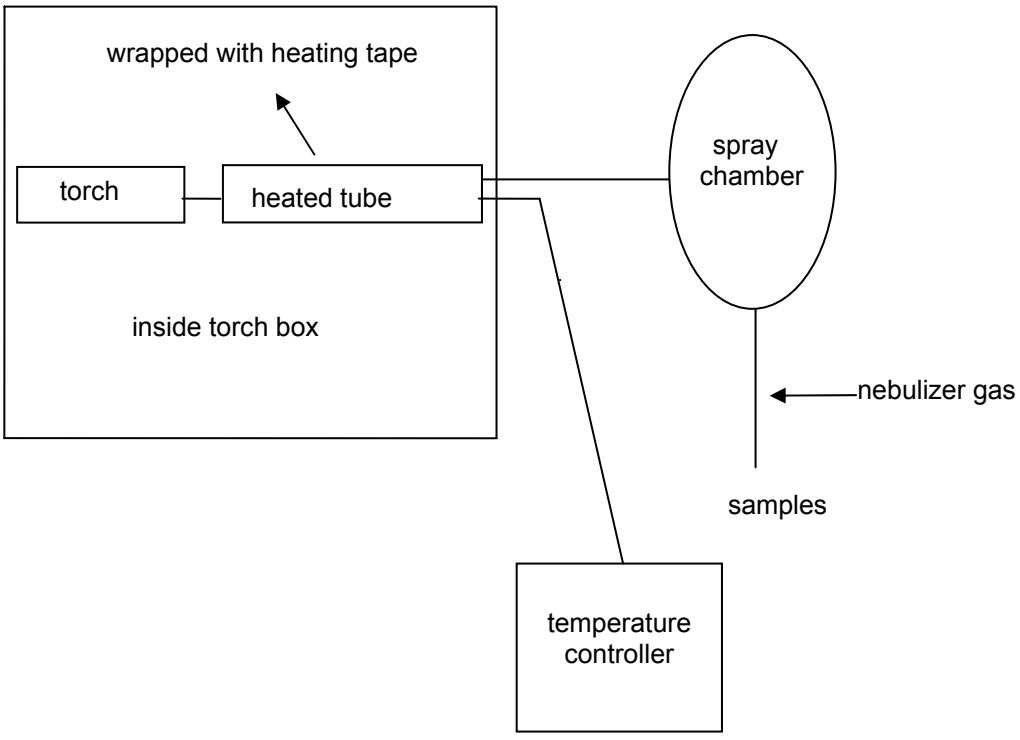

Figure 2.6 Schematic diagram of heated tube inside the torch box

2.3.6.3 Temperature in the pre-evaporation tube

The temperature inside the pre-evaporation extension tube was measured by inserting another probe inside the extension tube without touching its inner surface. This probe was connected to a thermometer (Fluke Corporation, USA). The nebulizer gas flow rate was then varied without igniting the plasma. The outside temperature was controlled by the above mentioned controller (see 2.1.2), inserting the probe outside the tube and inside the heating tape. By doing this the outside temperature together with inside tube temperature (which can not be measured with the plasma on) and their relationship was obtained.

2.3.7 Separation of As species by HPLC

A Dionex DX600/BioLC liquid chromatography system with GS50 gradient pump was coupled to the LECO Renaissance ICP-TOFMS instrument for the determination of four arsenic species. The separation conditions are summarized in Table 2.3.

A PTFE tee (0.02'' or 0.50mm through hole; 1/16'' tubing OD; 2.9 µL internal volume; Scientific Products & Equipment, North York, ON, Canada) was used to add concomitant ions to the eluent from the HPLC system prior to its introduction into ICP-MS when the heated pre-evaporation tube was applied to As speciation analysis.

Table 2.3 HPLC separation condition

Column	Dionex IonPac AS7 4x250mm
Precolumn	Dionex IonPac AG7 4x50mm
Mobile phase	A: 6.25mM NH_4NO_3 (pH 8.6)
	B: 25mM NH_4NO_3 (pH 8.6)
Flow rate	1.0mL/min
Gradient program	0-3min 100% A
	3-4min 100% A to 100% B
	4-13min 100% B
	13-15 100% A
Injection volume	50 µL

2.3.8 Data collection and processing

Although ion counting and analog data are simultaneously generated by the ICP-TOFMS instrument, only ion counting data were used in this thesis since the low analyte concentrations gave signals within the linear dynamic range of this mode (i.e. under 20,000 counts s^{-1}).

All raw data files were exported to Excel (Windows 2000 Professional) for processing and graphing. Except in the case of background ions, blank subtraction was systematically done, where the signals from an analyte-free solution in a given matrix was subtracted from the analyte signals from the standard in the same matrix, both having been measured under identical conditions.

Sensitivity was determined as the slope of the calibration curves, whereas detection limits were calculated from three times the standard deviation of the blank count rate (3xσ, n =10) divided by the corresponding sensitivity. Statistical analysis of the data (i.e. a Student's *t* test) was conducted to determine if significant differences existed at the 95% confidence level between results obtained under different sets of operating conditions.

Chapter 3 Investigation of the matrix effects caused by organic compounds

As discussed in Chapter 1 (section 1.2.1), introduction of a small amount of organic solvents (or compounds) can significantly enhance the signal of analytes with first IP in the range of 9-11 eV [86,89-91,95,97], such as As [89-91] and Zn [98, 99], because they are not completely ionized under standard plasma operating conditions [115]. This selective enhancement cannot be attributed to higher sample transport efficiency from a smaller mean droplet size distribution of the aerosol [112], as it would then also affect analytes with lower IP. Instead, a carbon charge transfer mechanism was proposed, where carbon ions (such as C^+ or other carbon-containing ions) extract electrons from analyte atoms [89], leading to an improvement in the degree of ionization of these analytes. Support for this proposed mechanism may be obtained through spatial profiling of the distribution of analytes ions and background carbon-containing ions in the plasma.

Literature on organic modifiers is not limited to organic solvents. Surfactants can also change the physical properties of the sample solution, including its density, viscosity and surface tension. In fact, they have been used to improve the sensitivity of As detection [91]. A surfactant contains carbon that may become involved in a charge transfer mechanism and, hence, result in signal enhancement of analytes with higher IP. Alternatively, it can change

the physical properties of the sample solution, resulting in an improvement of nebulization efficiency, which would result in signal enhancement for all analytes, irrespective of their IP.

Unfortunately, essentially no fundamental research based on spatial profiling was published on the signal enhancement mechanisms of these different organic compounds, including organic solvents with different volatilities. Therefore, the first objective of this chapter was to investigate the matrix effects on several analytes resulting from the introduction of different organic solvents and surfactants. The second objective was to investigate the mechanisms of the resulting signal enhancement by radial profiling of analyte ion and background ion distributions since spatial profiling can provide insight on ionization mechanism in the plasma, which is not known intuitively [116]. To rule out that a change in nebulisation efficiency was the culprit, the sample introduction efficiencies were also determined for different matrices.

The work in this chapter was published in Spectrochimica Acta Part B as “Effect of methanol and sodium dodecylsulfate on radial profiles of ion abundance in inductively coupled plasma mass spectrometry” (2006).

3.1 Analyte and matrix elements

Analytes selected in this study (which were mostly the same as for the following Chapters 4 to 6) covered a range of m/z and IP. Their relevant properties are summarised in Table 3.1 (including their enthalpy of vaporisation that is useful for the research on the effect of a pre-evaporation tube). In addition to these analytes, several other ions were also monitored. These included the LaO^+ and La^{2+}. Additionally, because an Ar-based plasma was used, some Ar-containing ions ($^{40}Ar^{12}C$, and ^{36}Ar) were monitored. Finally, $^{12}C^+$ and $^{12}C^{16}O^+$, arising from the different matrices, were monitored to identify the mechanism of signal enhancement. Sodium, which was also a matrix element in SDS, has a mass of 22.9898 with a first IP of 5.138 eV.

It should be noted that some of these background ions were at least partly deflected to protect the detector. Although this would lead to significant changes in their absolute signal intensity from day to day, their spatial profiles should nonetheless be comparable on a given day. The correction of partial deflection was done by calculating the signal ratio (beginning to end of the experiment) of the analyte (near deflection window, such as ^{55}Mn (1.04), and ^{78}Se (1.04)) and the analyte that is far from deflection window (La (1.06) or Pb (1.07)).

Table 3.1 Properties of analyte elements [4,147]

Element	m/z monitored	Atomic abundance (%)	1st I.P (eV)	2nd I.P (eV)	Enthalpy of vaporization (kJ/mol)*
Al	27	100	5.99	18.83	293
V*	51	99.75	6.75	14.16	453
Cr*	52	83.79	6.77	16.49	339
Mn	55	100	7.43	15.64	220
Ni	58	68.08	7.64	18.17	378
Ni	60	26.10	7.64	18.17	378
Co	59	100	7.88	17.40	375
Cu	63	69.17	7.73	20.28	300
Cu	65	30.83	7.73	20.28	300
Zn	64	48.60	9.39	17.96	119
Zn	66	27.90	9.39	17.96	119
As	75	100	9.82	20.20	32
Se	78	23.60	9.75	21.69	26.3
Mo	98	24.13	7.09	16.16	600
Cd	114	28.73	8.99	16.91	100
Sb	121	57.36	8.64	18.53	68
La	139	99.91	5.58	11.43	400
Pb	208	52.4	7.42	15.04	178

*Not used in this chapter, but used in the investigation of the effect of a pre-evaporation tube in the following chapters.

3.2 Secondary discharge

As mentioned in Chapter 1, the interface region is the most critical part of ICP-MS as it functions is to transport ions effectively and consistently from the plasma to the mass spectrometer with electrical integrity. Any undesired electrostatic coupling between the load coil and the plasma can induce a secondary discharge [46]; if the potential difference between the RF coil and the interface cones is high enough (up to 100-200 V), a secondary discharge (also called pinch effect) occurs [47]. It is observed as arcing in the region where the plasma is in contact with the sampling cone. In general, the cone and the load coil should be grounded and the potential between them kept around zero to avoid extra discharge. Otherwise, it changes the electrical characteristics of the plasma causing an increase in the percentage of doubly charged ions and broadens the kinetic energy distribution of ions making ion focusing more difficult [47]. As a result, a secondary discharge lowers the mass resolution of the instrument and also reduces the lifetime of the sampler cone. It would also affect ion distributions, which would prevent representative spatial profiling of the plasma.

Therefore, before doing profiling, an assessment of the extent of secondary discharge on the ICP-TOFMS instrument was necessary. This was accomplished by monitoring La^{2+} and LaO^{+} as either the nebulizer flow rate was increased or the sampling depth decreased. Any secondary discharge would be exacerbated by an increase in the aerosol carrier gas flow rate, as it

would concurrently increase the solvent load in the plasma. Alternatively, such an increase in discharge would occur by moving the plasma load coil towards the sampling orifice (i.e. decreasing the sampling depth or axial Z position), which is roughly proportional to increasing the nebulizer gas flow rate (if the sample introduction efficiency does not change significantly) [1]. This would, in turn, increase the level of doubly charged ions while decreasing that of oxides [146].

In the absence of a discharge, the oxide level should increase (the doubly charged level should decrease), especially low in the plasma, whereas it would decrease in presence of a discharge. Figure 3.1 shows that the former trend was observed, i.e, with an increase in sampling depth, the proportion of doubly charged ion (La^{2+}) increased (Figure 3.1a) whereas the proportion of La oxide (LaO^{+}) concurrently decreased (Figure 3.1b). Similar trends were also obtained by changing the nebulizer gas flow rate (not shown). Therefore, the torch configuration on this instrument seems to minimise the secondary discharge, and representative ion distributions of the plasma should be obtained by spatial profiling [116].

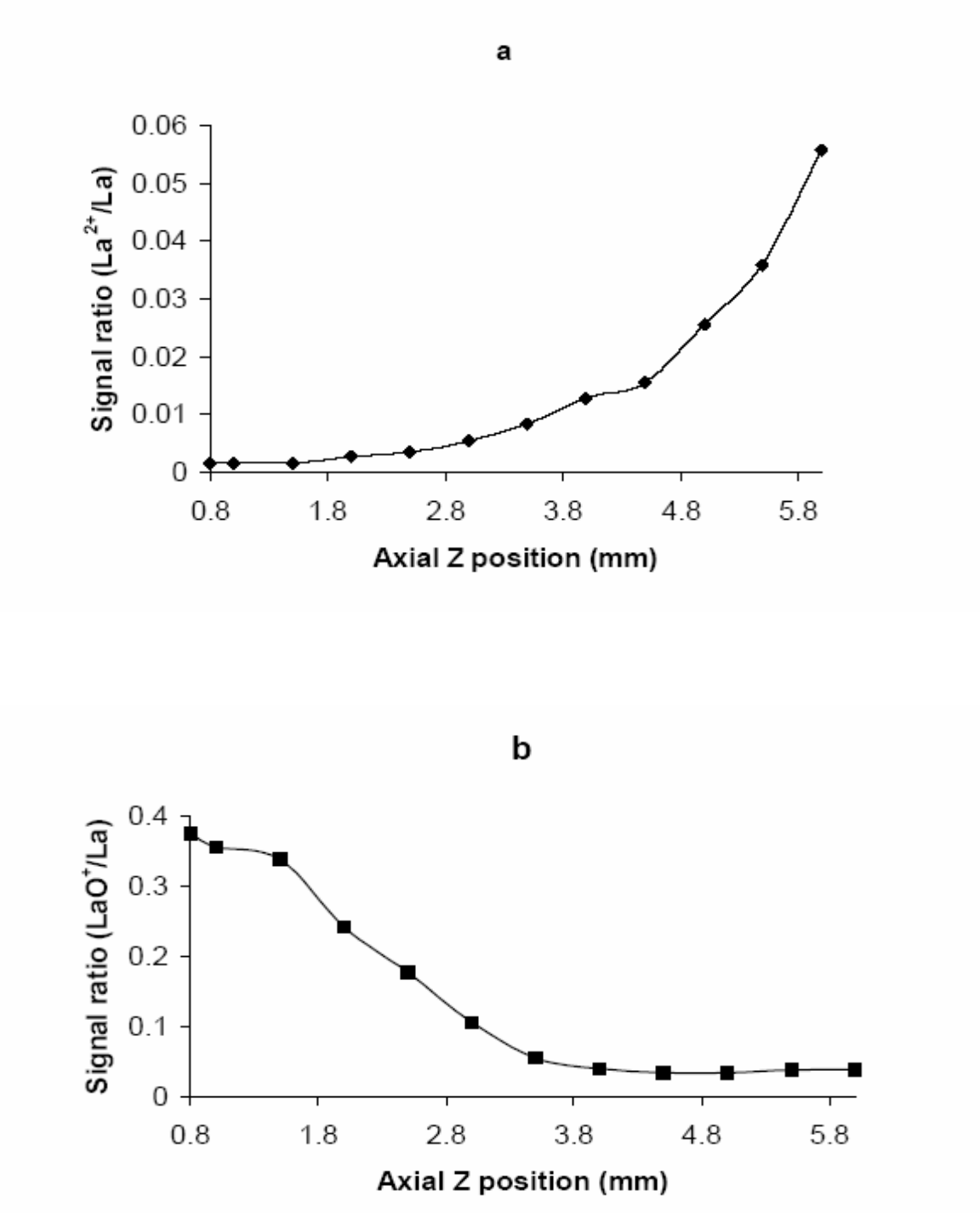

Figure 3.1 Axial profile observed for a) the ratio of doubly charged La ($La^{2+}/LaO^{+}+La^{+}+La^{2+}$) and b) the ratio of La oxide ($LaO^{+}/LaO^{+}+La^{+}+La^{2+}$)

3.3 Effect of matrix modifier on optimum RF power

The RF power is a very important plasma parameter that affects the performance of the instrument. Both the matrix composition and analyte IP influence the optimum RF power. The effect of organic modifiers on the optimum RF power was thus studied.

With the addition of 2% v/v methanol to the 1% HNO_3 matrix, the optimum RF power shifted to 1.5 kW for all analytes (Table 3.2). This is in agreement with the increase in RF power that is required to transform an organic solvent into carbon dioxide and water [148]. An increase of optimum RF power was also obtained for all analytes when 1% acetone was added in 1% HNO_3 (Table 3.2). A decrease in aerosol carrier gas flow rate, which can compensate for the increased nebulisation efficiency with solvents that are more volatile than water [149], could have been implemented instead, but was avoided in order to minimise variations in nebulisation efficiency that could be induced by a different nebuliser flow rate. Similarly, the optimum sampling depth increased if both the nebulizer gas flow rate and RF power were kept constant, indicating that a longer residence time in the plasma was then needed by the analyte to eventually undergo ionisation. However, since the power could be changed with more precise reproducibly than the sampling axial position, the latter was kept constant.

Table 3.2 Optimum RF power for each analyte in different matrices (all containing 1% HNO_3)

Elements	RF power (kW)*			
	1%HNO_3 (0.2 M)	2%MeOH (0.6 M)	0.2% SDS (0.007 M)	1% acetone (0.2 M)
^{27}Al	1.35	1.5	1.4	1.5
^{75}As	1.35	1.5	1.4	1.5
^{114}Cd	1.3	1.5	1.3	1.45
^{59}Co	1.4	1.5	1.4	1.5
^{65}Cu	1.3	1.5	1.35	1.5
^{139}La	1.3	1.5	1.3	1.4
^{98}Mo	1.3	1.5	1.3	1.45
^{60}Ni	1.3	1.5	1.4	1.45
^{208}Pb	1.2	1.5	1.25	1.4
^{121}Sb	1.3	1.5	1.3	1.45
^{78}Se	1.35	1.5	1.35	1.5
^{64}Zn	1.35	1.5	1.4	1.5
^{66}Zn	1.35	1.5	1.4	1.5

* The aerosol carrier gas flow rate was kept at 0.86 L/min while the axial Z position was 3 mm.

In contrast, the optimum RF power remained similar or increased slightly compared to that for a 1% HNO_3 matrix upon addition of 0.2% m/v SDS to 1% HNO_3 solutions (Table 3.2). This indicates that there is far less local cooling of the plasma with SDS than with MeOH, because SDS is a long-chain molecule that will not evaporate or dissociate readily from the sample. As will be seen later, this is further supported by the radial profiles of C^+ and CO^+, which are similar to those of analytes (i.e. with a peak in the central channel). The lower

concentration of SDS (0.2%) compared to 2% MeOH may also contribute to the different plasma RF power needed. Nonetheless, the volatility of the organic compound along with its concentration had an effect on plasma energy consumption, resulting in very different optimal RF power under otherwise identical conditions. With a 0.2% v/v methanol matrix (where the 0.08 M carbon content matches that of 0.2% m/v SDS), the optimal RF power was similar to that for 1% HNO_3 and 0.2% m/v SDS. A similar optimum power was also observed in solutions containing other surfactants (methoxy polyethylene glycol and Triton X-100).

3.4 Effect of matrix modifier on analyte sensitivity

Two types of surfactant (non-ionic and ionic) can be used as matrix modifier. The two non-ionic surfactants (methoxy polyethylene glycol and Triton X-100), over a range of concentrations encompassing their critical micelle concentration (CMC), either had no effect or induced a suppression (up to 20%) of almost all analytes signals except for that of Pb, which did not change. This may be linked to the limited ability of non-ionic surfactant to breakdown surface tension in combination with the increased plasma energy required to atomise these large molecules that is no longer available for analyte ionisation. Triton X-100, which is the largest (with a total of 34 carbons) of the two and contains a benzene ring, has carbon-carbon double bonds that are more difficult to break induced the most suppression. This behaviour is in contrast to the enhancement reported by Campbell *et al.* [91]. However, they

used up to 9% Triton X -100, a completely different instrument (VG PlasmaQuad II ATE) and reduced the aerosol carrier gas flow rate in order to observe an enhancement for As only (no such enhancement resulted for the other three analytes monitored). In this work, the concentration of Triton X-100 (CMC 0.015%, 0.25 mM) was kept under 0.8% v/v to avoid signal degradation of the ICP-TOFMS instrument performance through soot deposition on the sampler cone. On the other hand, a small improvement of the signal intensity of several analytes was observed in presence of the SDS anionic surfactant, as shown in Figure 3.2. Only selected analytes are shown for clarity. With the exception of Pb, whose signal behaved like that of Cd, the signals of all other analytes that are not shown were affected similarly to that of Zn. In all cases, the optimum concentration of SDS was around its CMC of 0.24% m/v (2.3 mM).

This result is in agreement with the observation that a surfactant is most efficient at breaking down the surface tension of a solution at its CMC since, beyond the CMC, surfactant molecules self-aggregate and form micelles. Under these conditions, all analyte signals might be enhanced by 37% since the sample transport efficiency increased by 37%. However, the enhancement clearly had some inverse dependency on mass, as shown in Figure 3.3c.

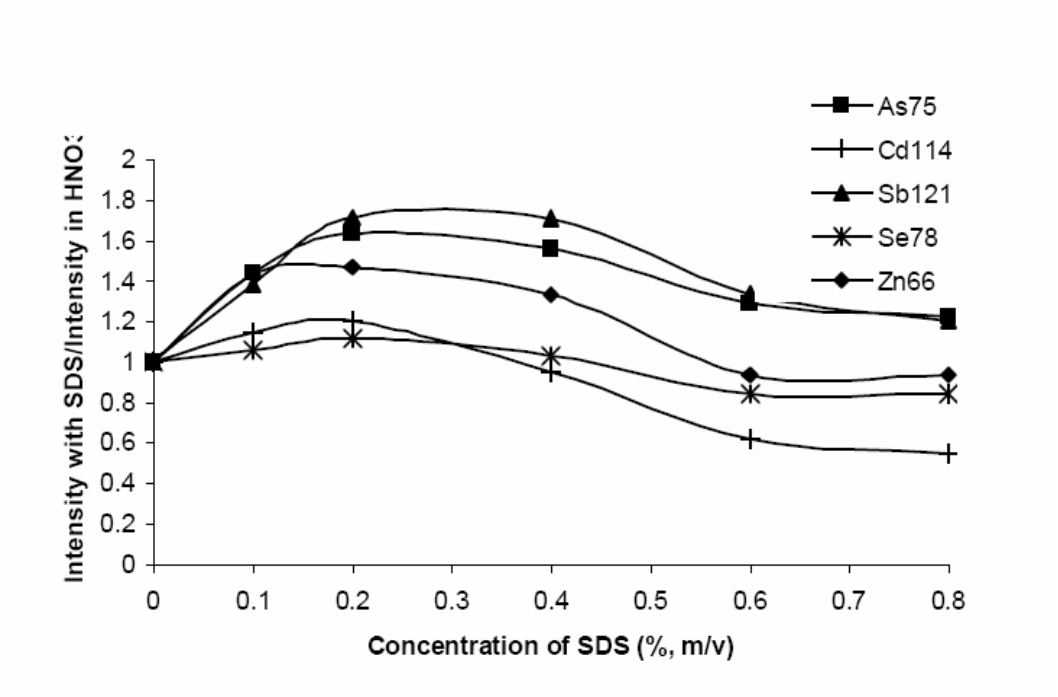

Figure 3.2 Effect of an addition of SDS(%, m/v) on the signal from selected analytes

A mass-dependent enhancement was reported using a 0.01 M Na matrix [150], therefore, a blank and standard solution prepared in 0.007 M Na^+ (i.e. equimolar to the SDS solution) and was used to check if the enhancement was simply due to the Na^+ from the SDS matrix. However, no trend with mass was observed, the signal remaining constant or decreasing slightly compared to that observed in 1% HNO_3 (Figure 3.4).

This anionic surfactant possesses negative charges. Therefore, electrostatic effect may be involved. Xu et al. [114] reported a change in the aerosol droplet size distribution upon the addition of an ionic matrix (including SDS) that was not observed when the matrix was non-ionic. This droplet size distribution alteration was attributed to a change in the net charge acquired by

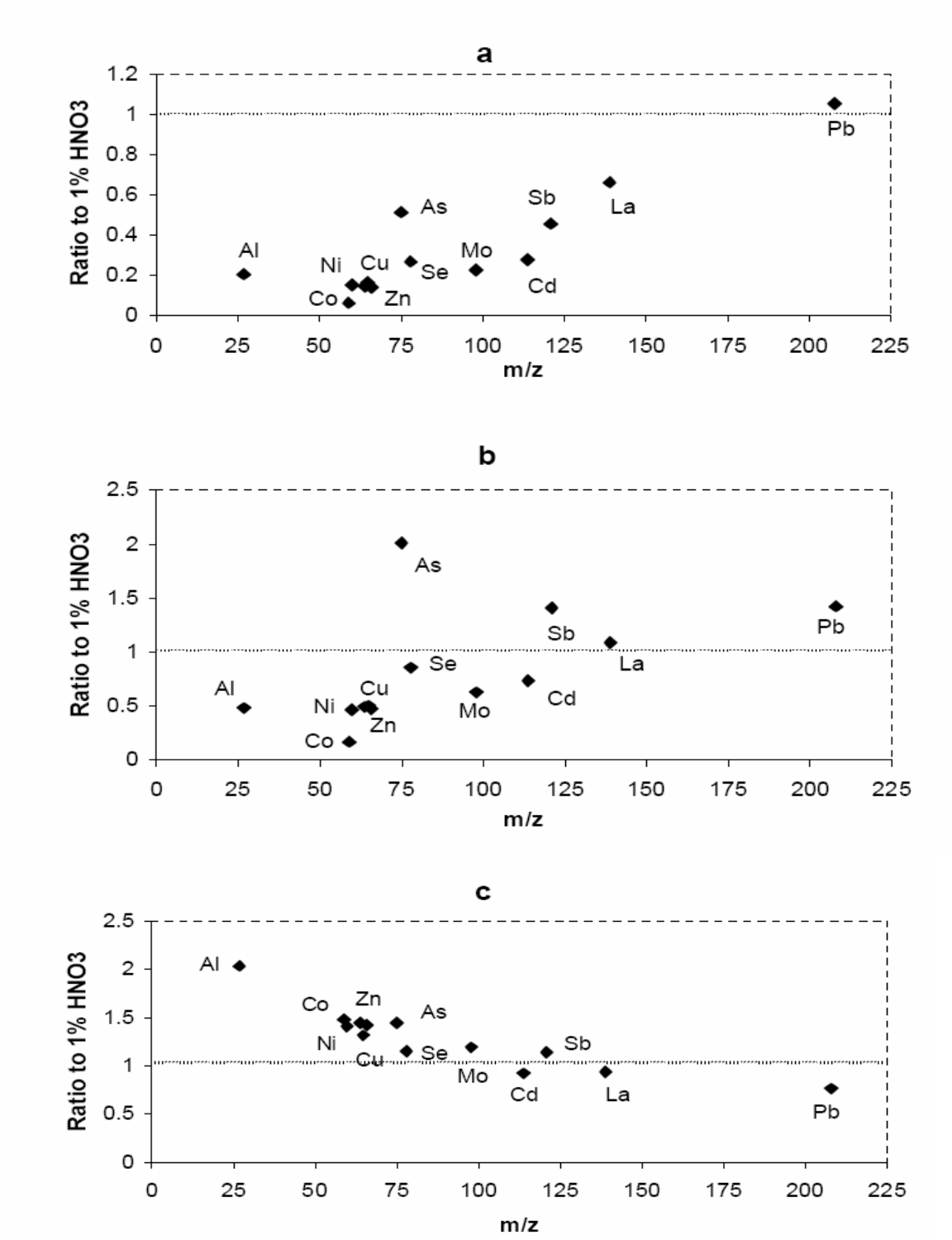

Figure 3.3 Change of analyte signal observed when adding methanol or SDS to 1% HNO_3: (a) with 2% v/v MeOH (at 1.35 kW); (b) with 2% v/v MeOH (at 1.5 kW); (c) with 0.2% m/v SDS (at 1.35kW).

the primary droplets during the nebulisation step that resulted from a change in ionic strength of the starting solution. The net charge acquired by a primary droplet can affect the extent of Coulomb fission events that may occur during the desolvation taking place through the spray chamber, a process that causes a droplet to split into numerous smaller droplets. The results in Figure 3.3c suggest an additional effect, specially that the negatively charged droplets induced by the SDS matrix attract cations, hence inducing analyte enrichment in aerosol droplets. This process should be most efficient for light analytes because they are more mobile than heavier ones, which could explain the trend in Figure 3.3c. Although SDS would only attract cations and perhaps polar molecules, anions might be entrained along by the cations, which would also explain the slight enhancement observed for As, Se.

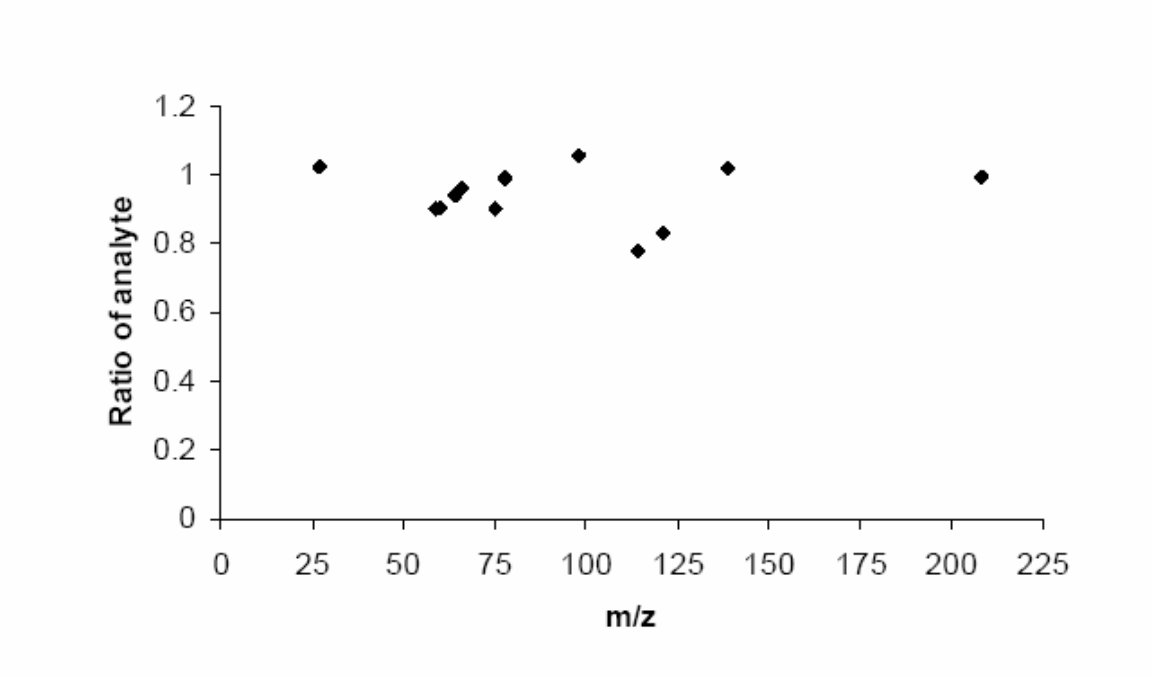

Figure 3.4 Ratios of analyte signal observed in 0.007 M Na/1% HNO_3 over that in 1% HNO_3

To verify this electrostatic analyte enrichment hypothesis, the analytes collected on the silica gel during the measurement of the sample introduction efficiency were eluted and their amount was determined. Figure 3.5 shows that smaller mass analytes are more likely to exit the spray chamber than heavier mass analytes in presence of 0.2% m/v SDS. Although the concentration of SDS was just below its CMC, i.e. no micelles were expected to be present in droplets, SDS may also play a role in the formation of films on the inner wall of the spray chamber, which could facilitate re-nebulisation.

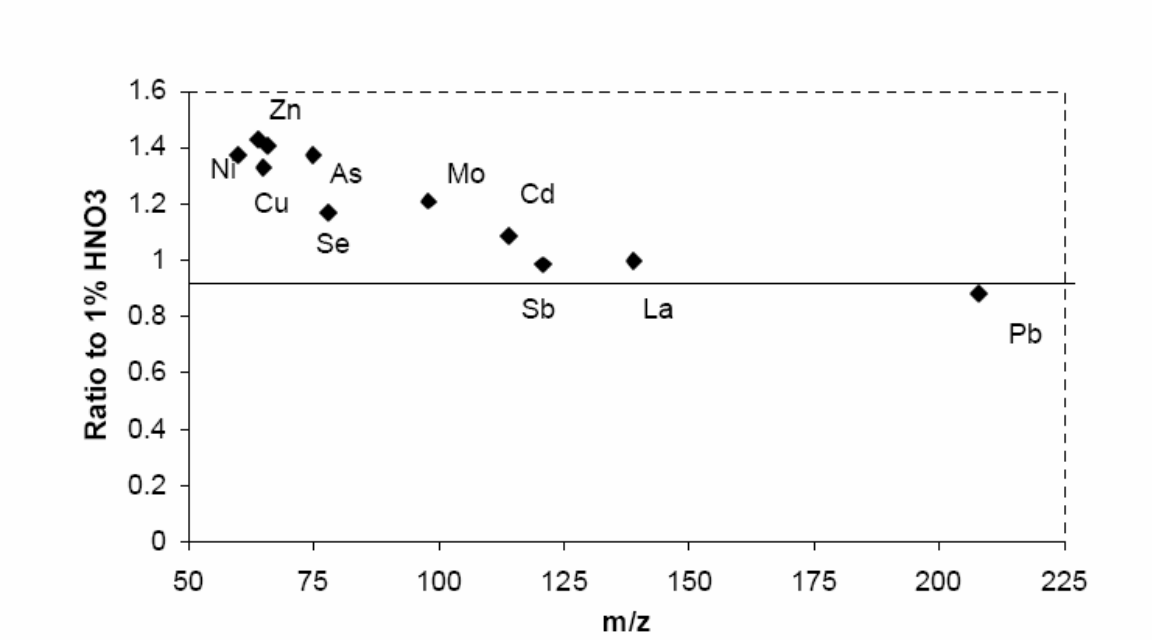

Figure 3.5 Recovery of analytes from the silica trap as a function of analyte m/z following nebulisation of an analyte solution containing 0.2% m/v SDS, relative to that obtained in 1% HNO_3.

In contrast, 2% v/v MeOH induced analyte signal suppression that decreased with m/z (Figure 3.3a), despite an increase in sample transport efficiency of 36% compared to that measured in 1% HNO_3 alone and similar to that

observed with 0.2% m/v SDS. Although increasing the RF power could decrease suppression, significant enhancement could only be achieved for As, Sb and Pb (Figure 3.3b). The radial profiles provided an explanation for this suppression: a widening of the analyte distribution with a bimodal shape occurred, as shown in Figure 3.6. Only in the case of As, Sb and Pb did an enhancement also result when power was increased to 1.5 kW. In fact, scrutiny of the data revealed that the widening of the analyte distribution appeared to have some inverse dependency on mass, as shown in Figure 3.7. This would suggest that light analytes were more easily spread out with MeOH.

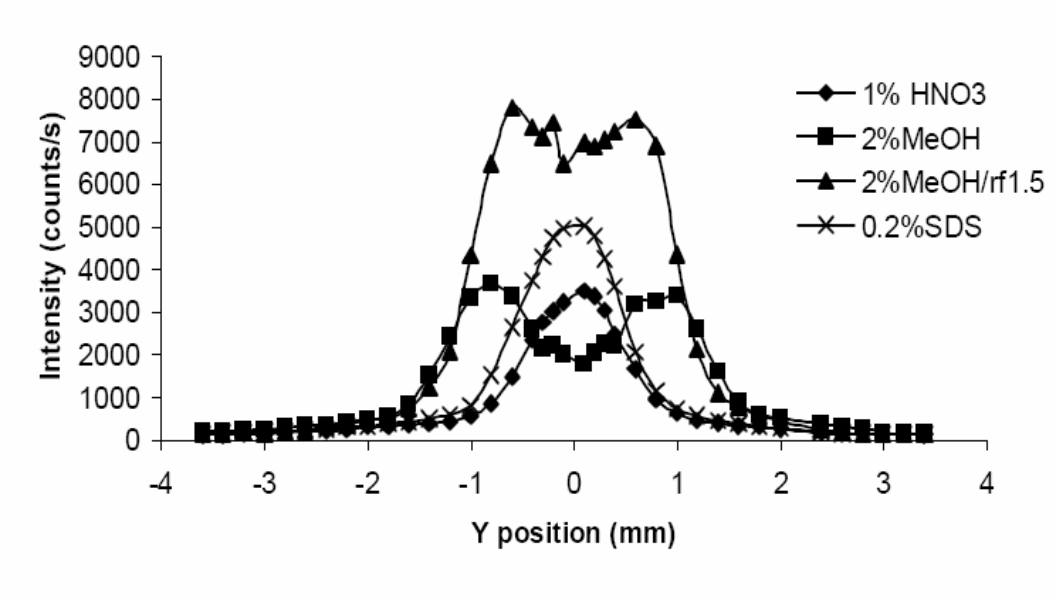

Figure 3.6 Radial profile of $^{75}As^{+}$ distribution in the ICP with different matrices: 1% HNO3; 1% HNO_3 and 0.2% m/v SDS; 1% HNO_3 and 2% v/v MeOH; 1% HNO_3 and 2% v/v MeOH at RF 1.5 kW.

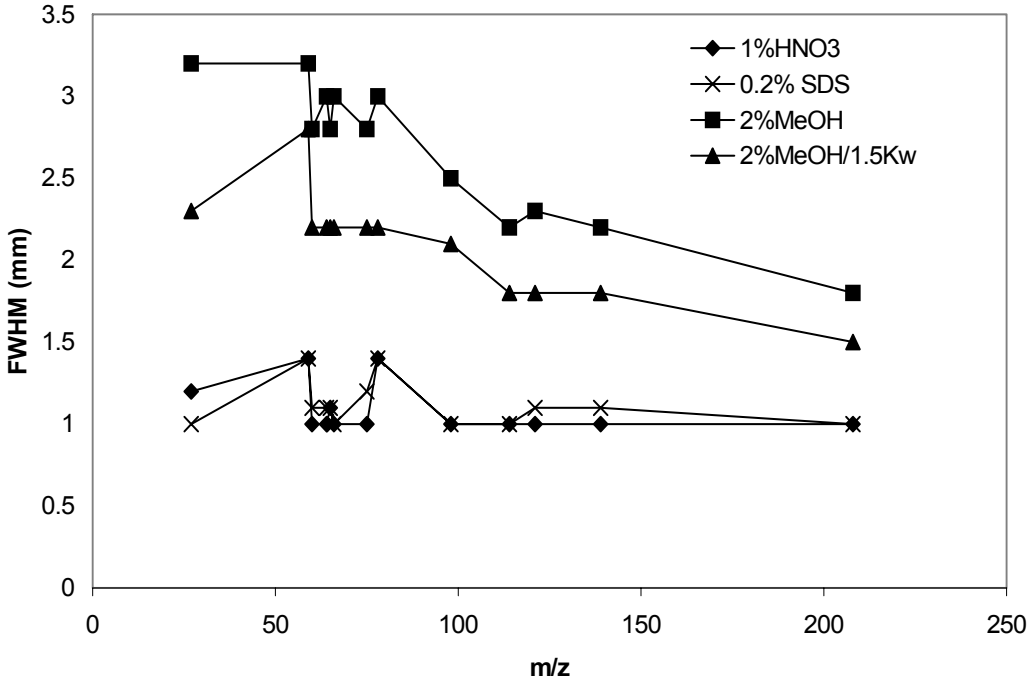

Figure 3.7 Full width at half maximum of the radial profiles of the analytes as a function of m/z for each of the matrices: 1% HNO_3; 1% HNO_3 and 0.2% m/v SDS; 1% HNO_3 and 2% v/v MeOH; 1% HNO_3 and 2% v/v MeOH at 1.5 kW.

3.5 Effect of matrix modifier on ionisation mechanisms in the ICP

Figure 3.6 shows that the bell-shaped analyte distribution, which is typically observed in 1% HNO_3 [116], did not change in presence of 0.2 % m/v SDS but turned into a bimodal analyte distribution with 2% v/v MeOH. Furthermore, this bimodal distribution is similar to that observed for C^+ (Figure 3.8) as well as CO^+ (Figure 3.9) and ArC^+ (Figure 3.10). On the other hand, the 0.08 M carbon content of 0.2% SDS did not significantly change the C^+ signal while it increased both CO^+ and ArC^+ in the central channel. Note that the absolute signal intensities of these background ions cannot be compared since they

were deflected to a different extent to protect the instrument detector. Only the relative changes in intensities and profiles are comparable, since the data were acquired simultaneously for a given matrix, and on the same day, when matrices are compared.

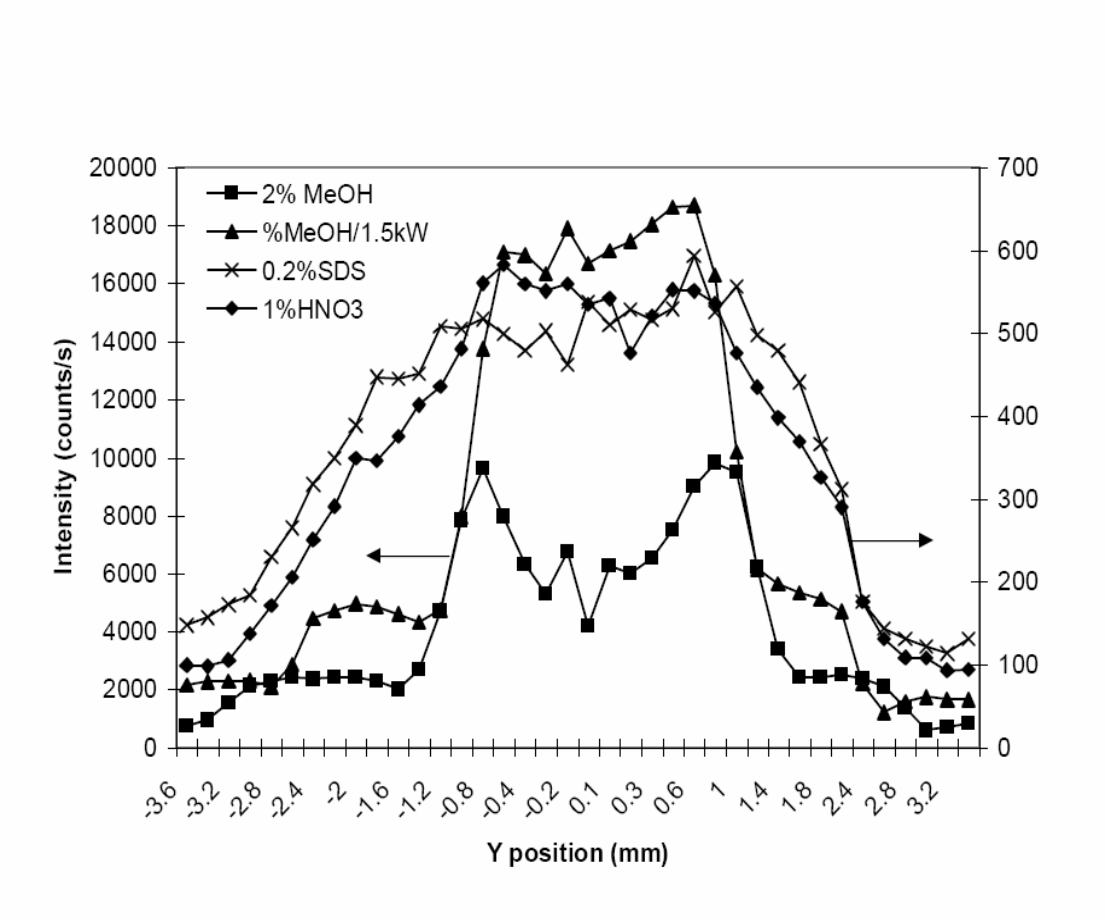

Figure 3.8 Radial profile of $^{12}C^{+}$ distribution in the ICP with different matrices: 1% HNO_3 (right scale); 1% HNO_3 and 0.2% m/v SDS (right scale); 1% HNO_3 and 2% v/v MeOH (left scale); 1% HNO_3 and 2% v/v MeOH at 1.5 kW (left scale).

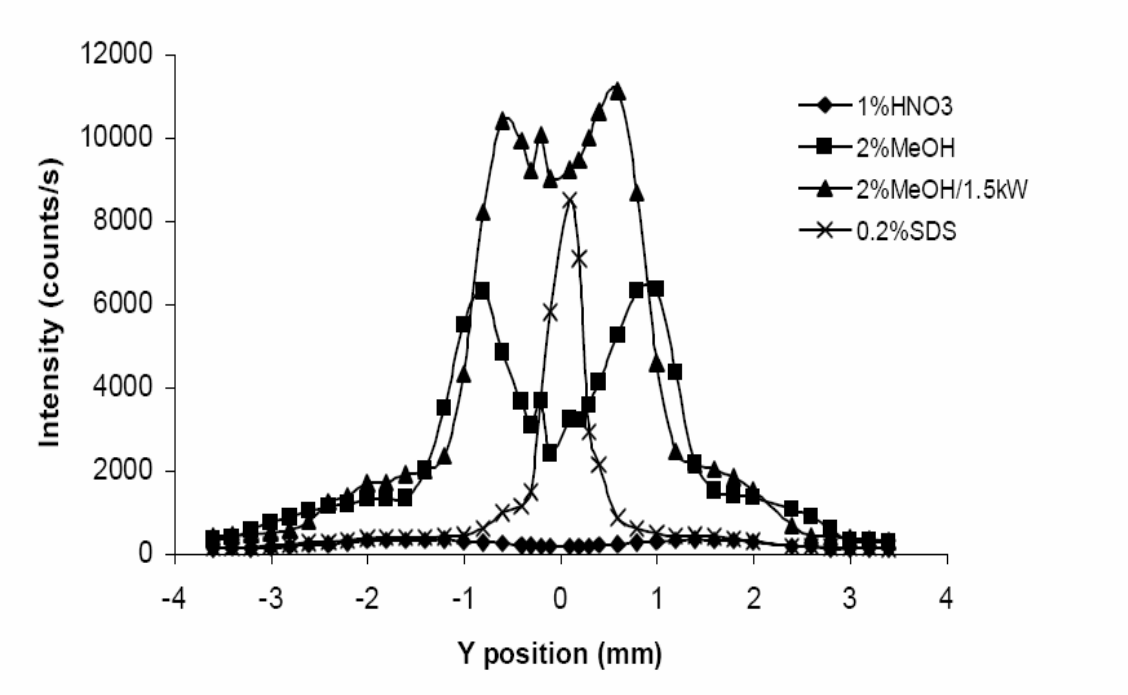

Figure 3.9 Radial profile of m/z 28 (CO^+) distribution in the ICP with different matrices (similar profiles were observed for ArC^+) matrices: 1% HNO_3; 1% HNO_3 and 0.2% m/v SDS; 1% HNO_3 and 2% v/v MeOH; 1% HNO_3 and 2% v/v MeOH at 1.5 kW.

In fact, the ArC^+ signal in the central channel increased by over an order of magnitude with either 0.2% m/v SDS or 2% v/v MeOH, as shown in Figure 3.10. However, the 0.2% m/v SDS had little effect on the $^{36}Ar^+$ signal, whereas 2% v/v MeOH concurrently suppressed it by almost an order of magnitude. This provides clear evidence that more Ar^+ was used up in presence of MeOH than was consumed to form ArC^+, which supports a charge-transfer mechanism between and C. Ar^+ can then transfer its charge to analytes that possess an IP lower than that of C (i.e. 11.26 eV), such as As (9.82eV), Se (9.75eV), Zn (9.39eV), and Sb (8.64eV), and that are partially

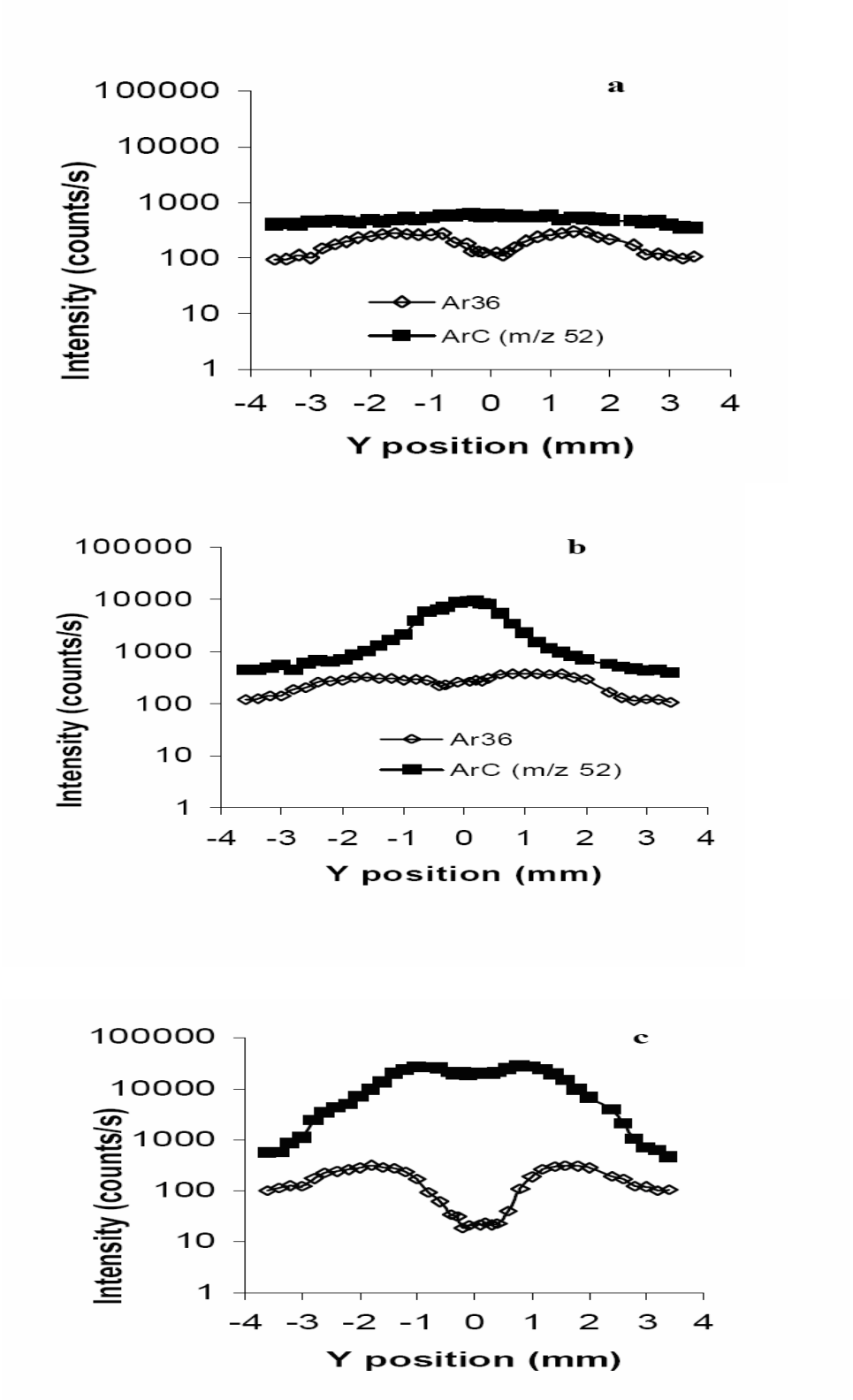

Figure 3.10 Radial profiles of ArC^+ (m/z 52) and $^{36}Ar^+$ in different matrices: (a) 1% HNO_3; (b) 1% HNO_3 and 0.2% m/v SDS; (c) 1% HNO_3 and 2% v/v MeOH.

ionised under normal plasma operating conditions [92, 93,151]. This effect, which was increasingly counteracted by the radial spread of analyte as their mass decreased, explains why an enhancement was only observed for As, Sb and Pb with 2% MeOH at 1.5 kW (Figure 3.3b). The profiles (Figures 3.8-3.10) suggest that when the matrix contains an organic solvent such as methanol, methanol is preferentially desolvated from aerosol droplets because of its lower boiling point (BP), evaporated, and spread around the central channel where the plasma temperature is higher than in the central channel.

Additional experiments with other organic solvents (acetone, BP 56°C and ethylene glycol, BP 198°C) were carried out. The radial profiles of the analytes in the 1% HNO_3 matrix also containing 2% v/v acetone became very wide, with a well in the middle for most of them, except for La and Pb (see Figure 3.11 for example). In contrast, with 2% of ethylene glycol in 1% HNO_3, little increase resulted in the peak width of the analytes radial profiles. Figure 3.12 summarises the FWHM of the radial profiles of all analytes in these different matrices. These results confirmed the effect of solvent volatility on the width of the radial profile: the lower the BP of the solvent, the wider the radial peak became, with a larger well in the middle (i.e. in the central channel), which was more important for analytes with lower mass.

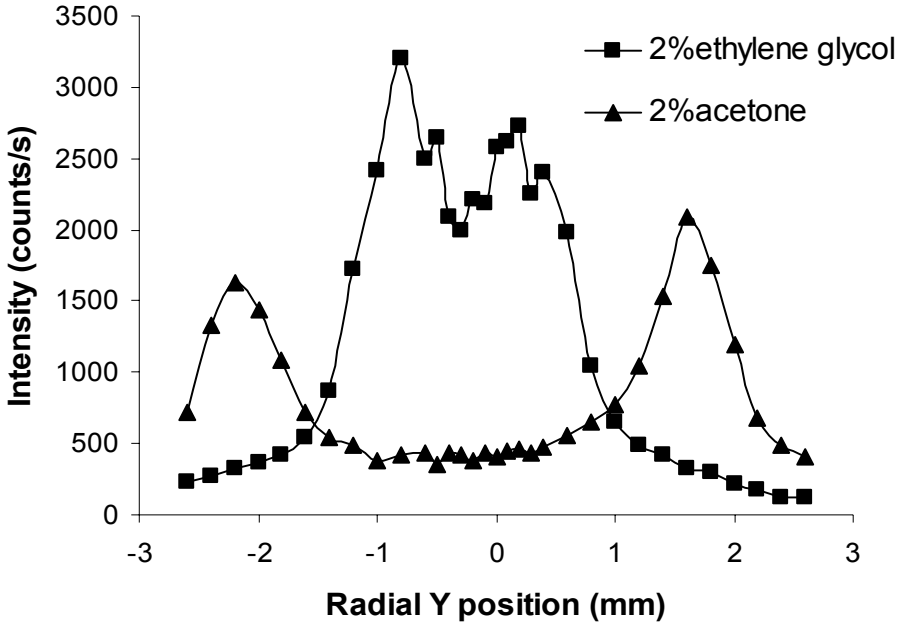

Figure 3.11 The radial profile of As^+ distribution in the ICP with different matrices: 1% HNO_3 and 2% v/v acetone; 1% HNO_3 and 2% v/v ethylene glycol.

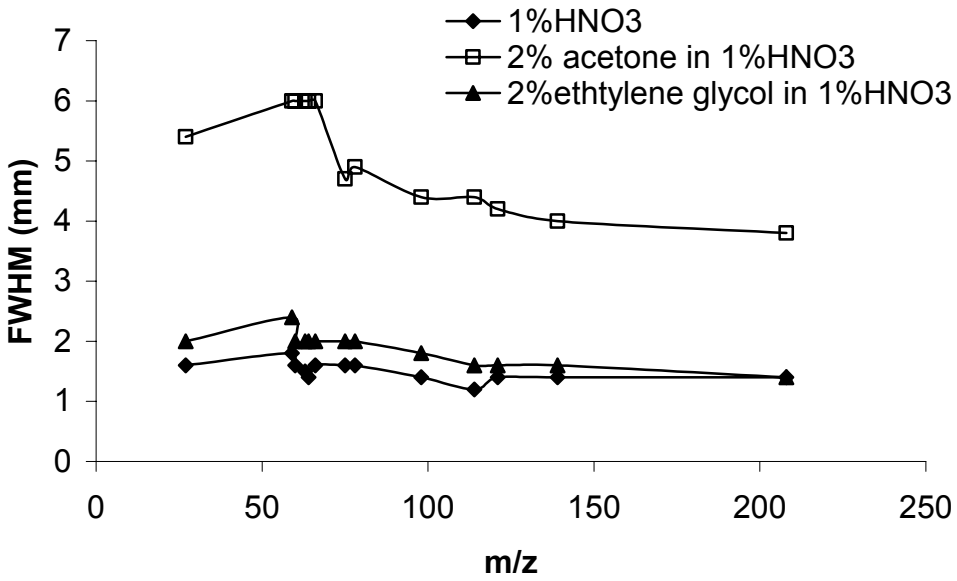

Figure 3.12 Full width at half maximum of the radial profiles of the analytes as a function of m/z for each of the matrices: 1% HNO_3; 1% HNO_3 and 2% v/v acetone; 1% HNO_3 and 2% v/v ethylene glycol.

On the other hand, the introduction of organic compounds (both organic solvents and surfactant) reduced the level of LaO^+ as a result of the scavenging of oxygen by carbon to form CO^+ [99], as can be seen in Figure 3.13. Although the carbon concentration in 0.2% m/v SDS was an order of magnitude lower than that with 2% v/v MeOH, it reduced the oxide level more. Only when the power was increased to 1.5 kW did an even larger decrease in LaO^+ result with 2% v/v MeOH.

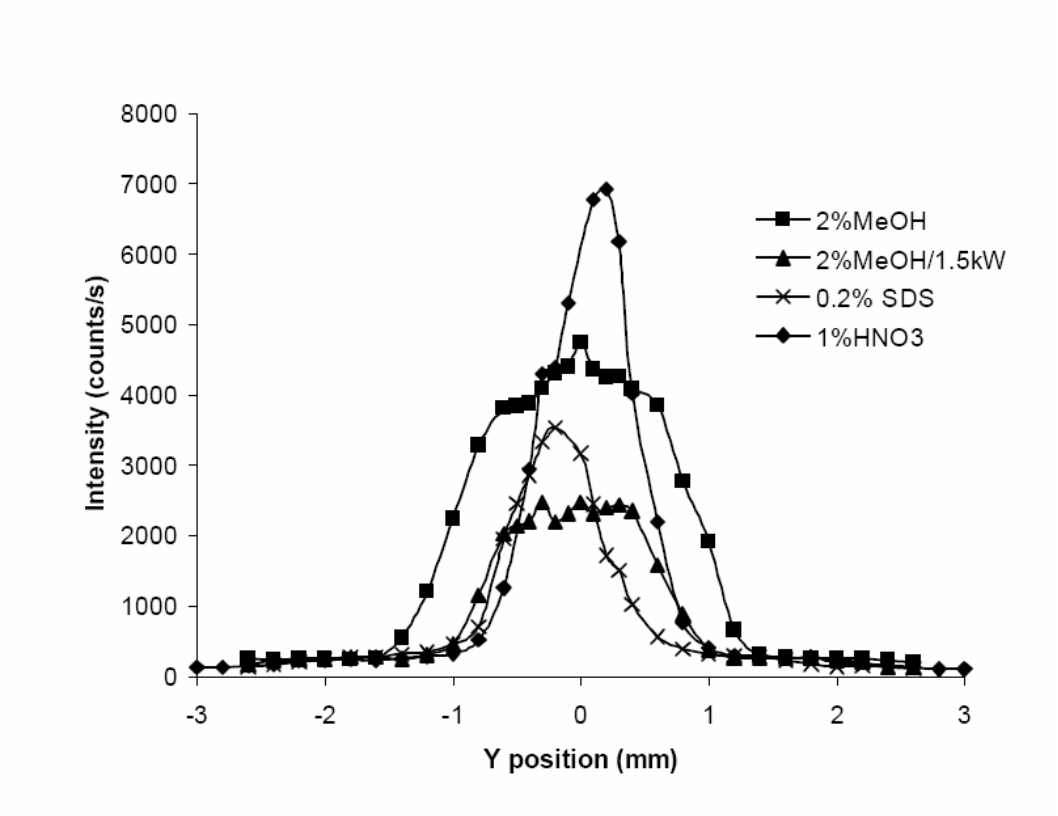

Figure 3.13 The effect of different matrices on the signal of LaO^+: 1% HNO_3; 1% HNO_3 and 0.2% m/v SDS; 1% HNO_3 and 2% v/v MeOH; 1% HNO_3 and 2% v/v MeOH at 1.5 kW.

Higher RF power was needed to compensate for the local cooling effect and the ionisation of carbon species when an organic solvent was introduced into the plasma (Table 3.2). Alternatively, a longer residence time in the plasma might have also been allowed since, as can be seen in Figure 3.14, the optimum axial Z position increased in presence of MeOH. However, the optimum Z position (also RF power, Table 3.2) did not change much for 0.2% SDS, in comparison with that for 1% HNO_3. The above results indicate that the carbon charge-transfer mechanism only happened in presence of an organic solvent (such as MeOH) but not in presence of SDS.

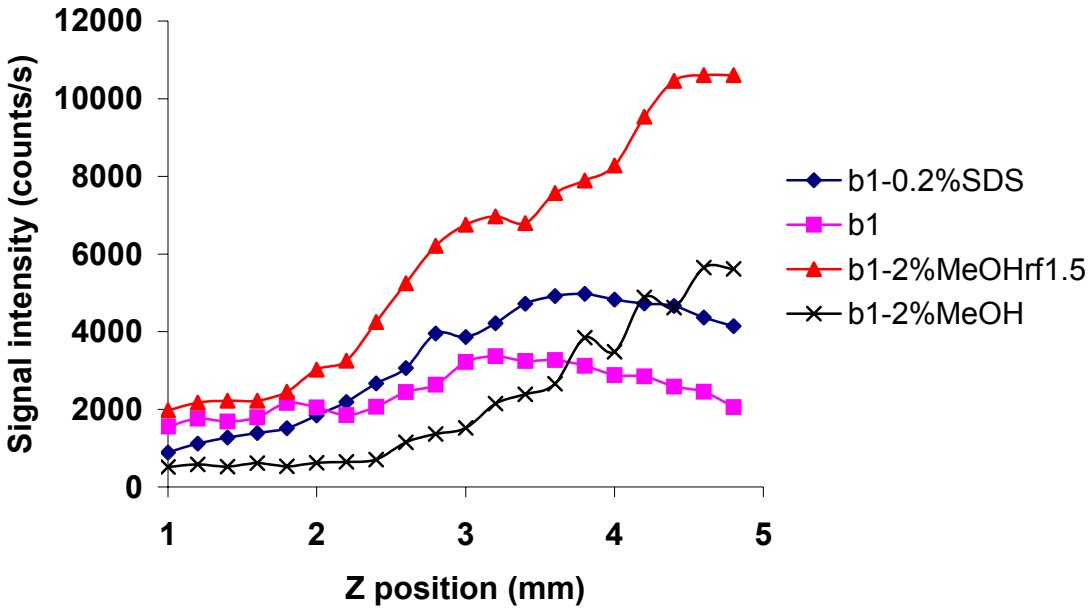

Figure 3.14 The axial profile of As^+ in: 1) 1% HNO_3 (b1); 2) 2% MeOH in 1% HNO_3 at RF power 1.35 kW and 1.5 kW; 3) 0.2% SDS in 1% HNO_3

3.6 Summary

The matrix effects caused by organic compounds and the possible mechanisms involved were investigated by radial profiling the distribution of analytes and background ions in the plasma. The addition of different organic compounds to 1% HNO_3 caused different matrix effects, which arose from different mechanisms. The negative charge of the ionic SDS (0.2% m/v) preferentially attracted lighter cations, resulting in an increase in analyte transport efficiency that was inversely dependent on mass. Although 0.2% SDS had no significant effect on the plasma itself, the addition of 2% v/v MeOH induced a widening of the radial distribution of both analytes and polyatomic background ions because of a spread of MeOH in the plasma, which carried along ions. A suppression of analyte signal was therefore observed, which was inversely dependent on mass, because lighter ions diffuse more rapidly than heavy mass analytes. A change in the analyte ions radial distribution from bell-shaped to bimodal also resulted from an addition of 2% v/v MeOH, which then matched those of carbon-containing polyatomic ions. This observation in combination with the fact that Ar^+ was simultaneously suppressed in the central channel, increases the significance of charge transfer with C^+ as an ionisation mechanism in the plasma. In any case, a study of the combined effect of SDS and MeOH is warranted, as it could lead to analyte signal enhancement across the mass range. This chapter further demonstrated that spatial profiling of both analytes and

background ions distribution in the plasma is an efficient way of investigating matrix effects.

Chapter 4 The effect of pre-evaporation on ion distributions in inductively coupled plasma mass spectrometry

With a conventional sample introduction system consisting of a pneumatic nebulizer and a spray chamber, only about 2% of the sample reaches the plasma, which limits sensitivity. Thus, alternative sample introduction systems have been developed, such as the DIN [26] or an USN with desolvator [22, 18], which both greatly increase the sample introduction efficiency and, hence, sensitivity. However, they also concurrently exacerbate matrix effects since more matrix then reaches the plasma (which is additionally preconcentrated when a desolvator is used). In fact, the complete removal of water is not advisable as the presence of a small amount of water vapour may improve sensitivity as well as the stability of the analyte signal [141].

A pre-evaporation interface was first implemented by Peter and Beauchemin in an old Perkin-Elmer/SCIEX quadrupole-based ICP-MS instrument [143]. They then reported that the compromise nebulizer gas flow rate was optimal for a greater number of elements with a pre-evaporation interface than without it, which would be quite advantageous for multielemental analysis. However, only changes in signal as a function of nebuliser gas flow rate were reported i.e. the resulting profiles may not correspond to the actual axial ion distribution in the plasma, as a change in nebulizer gas flow rate may also change the sample introduction efficiency. In order to truly assess the effect of the pre-

evaporation interface, spatial profiles of analytes and background ions distribution in the plasma should be obtained under constant nebulizer gas flow rate. Furthermore, the Leco Renaissance ICP-TOFMS instrument that was used in this thesis is completely different from the quadrupole one from the previous study [143].

Thus, the main objective of this chapter was to test several pre-evaporation tubes of different sizes on the Leco ICP-TOFMS instrument to determine which would best improve the sensitivity and detection limits for different analytes, and would therefore warrant further investigation and application. To this end, spatial profiling (both axial and radial profiling) of analytes and background ions distribution in the presence and absence of a pre-evaporation tube was carried out while keeping the nebulizer gas flow rate constant.

The research described in this chapter was published in Volume 61 of Spectrochimica Acta Part B, as “The effect of pre-evaporation on ion distribution in inductively coupled plasma mass spectrometry” (2006).

4.1 Axial profiles of analytes ions

Fourteen analyte elements in the m/z range of 27 (Al) to 208 (Pb) and with a first IP from 5.58 eV (La) to 9.81 eV (As) were selected. In each case, the most abundant isotope was monitored, except for Se: $^{27}Al^{+}$, $^{51}V^{+}$, $^{52}Cr^{+}$, $^{58}Ni^{+}$,

$^{60}Ni^{+}$, $^{63}Cu^{+}$, $^{55}Mn^{+}$, $^{66}Zn^{+}$, $^{75}As^{+}$, $^{78}Se^{+}$, $^{98}Mo^{+}$, $^{114}Cd^{+}$, $^{121}Sb^{+}$, $^{139}La^{+}$, $^{208}Pb^{+}$. Arsenic, $^{75}As^{+}$, was used as a representative analyte for graphing spatial profiles.

Axial profiling can provide information about the energy and time needed to form ions [120]. When an unheated tube (5-mm i.d. and 11-cm long, or 2-mm i.d. and 11- or 22-cm long) replaced the plastic connection tube inside the torch box, the axial profile remained unchanged compared to that obtained in the standard configuration as can be seen in Figure 4.1. Similarly, inserting a 11- or 22-cm extension tube outside the torch box had no significant effect on the analyte axial profile (not shown) (see the set-up diagram in Figure 2.5).

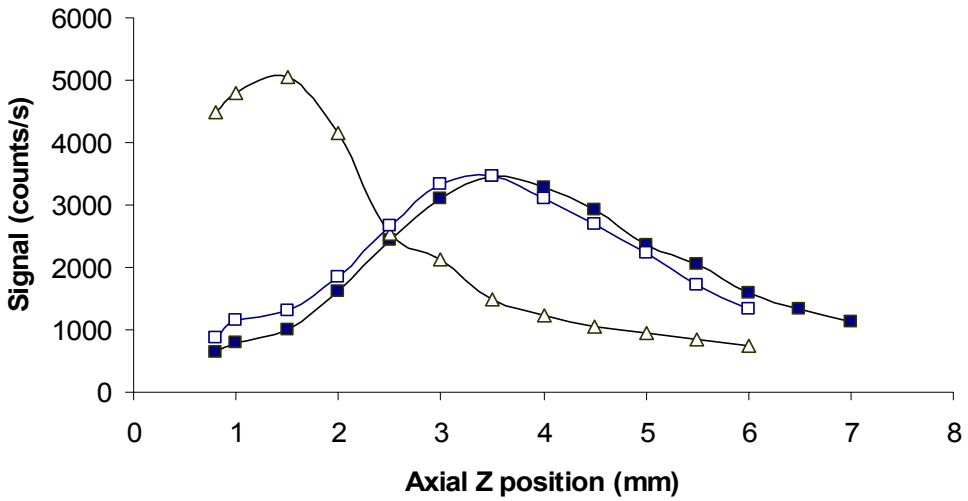

Figure 4.1 Axial profiles observed for $^{75}As^{+}$ with a heated tube (open triangles), in the standard configuration (open squares) or with an unheated tube (black squares).

The optimal Z position for each analyte had some dependence on the mass of the analyte (Figure 4.2). For instance, the optimal axial position of the heaviest analytes was significantly closer (by up to 2 mm) to the load coil than that of the lightest analytes monitored, whether a heated tube was used or not. This mass dependence may come from the velocity of heavier analytes being lower than that of lighter analytes with the same kinetic energy ($E = 1/2mv^2$) in the plasma. Hence, their optimum sampling depth would be smaller (i.e. lower in the plasma) compared to that of lighter mass analytes. This mass dependence was not observed in previously published axial profiles because the plasma operating conditions had not been set so as to see a peak within the Z-translation range [85]. On the other hand, a dependence of the optimal nebulizer gas flow rate on analyte mass was reported previously and attributed to mass transport effects [152].

Upon heating the tube to 400 °C (which resulted in the temperature inside the tube rising to 330 °C), the optimal axial positions of all 14 analytes moved closer to the load coil (illustrated by As in Figure 4.1) by, on average, 1.5–2.0 mm. Furthermore, as can be seen in Figure 4.2, the compromise axial position of 3.5 mm for multi-elemental analysis without the heated tube was optimal for 6 analytes. However, with the heated tube, this position became 1.5 mm, which was then optimal for 9 of the 14 analytes i.e., a single Z sampling position (1.5 mm) was optimal for a greater number of elements than any single position selected without the extension. Clearly, the plasma

energy preserved by pre-evaporating the solvent resulted in a shift of the sequential processes of desolvation, vaporisation, atomization and ionisation, which then occurred lower in the plasma and over a narrower region.

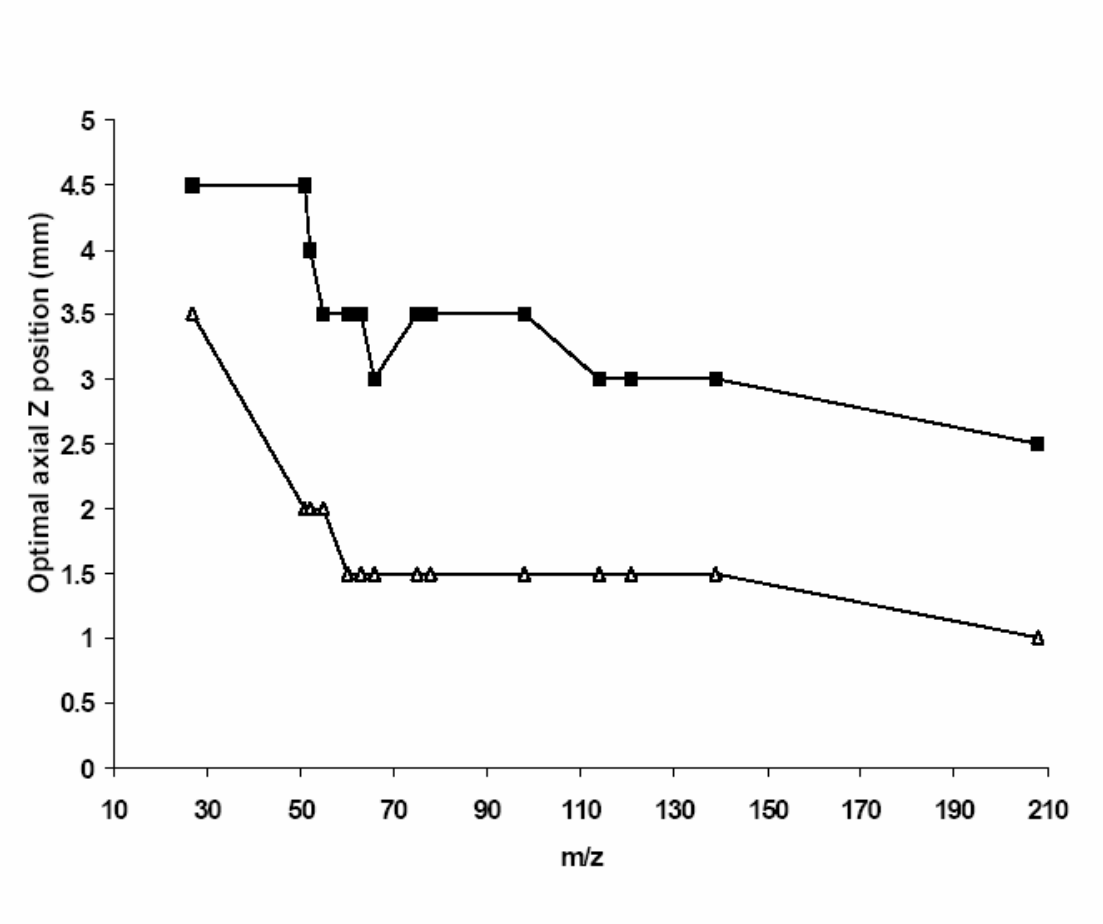

Figure 4.2 Effect of the heated pre-evaporation tube on the optimal axial position: without it or with unheated tube (black squares); with heated tube (open triangles)

When a heated extension tube (11 or 22 cm) was located outside the torch box, the compromised axial Z position for multielemental analysis moved closer to the sampler cone (Figure 4.3), similarly to when the heated tube was placed inside the torch box. However, no enhancement of the analytes signals resulted, which remained similar (with the 11-cm tube) or even slightly

decreased (with the 22-cm tube) compared to those observed without heating. The optimum Z position with heating was also 2 mm (as opposed to 1.5 mm when the heated tube was in the torch box). This is likely a result of some cooling or condensation of aerosol in the connection tube between the extension and the torch.

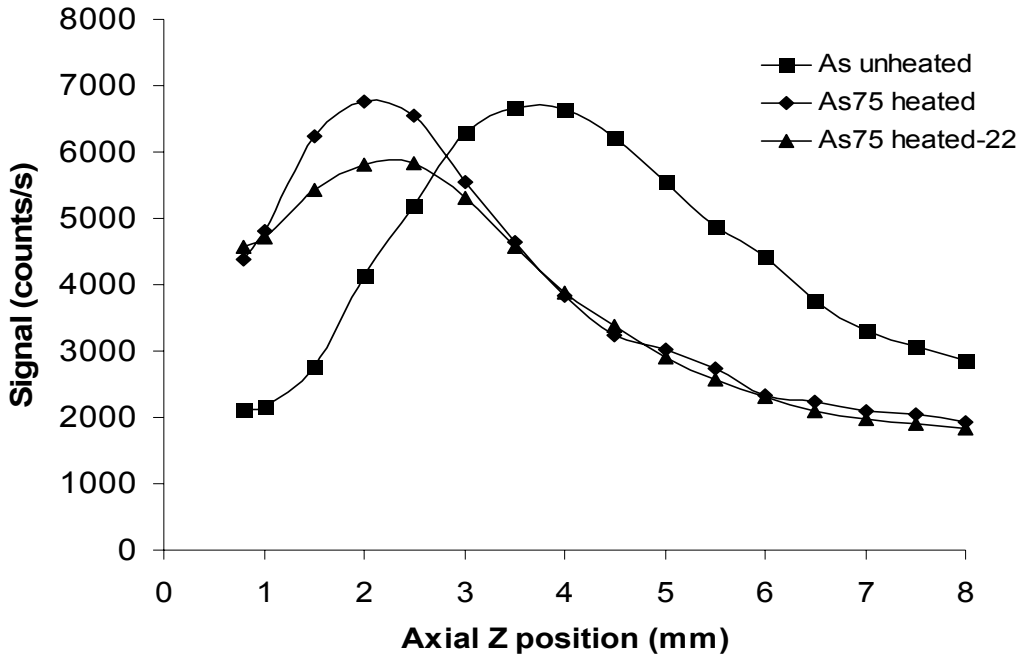

Figure 4.3 Axial profile of As^+ with: the standard configuration (without pre-evaporation tube, black squares), a 11-cm pre-evaporation tube (black diamond) or 22-cm pre-evaporation tube outside the torch box (black triangles)

Presumably because of a cooling effect in the connection tube when the heated tube was outside the torch box, no enhancement of the analyte signal intensity was observed. A 3-min washout with 1% HNO_3 was used when changing solutions and, especially, when switching from unheated to heated tube. As a result, the remainder of the work in this thesis was done with the

pre-evaporation tube located inside the torch box. For the measurement of radial profiles, sensitivities and detection limits, the sampling position was therefore kept at 3.5 mm for the standard configuration (or with an unheated tube replacing the connection tube) and at 1.5 mm with a heated tube inside the torch box. The axial profile obtained with the standard configuration was identical to that observed with an unheated glass tube replacing the plastic connection tube inside the torch box.

4.2 Radial profiles of analytes ions

Insertion of a heated tube (either inside or outside the torch box) resulted in a narrowing of the radial profile for all 14 analytes, which became more Gaussian than that observed without heating. It should be noted that the radial profiles obtained with an unheated 5-mm i.d. tube replacing the plastic connection tubing in the torch box were identical to those observed with the latter (i.e., in the standard configuration). However, in addition to becoming narrower, the profiles also generally became taller upon heating the pre-evaporation tube, as illustrated in Figure 4.4a. No such systematic increase in profile height (compared to that seen without the heated tube) was observed when the same heated tube was placed outside the torch box (Figure 4.4b), which is likely because of loss of analyte by condensation in the connecting tube between the extension and the torch. Similar observations were made with either a 2-mm or 5-mm i.d. tube. Nonetheless, the fact that the radial profiles of all analytes became narrower and more Gaussian indicates that the

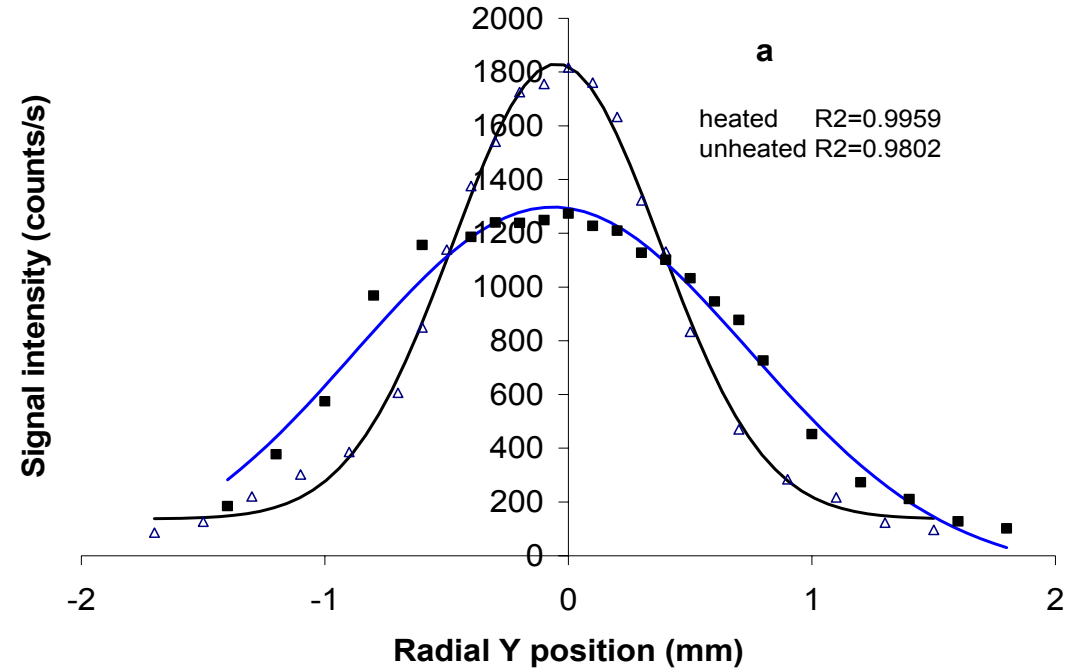

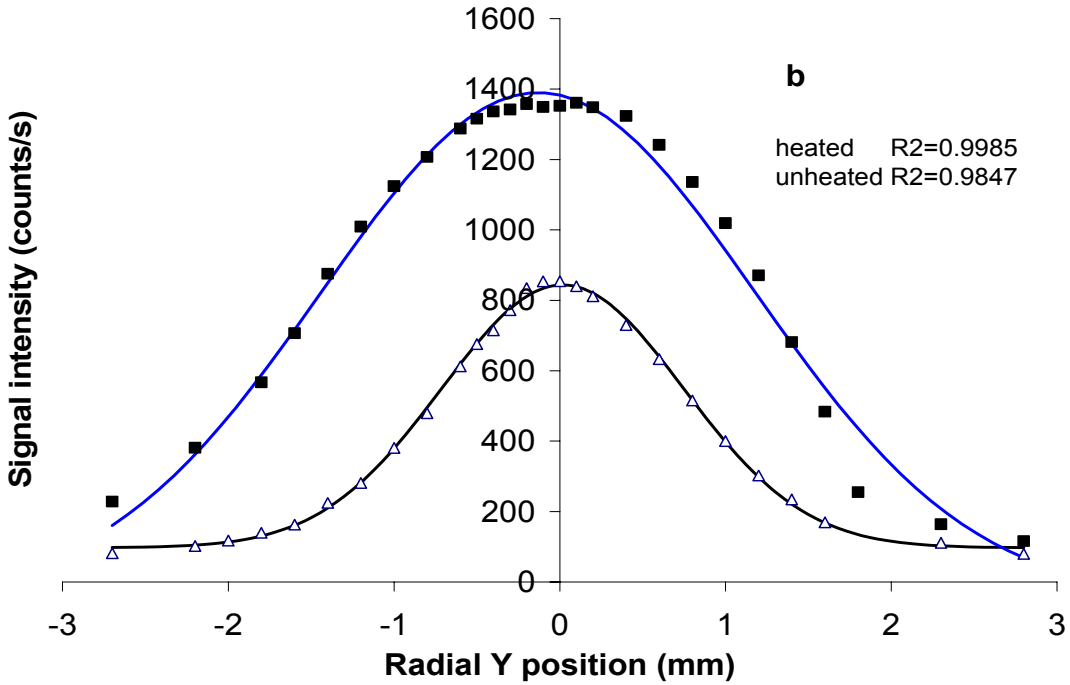

Figure 4.4 Radial profiles observed for $^{75}As^{+}$ with heated (open triangles) and unheated (black squares) pre-evaporation tube placed a) inside the torch box, b) outside the torch box, fitted to Gaussian distribution curves, with the corresponding correlation coefficients

pre-evaporation interface affects the ion distribution profiles and the signal intensity.

Although replacement of the plastic connection tube with an unheated 5-mm i.d. tube had no effect on the radial profile, using an unheated 2-mm i.d. tube instead resulted in a narrowing of the radial profile (Figure 4.5) since its dimension is narrower than that of the torch inlet and the nebulizer outlet (5 mm). Upon heating either tube, however, profiles with the same narrowed FWHM were obtained as can be seen in Figure 4.5. This narrowing is likely linked to the lower sampling depth that is used with the heated tube, i.e., the analytes have less time to diffuse between the time they reach the plasma and when they traverse the sampler cone. Lateral diffusion would also be minimized by the increased gas volume, and hence flow rate through the torch injector tube, resulting from heating the aerosol. Although a fair amount of cooling was previously observed to occur over the length of the torch [143], the aerosol exiting the injector tube would be at a higher temperature than without a pre-evaporation tube, which would increase its flow rate. In any case, using a 2-mm i.d. tube did not result in additional narrowing of the radial profile compared to that observed when heating a 5-mm i.d. tube. This may be a result of some turbulence that might be present at the joints (even if the tube was gradually tapered to 2-mm i.d. from the 5-mm i.d. joints over a 1-cm length), which could also not be covered with heating tape.

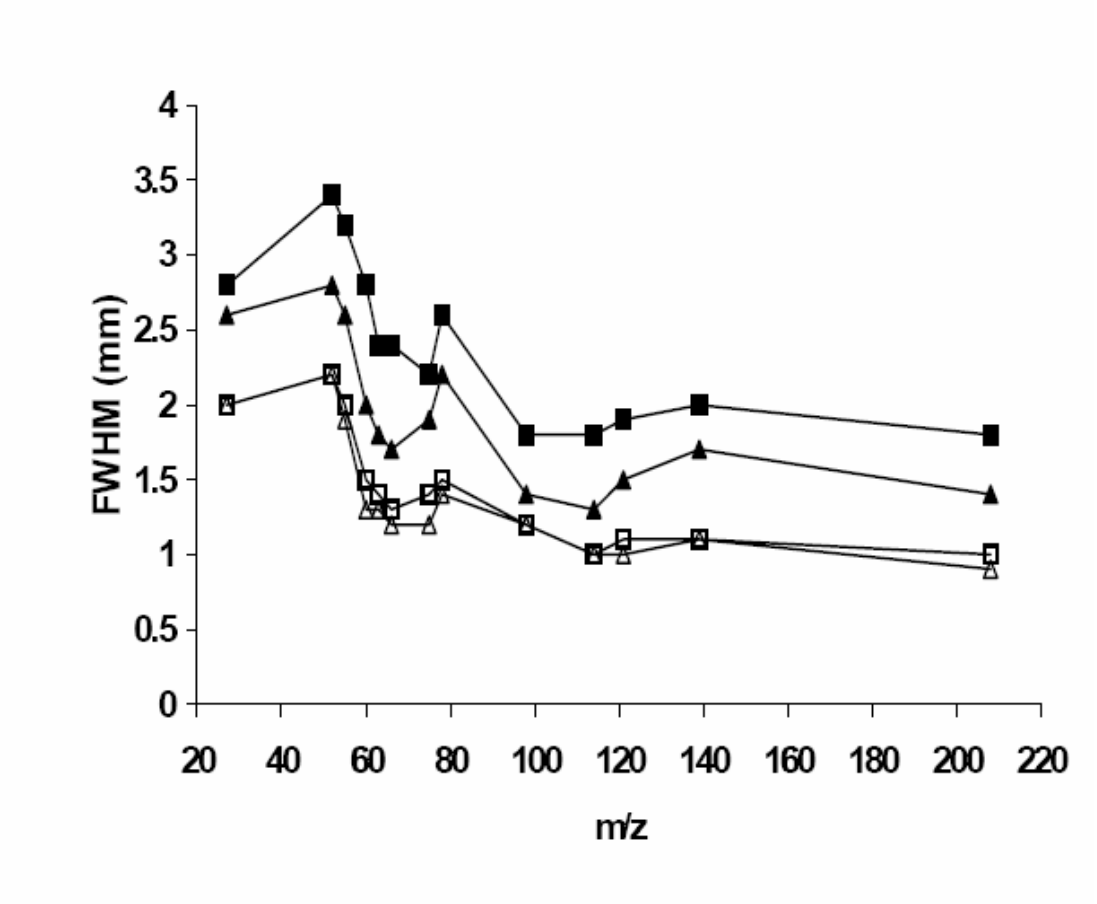

Figure 4.5 Full width at half maximum of the radial profiles observed for various analytes with a 5-mm i.d. (squares) and 2-mm i.d. (triangles) tube inside the torch box, which was heated (open symbols) or not (full symbols).

On the other hand, Figure 4.5 shows that, whether the instrument was used in its standard configuration or with an unheated or heated tube, the peak width was dependent on the analyte m/z, with the low-mass analyte having a peak width that was about twice that of Pb. Although this apparent dependence on mass may be a spurious effect of the compromise sampling depth that was used in each case, the fact that heating did not affect this trend suggests that it originates downstream of the ICP i.e., within the mass spectrometer or its interface. In fact, a very similar trend was observed on a quadrupole-based

ICPMS instrument (UltraMass 700 from Varian) in its standard configuration [144]. In both cases, analytes with a similar or higher mass than that of the optimisation element (In for the Renaissance; Rh with the UltraMass) had bell-shaped distributions whereas lower mass elements had a flatter distribution in the middle of their radial profile (as can be seen for As in Figure 4.4). The aerosol flow through the tube is turbulent [153]

4.3 Blanks, sensitivity and detection limits

Two 11-cm tubes (2-mm and 5-mm i.d.) were used to replace the connection tube inside the torch box for the sensitivity and detection limits comparison. Figure 4.6 shows that, in several elements (Cr, Cu, La, Se, Mn, V), a loss of sensitivity resulted when the 2-mm i.d. tube was inserted. In contrast, sensitivity was either similar (La, Mn) or improved by a factor of up to 2 (for the majority of elements) when a 5-mm i.d. heated tube was inserted (Figure 4.7). Although an increased heating efficiency might have been expected with the narrower tube, the greater velocity and shorter residence time of the aerosol in the heated region evidently compensated it. Furthermore, some turbulence might also be present at the joints even if the tube was gradually tapered to 2-mm i.d. from the 5-mm i.d. joints, over a 1-cm length. Moreover, these tapered regions could not be covered with heating tape. In any case, the increase in sensitivity with the 5-mm i.d. heated tube resulted from it at least partially evaporating the solvent prior to its entry in the plasma. Hence, it preserved the plasma energy that would have otherwise been consumed for

this step, which was then available for subsequent processes, including analyte ionisation.

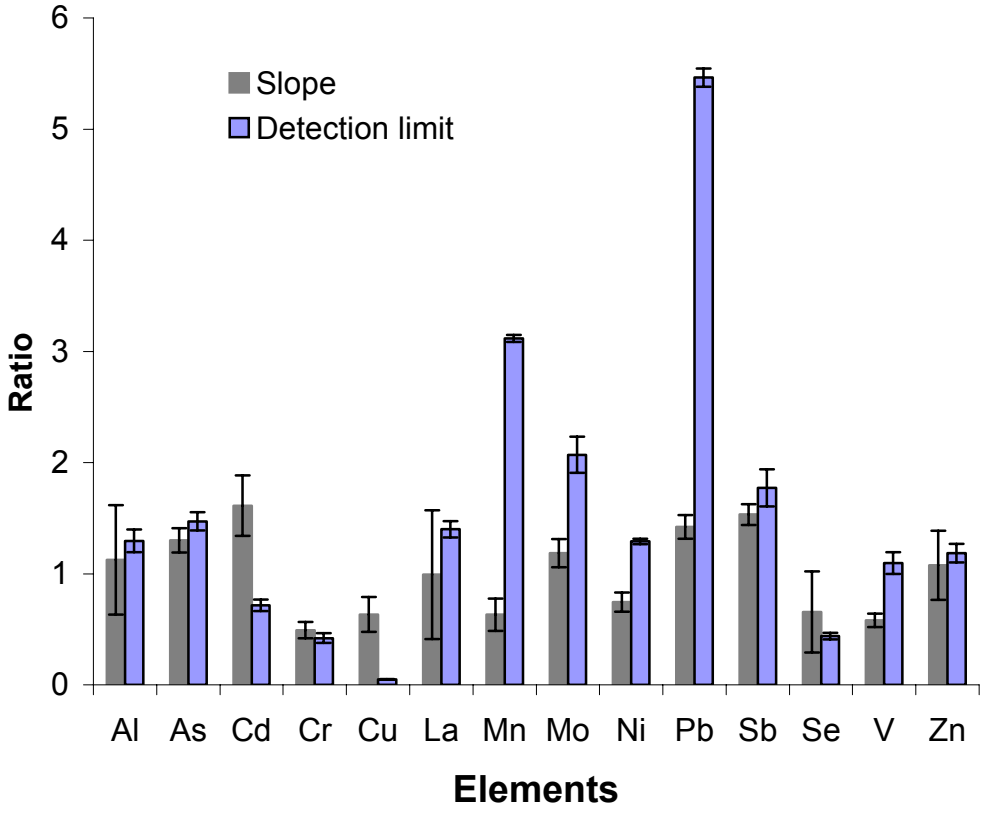

Figure 4.6 Comparison of sensitivity (heated/unheated) and detection limits (unheated/heated) for 14 analytes (2-mm heated tube inside the torch box).

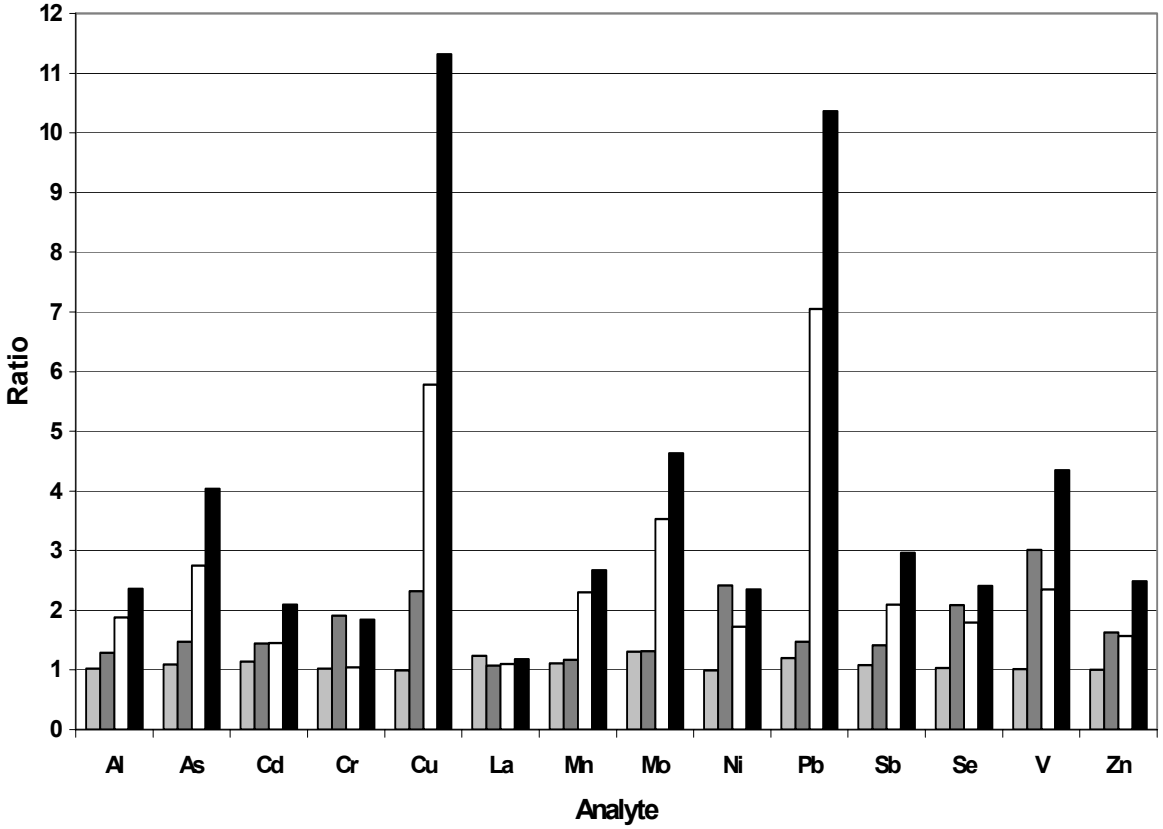

Figure 4.7 Effect of heating a 5-mm i.d. pre-evaporation tube: ratio of blank signals (heated/unheated tube) (light grey bars); ratio of sensitivities (heated/unheated tube) (dark grey bars); ratio of standard deviations of the blank signals (unheated /heated tube) (white bars); ratio of detection limits (unheated/heated tube) (black bars). A ratio greater than unity indicates an increase in blank signal and sensitivity, but a decrease in standard deviation of the blank and detection limit upon heating the tube.

Since the detection limits depend on background noise and sensitivity, and that the background noise should decrease as a result of the smaller droplets entering the plasma when the pre-evaporation tube is present, the improvement in detection limit should be greater than the corresponding one in sensitivity. This was in general true, even with the 2-mm i.d. extension tube

where a degradation of detection limit was observed for fewer elements (Figure 4.6) than the degradation in sensitivity.

Figure 4.7 shows the effect of heating the 5-mm i.d. tube on blank signals, sensitivities, standard deviation of the blanks and detection limits. Although the blank signals were not much affected by heating, their corresponding standard deviations decreased significantly for 9 of the 14 elements (as confirmed by F test at the 95% confidence level [154]) as a result of the smaller droplets entering the plasma when the pre-evaporation tube was present. Fig. 4.7 also shows an increase in sensitivity, which a Student's t-test at the 95% confidence level [154] revealed to be significant for all elements but Mn (where the standard deviation is large presumably as a result of the deflection of m/z 56). Since the detection limits depend on background noise and sensitivity, and that the background noise decreased, the improvement in detection limit was in general greater than the corresponding one in sensitivity. In any case, no correlation could be made between the improvement in sensitivity or detection limit and the first ionisation potential of the analyte. Therefore, using a pre-evaporation tube did not significantly save plasma energy as one might have expected (otherwise, the greatest improvement would have been observed for elements with a high first ionization potential). Evidently, the heated tube mainly reduced noise in the blank through a reduction in the size of aerosol droplets entering the plasma.

The above results show that both pre-evaporation tubes preserved plasma energy by decreasing droplet size distribution when the tubes were inside the torch box. The 5-mm i.d. tube resulted in a better improvement of sensitivity and detection limits. Furthermore, since 5 mm is the i.d. of the regular tube connecting the spray chamber to the torch, which matches the i.d. of the torch inlet, which prevents turbulence at the joints, the remainder of this work therefore focused on the changes observed upon heating a 5-mm i.d. tube.

4.4 Analyte oxide and doubly charged ions

Inserting a pre-evaporation tube has previously been reported to decrease the oxide level of oxide-forming elements [143]. This observation was reproduced in this work, as can be seen in Figure 4.8a. In fact, this improvement seems to result from a shift in the oxide ratio to lower depth in the plasma. The increase in oxide ratio at lower depth (that was observed with or without a heated tube), which is also indicative of freedom from a secondary discharge, was observed on both an UltraMass 700 [116] and an ELAN 500 [155]. The shift of the profile to lower depth indicates that oxides are formed lower in the plasma and have more time to be dissociated when pre-evaporation occurs than without it. A similar shift in the doubly charged ion ratio was observed, which in turn lead to an increase in ratio at high depth (Figure 4.8b). However, since all the measurements were made at lower depth, this shift was of no consequence. This is further illustrated in Figure 4.9 where a decrease in oxide ratio and negligible change in doubly charged ion ratio is evident in the

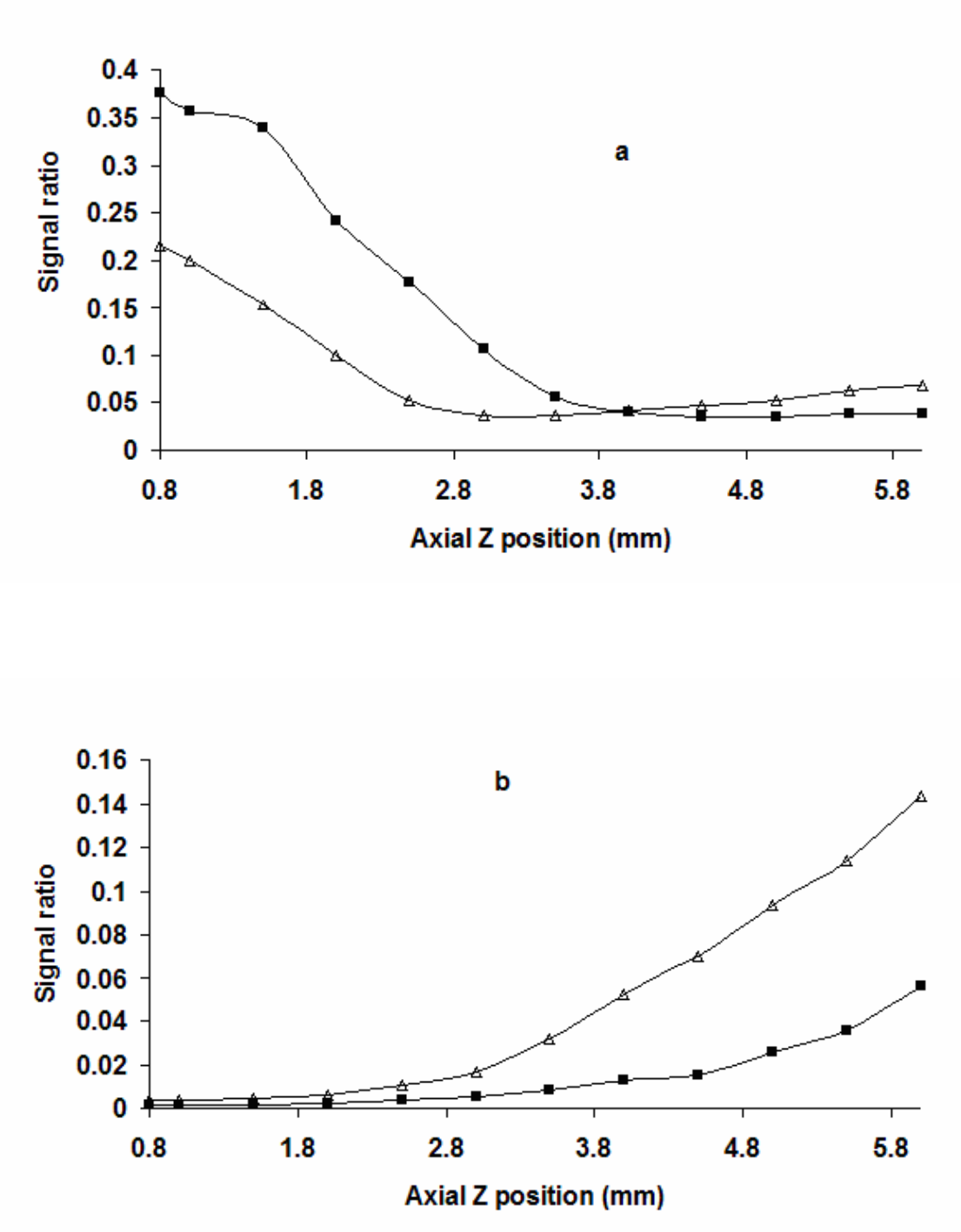

Figure 4.8 Axial profiles observed for a) La oxide ratio (i.e. $LaO^+/[LaO^+ + La^+ + La^{2+}]$) and b) doubly charged ratio (i.e. $La^{2+}/[LaO^+ + La^+ + La^{2+}]$) with a heated (open triangles) and unheated (full squares) 5-mm tube inside torch box.

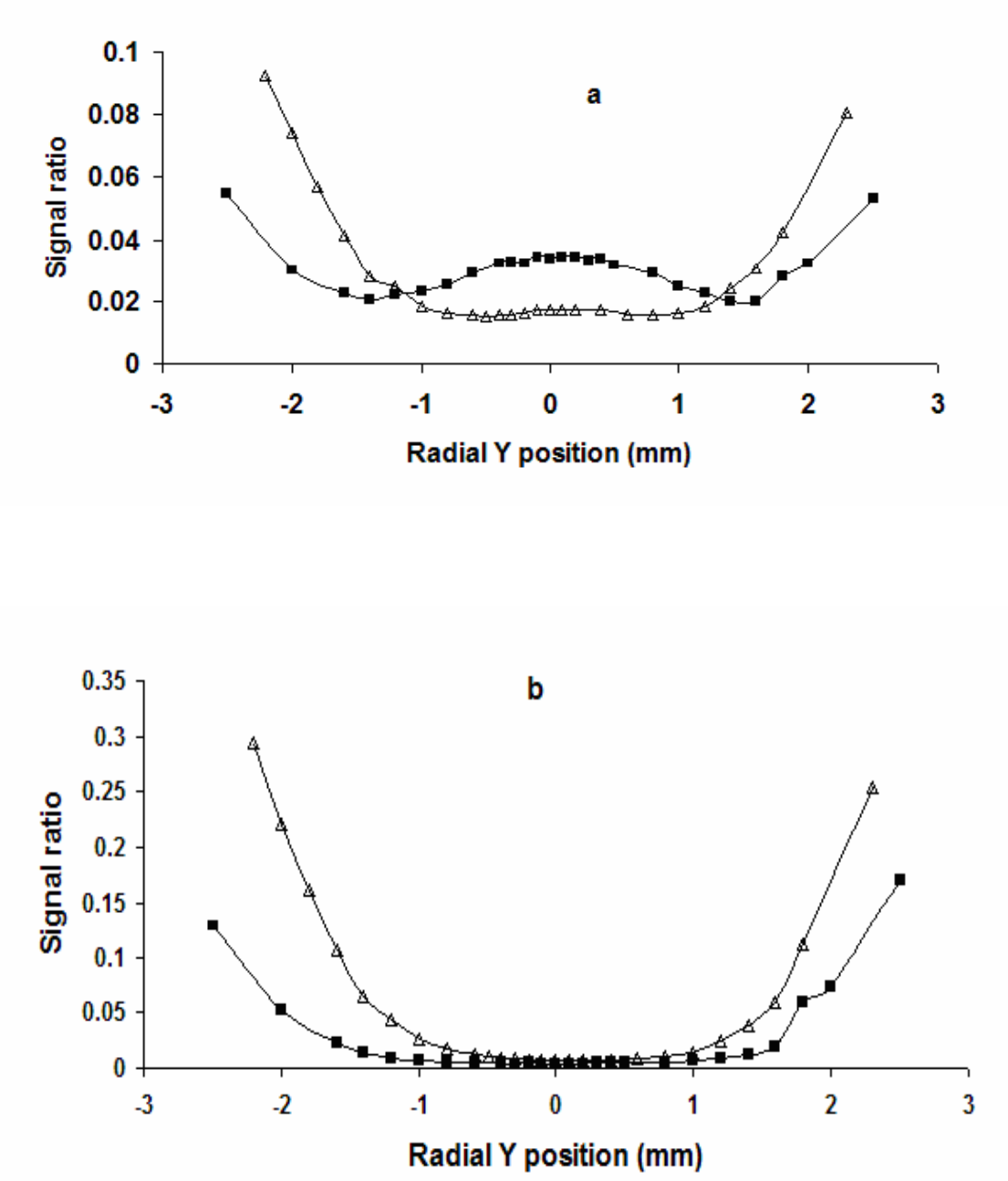

Figure 4.9 Radial profiles observed for a) La oxide ratio (i.e., LaO^+ /[LaO^++ La^++La^{2+}]) and b) doubly charged ratio (i.e., La^{2+} /[LaO^++La^++La^{2+}]) with a heated (open triangles) and unheated (full squares) 5-mm tube inside torch box.

centre of the plasma at a 1.5-mm sampling position. This figure also shows a narrowing of the profile upon heating the tube, which may indicate a shrinkage of the central channel of the ICP.

Table 4.1 Temperature inside and outside the heated tube

Outside tube temp.(ºC)	Inside tube temp.(ºC) with different nebulizer gas flow rates			
Neb. Gas flow rate (L/min)	0.85	0.87	0.90	0.95
400	332	332	332	330
380	292	292	292	292
330	273	272	272	271
300	243	242	242	242
250	201	202	202	202
200	163	163	163	163
150	123	123	121	120
100	77	77	77	76

4.5 Temperature inside the heated tube

The temperature inside the heated tube is very important since it directly influences the aerosol droplet size. However, it can not be measured when the plasma is on due to physical constraints. Therefore, it was measured without igniting the plasma, by inserting a probe inside the tube without touching its inner wall. Another probe placed outside the tube, as described in chapter 2, measured the temperature on its outside surface. The nebulizer gas flow rate was adjusted to the same value as when the plasma was on.

The resulting temperatures are reported in Table 4.1 over the range of nebulizer gas flow rate that was used. A small change in nebulizer gas flow rate had an insignificant effect on the temperature inside the tube, which was stable and high enough (330 °C) to pre-evaporate water and even the nitric acid-water azeotrope (BP: 122 °C) when the outside temperature reached 400 °C.

4.6 Summary

The effect of several pre-evaporation tubes (11- and 22-cm long, 2- and 5-mm i.d.) placed either outside or inside the torch box was studied in this chapter. Pre-evaporation using a 5-mm i.d., 11-cm long heated glass tube instead of the plastic connection tubing that is currently used inside the torch box of the Renaissance instrument was the best for improving multi-elemental sensitivity and detection limits. This pre-evaporation tube changed the ions distribution in the plasma, where radial profiles of analytes became narrower and more Gaussian. Furthermore, the analyte oxide ratio decreased while the doubly charged analyte ratio remained unchanged at the axial position used for multi-elemental analysis, which was truly optimal for a greater number of elements. Moreover, slightly improved sensitivity and detection limits resulted across the mass range. Since similar results were obtained with other torches and spray chambers as well as on a quadrupole-based instrument [143], this simple approach should be beneficial to all ICPMS instruments.

Chapter 5 Effect of concomitant analytes on the As signal during pre-evaporation of the solvent

As discussed in Chapter 1, ICP-MS is an extremely sensitive and powerful technique for multielemental analysis [8]. However, the broad droplet size distribution of the aqueous aerosol, which results from the nebulisation process, increases the noise level of the signal, including of the background signal, while water itself decreases both the ionization temperature and electron density of the ICP. The complete removal of water using a desolvation system is not advisable as the presence of a small amount of water vapor may improve sensitivity as well as the stability of the analyte signal [141]. Little change was observed on the ICP ionization temperature and electron density when water was introduced in vapour form that suggests that it interacts differently with the plasma than a water aerosol [142].

Chapter 4 showed that the pre-evaporation tube pre-vaporized at least part of the aerosol prior to its introduction into the plasma. Both sensitivity and detection limits for multielemental analysis were improved as this pre-evaporation tube decreased the average droplet size of the aerosol entering the plasma, hence reducing noise [156, 143]. However, it did not significantly change the plasma ionisation temperature since the greatest improvement was not systematically observed for elements with a high first IP such as As, which should be more susceptible to these effects since they are not

completely ionised in the ICP. Anything affecting the ionisation temperature and electron density of the latter should change their degree of ionisation and, hence, the sensitivity of ICP-MS for these analytes.

Organic solvents [89, 92] and surfactants [91,157] can be used to improve the sensitivity of high IP elements, as was shown in Chapter 3 [89-92,157]. However, the situation is often complicated by matrix effects from the carbon that is concurrently introduced in the plasma, as well as from changes in the nebulisation and sample transportation processes. For example, the amount and droplet size distribution of the aerosol exiting the spray chamber and solvent vapour loading, which are affected by the volatility of the solvent, influenced analyte signal [111]. Chapter 3 also showed that different organic solvents and surfactants could affect differently the predominant mechanism of ionisation in the plasma.

Alternative nebulisation techniques, such as direct injection nebulisation and thermospray nebulisation, can also be used to improve sensitivity [16]. However, they do so through an increase in nebulisation efficiency, which exacerbates matrix effects since more matrix then also reaches the plasma. In contrast to thermospray, which changes a liquid solution into an aerosol through direct heating of the solution, the pre-evaporation interface, which is inserted between the spray chamber and the torch, does not change the sample introduction efficiency (i.e. does not increase the amount of aerosol

going into the plasma). Instead, it only heats the aerosol exiting the spray chamber and evaporates the solvent. The temperature inside the heated extension tube (i.e. 272 ˚C when the external tube temperature was 330 ˚C; see Table 4.1 in chapter 4) is indeed high enough to evaporate water. The aerosol reaching the plasma then has an even smaller droplet size distribution as a result of this solvent pre-evaporation.

Another aerosol reducing phenomenon that may also occur is Coulomb fission that is an important mechanism in electrospray ionisation (ESI). In ESI, an electric field (3-6 kV) is applied between a capillary through which a solution flows at 1-10 μL/min and the entrance to a mass spectrometer. This field induces a charge accumulation on the liquid surface at the end of the capillary, which then breaks to form charged droplets. These charged droplets then pass through a heated inert gas curtain (N_2), or through a heated capillary to remove the solvent, which further shrinks the droplets and thus increases their charge density, hence causing further Coulomb fission events.

Droplets produced by nebulisation can be expected to have a net random statistical charge from fluctuations in ion density in the bulk solution [158], as well as a net charge depending on the matrix and its concentration [114, 158]. The shrinkage of the droplets that should occur as they pass through the pre-evaporation tube would increase their charge density and hence induce

Coulomb fission events that would further reduce their size. This is schematically represented in Figure 5.1

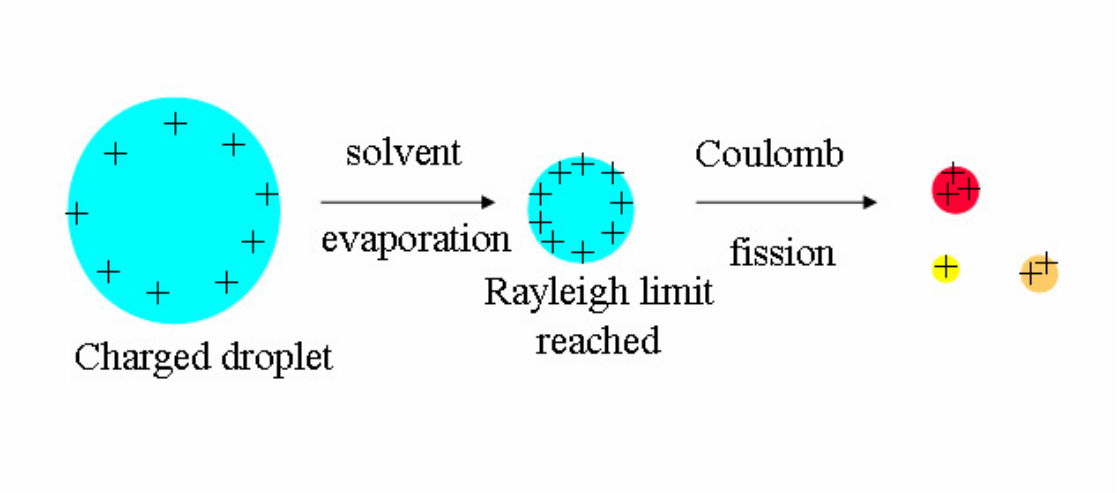

Figure 5.1 Coulomb fission event promoted by solvent pre-evaporation in the heated tube

Thus, as the droplet size decreases, the frequency of Coulomb fission events may increase, which can further decrease the size of the droplets entering the plasma and, hence, decrease noise, resulting in a further improvement in detection limits. Conversely, Coulomb fission is dependent on the matrix. For instance, Xu et al. [114] reported that a higher ionic strength matrix increased the abundance of small droplets in the aerosol going to plasma because of Coulomb fission events during the desolvation occurring through the spray chamber, which ultimately enhanced the analyte signal.

The signal enhancement observed for a multielemental solution in Chapter 4 was consistent with the above effects of pre-evaporation. However, while applying the pre-evaporation interface to the speciation analysis of As by HPLC-ICP-MS i.e., with a monoelemental As solution, a suppression of the As signal was observed. This is despite the fact that, as demonstrated in Chapter 6, a baseline separation of four major arsenic species was achieved by ion chromatography with a gradient of 0.00625 M to 0.025 M ammonium nitrate, the mobile phase caused insignificant matrix effects compared to 1% HNO_3. This thus prompted an investigation into this apparent contradictory behaviour, as the pre-evaporation would be expected to increase the frequency of Coulomb fission events, thereby reducing the droplet size distribution of the aerosol and thus enhancing sensitivity.

Therefore, the objective of this chapter was to further investigate by axial profiling how the pre-evaporation interface affects different analyte signals, with the ultimate goal of elucidating the unexpected As signal suppression mentioned above. This work was published in Spectrochimica Acta Part B as “Effect of concomitant analytes on As signal during pre-evaporation of the solvent prior to introduction into inductively coupled plasma mass spectrometry” (2006).

5.1 Comparison of analyte signals from mono- and multi-elemental solutions in 1% HNO_3

As described in chapter 4, to ensure that spatial profiling would be representative of the ions distribution in the ICP, the extent of secondary discharge was assessed, with and without the pre-evaporation tube. Continuous monitoring of LaO^+ was thus done while the aerosol carrier gas flow rate was increased, as the concurrent increase in solvent load to the plasma should exacerbate any secondary discharge [1], which would, in turn, decrease the level of oxides and increased that of doubly charged ions [146]. In fact, since the LaO^+ level increased and La^{2+} decreased, especially low in the plasma (see section 4.4), the torch configuration on this instrument minimised the secondary discharge, which was unaffected by the pre-evaporation tube. Hence, spatial profiling of the ICP should represent the distribution of ions in the ICP [116].

A reproducible axial profile of As^+ from a 20-μg/L multi-element solution (also containing Al, V, Cr, Mn, Ni, Cu, Zn, Se, Mo, Cd, Sb, La, Pb) in 1% HNO_3 is shown in Figure 5.2a. A signal enhancement ratio (heated/unheated) of 1.55 was obtained by taking the ratio of the maximum signal observed in each condition (i.e. at the optimal axial Z position for As in each case). This is similar to the previously observed enhancement ratio of 1.47 [156] for the same multielemental solution, although the latter ratio was observed with an

inner tube temperature of 330 instead of 270-272°C and corresponds to the As signal ratio at compromise sampling positions for multi-elemental analysis.

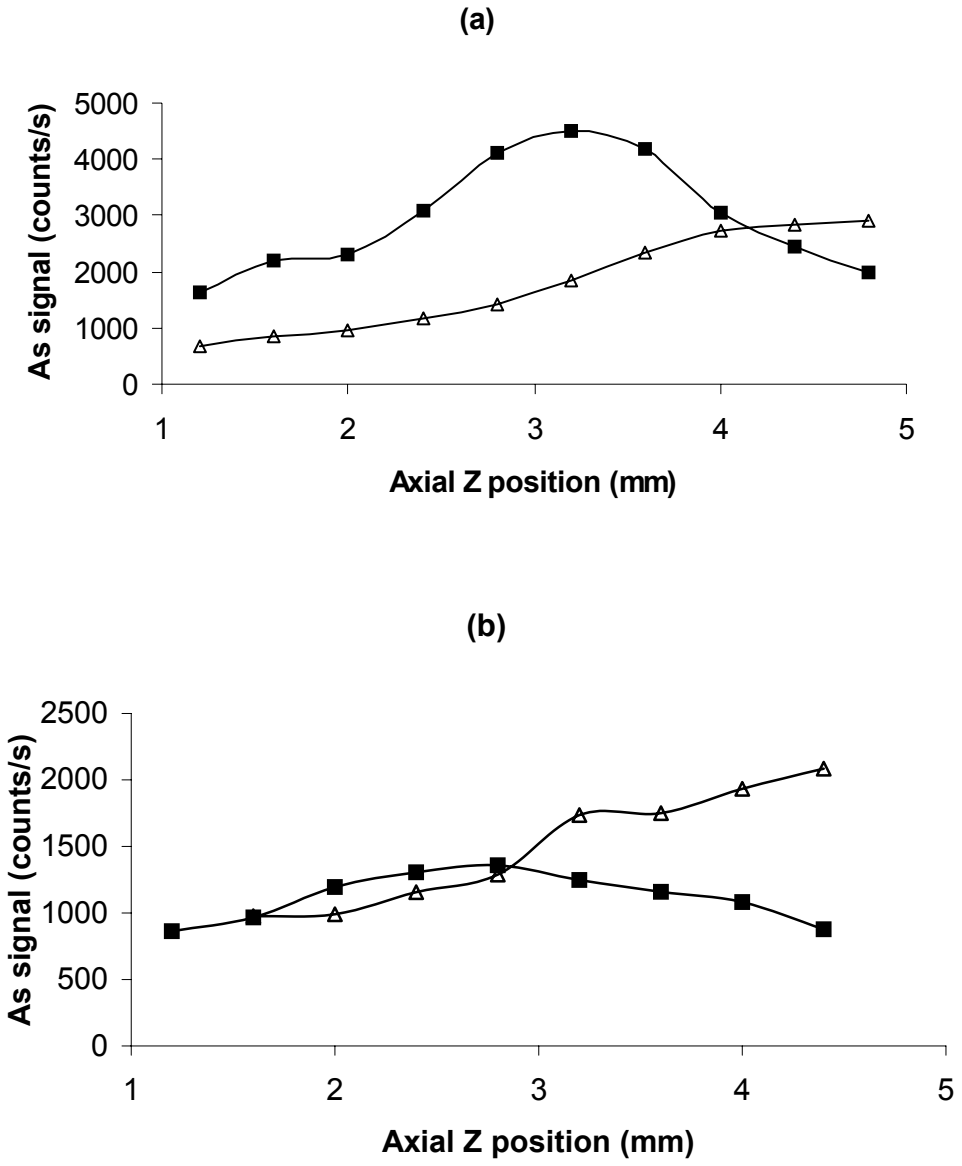

Figure 5.2 Axial profile of As in 1% HNO_3 with unheated (open triangles) and heated (full squares) tube using a) 20-μg/L multielemental solution (containing Al, V, Cr, Ni, Cu, Mn, As, La, Mo, Sb, Cd, Pb, Zn, Se, and b) 20 μg/L As solution

In contrast, the axial profile of a 20-μg/L mono-elemental As solution also in 1% HNO_3 showed a signal suppression (Figure 5.2b) upon heating the pre-evaporation tube. Similar observations were made for Se (Figure 5.3), with signal intensity ratios (heated/unheated) of 0.65 and 0.67 for As and Se respectively, in mono-elemental solutions. This difference between the optimal signal intensity from equi-concentrated multi-elemental and mono-elemental solutions in 1% HNO_3 was only observed for As and Se upon heating the pre-evaporation tube i.e. no such difference was observed with an unheated tube. Furthermore, no such suppression was observed for all the other analytes in the multi-elemental solution upon switching to a mono-elemental solution, as can be seen in Figure 5.4, where the optimal signal with the heated tube is similar or enhanced compared to that observed without heating it.

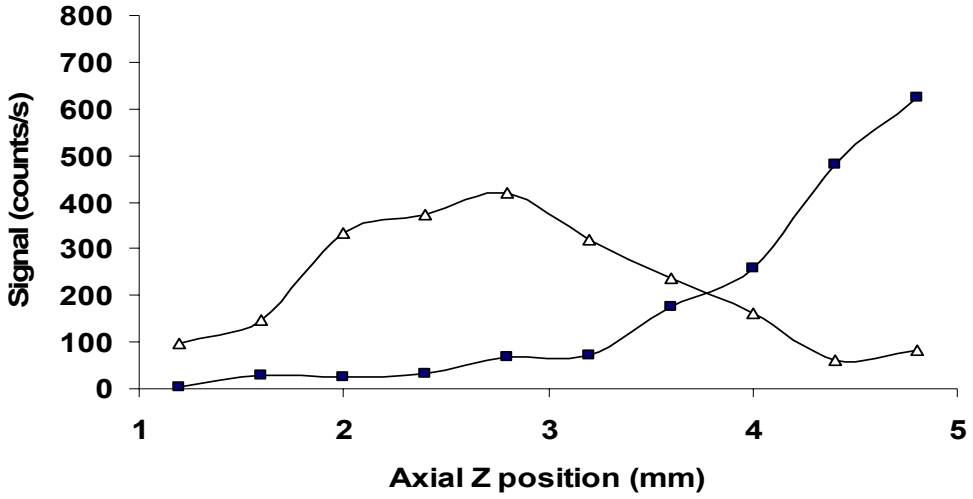

Figure 5.3 Axial profile of $^{78}Se^{+}$ in 1% HNO_3 with unheated (full squares) and heated (open triangles) tube using a 20 μg/L Se solution

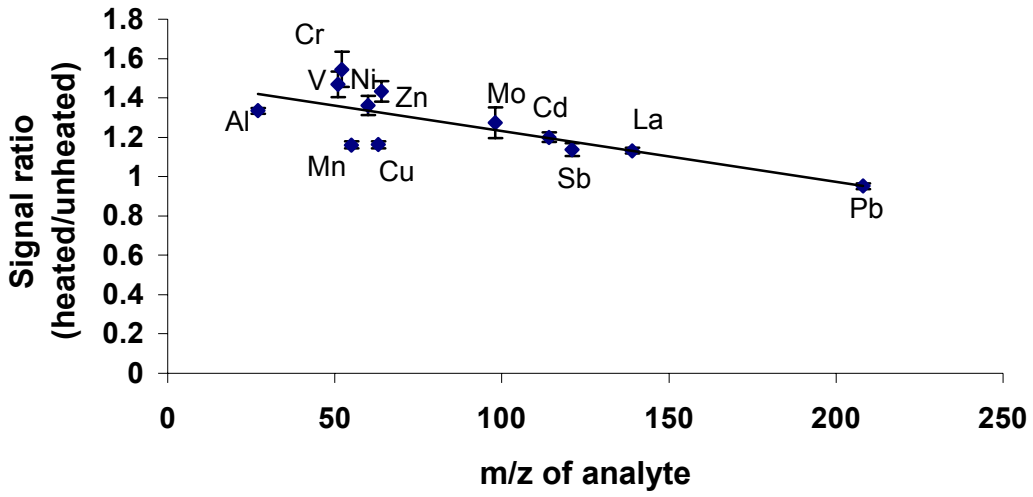

Figure 5.4 Ratio of the optimal signal observed with heated and unheated tube for 20 μg/L monoelemental solutions of various analytes as a function of the mass of these analytes with error bar. A trend line was added to illustrate an apparent mass-related effect (n=3).

5.2 Investigation of Coulomb fission as a possible explanation for signal enhancement

For a given matrix, the probability that a given droplet will undergo Coulomb fission increases as its radius decreases (which is promoted in the heated tube by pre-evaporation of solvent) [114] and as its charge density increases. This means that for droplets containing different analytes but the same number of water molecules, a Coulomb fission event would be most likely for the droplet containing the smallest ionic analyte with the highest number of charge (as its charge density would be greatest) and less likely for a larger ionic analyte. (It would, in fact, be the least likely for a neutral analyte).

Therefore, in the case of a multielemental solution, the signal of a light mass analyte would be expected to improve more than that of an equally charged heavy mass analyte upon heating the tube. This explanation is consistent with the trend with mass in Figure 5.4, which is linear from Mo to Pb ((R^2=0.96). It also helps to rationalise signal enhancement for analytes that would be expected to be completely ionised in the ICP. Indeed, a greater proportion of small droplets (as a result of evaporation and Coulomb fission) that result in ions in the ICP is then simply being introduced.

However, in Figure 5.4, the concentration of each analyte was 20 μg/L, which corresponds to a range of molar concentration for analytes of different mass, i.e. from 740 nM Al to 97 nM Pb, which might affect the extent of Coulomb fission if the solvent is completely evaporated. To verify that the inversely mass dependent trend of signal enhancement (showed in Figure 5.4) was not an artefact of having an unequal molar concentration of each analyte, the study was repeated with a 300-nM equi-molar solution of each analyte in 1% HNO_3. The results shown in Figure 5.5 are very similar to those in Figure 5.4, i.e. signal enhancement remains inversely dependent on analyte mass. This supports the Coulomb fission theory, whereby an increase in Coulomb fission frequency is expected upon heating the pre-evaporation tube, especially for light analytes.

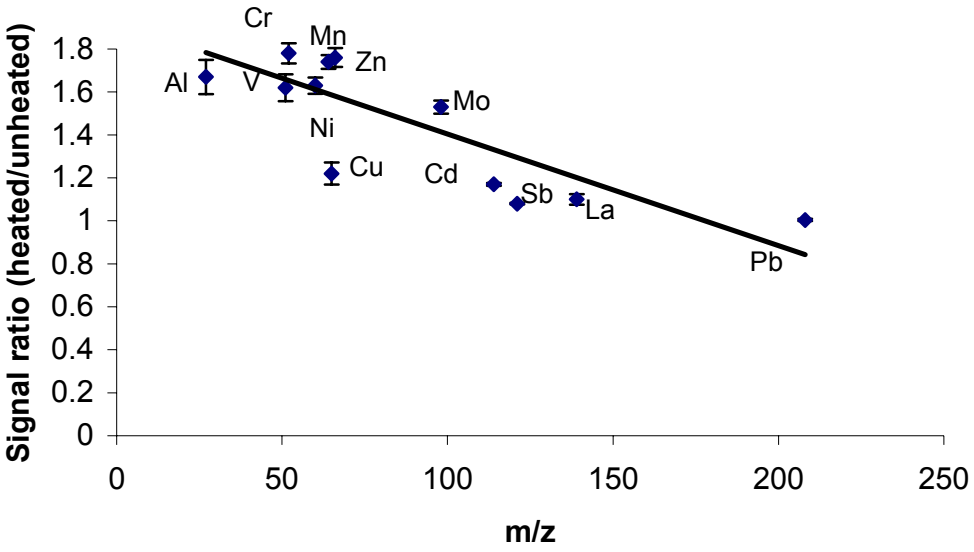

Figure 5.5 Ratio of the optimal signal observed with heated and unheated tube for 300 nM monoelemental solutions of various analytes as a function of the mass of these analytes. A trend line was added to illustrate an apparent mass-related effect (n=3).

Another possibility is that the heated tube may boil the neutral droplets and shatter them into smaller progeny droplets (which are neutral as well), i.e. a process that is reminiscent of the Coulomb fission process. However, although the temperature in the tube is 272ºC, the residence time of the droplets in the heated extension is only about 0.14 s, which is unlikely sufficient to induce such a boiling effect. Furthermore, such effect would affect the signals from all analytes similarly, in contrast to what is observed. A physical carrier effect, such as that observed with ETV can also be ruled out. Such effects are observed when a large excess of a physical carrier is added to the sample (such as µg amounts of carrier for ng of analytes) [159]. Similar effects have also been observed in desolvation systems under similar

conditions (i.e. with a large excess of carrier) [160]. If concomitant analytes could act as carriers then there would be no need for the addition of physical carriers to multielemental sample solutions during their analysis by ETV-ICP-MS. Yet, such addition is in fact essential for quantitative multielemental analysis using aqueous external calibration [159].

Similarly, aerosol ionic re-distribution (AIR) [161] cannot explain this mass-dependent enhancement. It can only explain a general enhancement in presence of a 50-200 fold excess of concomitant element. AIR can occur when the matrix causes an enrichment of the analyte on the surface of large droplets, which upon fragmentation create small analyte-enriched droplets that, in turn, result in an enhancement of analyte signal in the ICP [160].

The operating conditions of the heated interface are vastly different from those in typical desolvation systems. In the latter, the aerosol typically spends several seconds in the heating portion of the apparatus, which is typically held at 140ºC [160], and the vapour is then condensed out so that a dry aerosol reaches the ICP. In the heated interface, not only does the aerosol reside only 0.14 s in the tube that is held at 272 ºC, but the vapour is not removed i.e. the aerosol reaching the plasma is not completely dry. Under these conditions, only some evaporation of the solvent is expected since the BP of the nitric acid–water azeotrope is 122ºC, which is the lowest of all the components (nitrates, oxides, etc.) in solution. For example,

evaporation of 10-μm water droplets has been calculated to occur within several ms, as they are heated from 7 to 1200ºC [162]. Given the slightly higher BP of the HNO_3/H_2O azeotrope, the higher starting temperature of the droplets (20ºC), the lower final temperature (270ºC), and the polydispersity of the aerosol droplet distribution, 0.14 s would be expected to be sufficient to evaporate the solvent.

At room temperature, the ionic strength of the sample solution, which will determine the extent of Coulomb fission events, is dominated by the matrix (1% v/v HNO_3 or 0.15 M) as it is in much higher concentration than the analytes (20 μg/L i.e. 97 nM (for Pb) to 740 nM (for Al)). This explains why there was no difference in signal (for all analytes, including As) between multielemental and monoelemental solutions with an unheated tube. However, as the solvent evaporated upon heating, the contribution from concomitant analytes to the ionic strength eventually became significant and dominated the Coulomb fission events (Figures 5.4 and 5.5).

Evaporation alone cannot explain these results, as As and Se should then be enhanced similarly. Furthermore, vaporisation of As and Se is unlikely as their BP is higher than that of many of the other analytes (such as the nitrates of Cr, La, Mn, Ni, etc.) i.e. those would also be vaporised. Moreover, if premature evaporation of As and Se induced their signal suppression, then this should be evident in their radial profile, which should then become wider

upon heating the tube. However, the peak width of the radial profile originating from a mono-elemental As solution in 1% HNO_3 became narrower and more Gaussian (Figure 5.6), at the optimum Z positions for the heated and unheated tube. This is consistent with the results obtained from a multi-elemental solution in the same matrix [156 or chapter 3]. However, an As signal enhancement was concurrently observed in the latter case, whereas As (as well Se) signal suppression resulted from heating the tube when a mono-elemental solution was used.

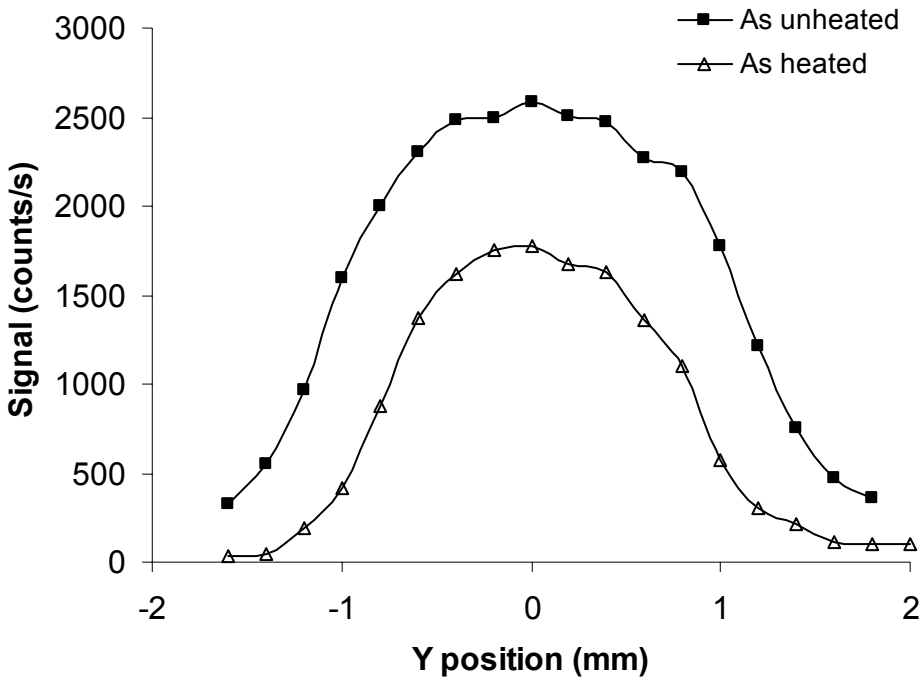

Figure 5.6 Radial profile of As from a mono-elemental solution in 1% HNO_3 with a heated or unheated tube (ratio 0.685)

Space-charge effects [48] and ambipolar diffusion [107] have been proposed to explain analyte signal suppression in presence of a matrix, such as one

containing salts. For example, the signal of some metal analytes in 0.125 M NaOH were suppressed by up to 80% compared to that observed in 1% HNO_3 [163], which is the most widely used matrix in ICP-MS because it does not add to the background spectrum and induces negligible matrix effects. However, such effects are observed across the mass range, i.e. not just on selected analytes, and are usually worse for analytes with high IP. Yet, there was no obvious relationship between the signal improvement ratio of each analyte and their IP upon using the heated tube.

On the other hand, the solution pH affects the analyte chemical form (cationic, anionic or neutral molecules). In 1% HNO_3, the signals of almost all cations in solution were enhanced upon heating (Figure 5.4). For As and Se to fall significantly below the trend in Figures 5.4 and 5.5, one must consider the main difference between these 2 analytes and all the others studied i.e., they are not ionic. In 1% HNO_3, As would be approximately 95% present as H_3AsO_4 and 5% as $H_2AsO_4^-$, even if prepared from an As(III) compound, since HNO_3 would oxidise it to As(V) [31]. The same reasoning applies to Se. In these cases, Coulomb fission could occur in multi-elemental droplets, since they then also contained ionic analytes, but would be far less likely in mono-elemental droplets containing neutral analytes. Hence, the As and Se signals from a multi-elemental solution would be greater than from a mono-elemental one with the pre-evaporation tube.

In contrast, the HNO_3 matrix controlled the ionic strength of the solution in the absence of heat. Hence, no difference in signal intensity resulted for either As or Se whether present in mono or multi-elemental HNO_3 solution. Only following evaporation of HNO_3 from the droplets, which is promoted by the heated tube, would the ionic strength be controlled by concomitant ionic analytes. However, since there is no concomitant ionic analyte in mono-elemental solutions of As or Se, no promotion of Coulomb fission events would occur. Hence, the signal of As and Se from those solutions was apparently suppressed compared to that obtained with equi-concentrated solutions that also contained concomitant ionic analytes, which increased the occurrence of Coulomb fission.

If the heated tube indeed promotes Coulomb fission events, then the extent of signal enhancement should depend on the concentration of other analytes. Several solutions were thus prepared, where the number and concentration of the concomitant analyte(s) were varied, as detailed in Table 5.1. (In all cases, the total concentration of concomitant analytes was at least two orders of magnitude lower than that required for a physical carrier.) The greatest effect was observed with the solution containing the greatest number of concomitant analytes. When the concentration of a single concomitant analyte was increased, the As signal enhancement observed upon heating the interface also increased. Even an apparent discrepancy i.e., the smaller enhancement observed in presence of 6 concomitant analytes (La, Mo, Sb, Cd and Pb) than

in the presence of only three (Ni, Cu and Mn, for example) can be explained by the different total molar concentration of these solutions. Indeed, the former solution had a total concomitant analyte concentration of 790 mM whereas that of the latter was 1000 mM (because of lighter concomitant analytes). These results thus support the above explanation.

Table 5.1 Effect of concomitant analyte elements on the As signal enhancement ratio

As signal ratio* (heated/unheated)	Concomitant analyte(s)	Concentration of concomitant analyte(s) (µg/L)
0.65 ± 0.02	None	0
1.18 ± 0.03	Al, V, Cr	20
1.27 ± 0.04	Ni, Cu, Mn	20
1.09 ± 0.02	La, Mo, Sb, Cd, Pb	20
1.22 ± 0.06	Al, V, Cr, Ni, Cu, Mn	20
1.55 ± 0.04	Al, V, Cr, Ni, Cu, Mn, La, Mo, Sb, Cd, Pb, Zn, Se	20
1.30 ± 0.03	V	250
1.30 ± 0.02	Cr	250
1.29 ± 0.03	Mn	250

* Uncertainty expressed as standard deviation (n=3)

For a two-analyte solution, the optimal As signal observed, which was within 10% of that without heating, was also dependent on the IP of the concomitant analyte, as shown in Figure 5.7, where a line was added to emphasize the

trend (R^2 = 0.82). This suggests that, with pre-evaporation, more plasma energy was available for the ionisation of As, and the available energy increased as the IP of the concomitant analyte decreased, since the latter then needed less plasma energy for its ionisation. Although the presence of 20 µg/L of a concomitant element may seem insignificant, this concomitant element would be present in the same region of the plasma as the analyte, which may affect the ionisation of the analyte. This is reminiscent of the effect of nearby desolvating droplets and vaporising particles on analyte ionisation, which was reported by Hobbs and Olesik [164].

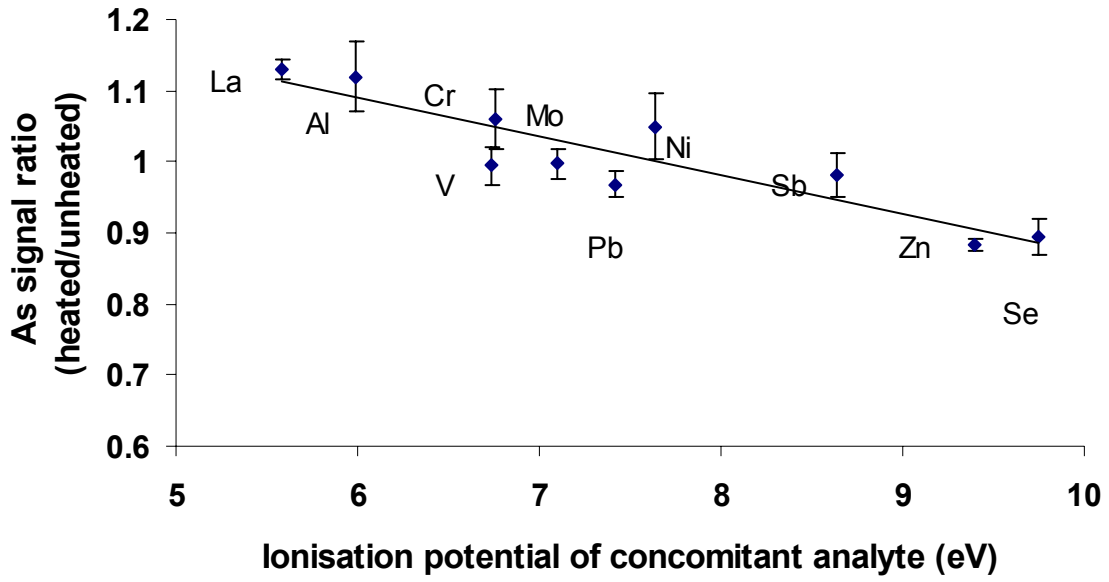

Figure 5.7 Ratio of the optimal As signal observed with heated and unheated tube for 20 µg/L solutions of As and one other analyte as a function of the first IP of the concomitant analyte element. A trend line was added to illustrate an apparent IP-related effect (n=3).

5.3 Comparison of analyte signals from monoelemental solutions in 0.01 M NaOH

To further test the above explanation, i.e. that the signal enhancement of ionic analyte is due to the pre-evaporation interface promoting Coulomb fission events, a 0.01 M NaOH (0.04 % m/v) matrix (pH 12) was used since As should be completely anionic at this high pH. The selection of this matrix is also relevant as an alkaline medium is increasingly used for sample preparation [165], especially for analytes, such as As, whose solubility increases with pH [166, 167]. Furthermore, this low matrix concentration is not expected to induce significant space-charge effects [85]. On the other hand, the NaOH might act as a physical carrier, if such an effect can still exist in presence of water vapour, since its concentration is several orders of magnitude greater than that of the analyte.

Axial profiles were obtained for As with and without the heated tube (Figure 5.8). Similar profiles (Figure 5.9) were obtained for I (also anionic at pH=12), although the optimum axial position was smaller than that for As, both with and without heat, which is commensurate with the higher IP of this element. Nonetheless, the analyte signal was enhanced upon heating the tube. The resulting signal enhancement ratio (heated/unheated) was 1.25 and 1.15 for As and I, respectively, which is in agreement with the ratios of 1.29 and 1.16 that are predicted by the trend line in Figure 5.4 at m/z 75 and 127, respectively. This therefore lends even more credence to the Coulomb fission

explanation, since the 0.01 M NaOH matrix, which would dominate the ionic strength, would lead to smaller droplets with the pre-evaporation interface. Although the enhancement may also be explained by some physical carrier effect, it does not explain why the enhancement factors fall exactly on the curve observed when no such effect existed (figure 5.5).

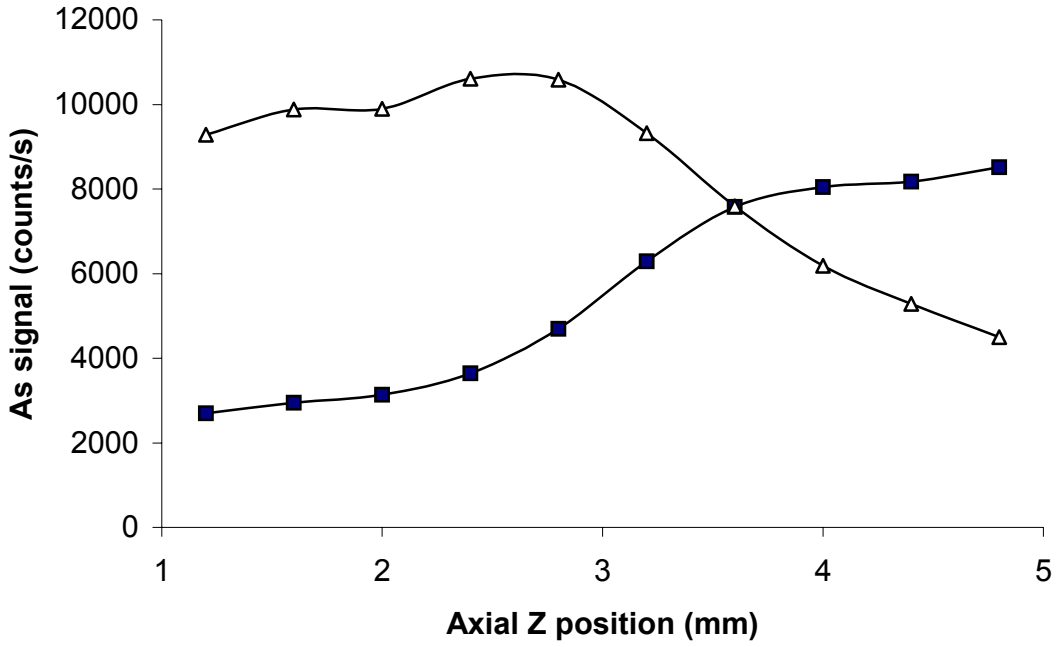

Figure 5.8 Axial profile of As in 0.01 M NaOH with unheated (full squares) and heated (open triangles) tube using a 20 μg/L As solution

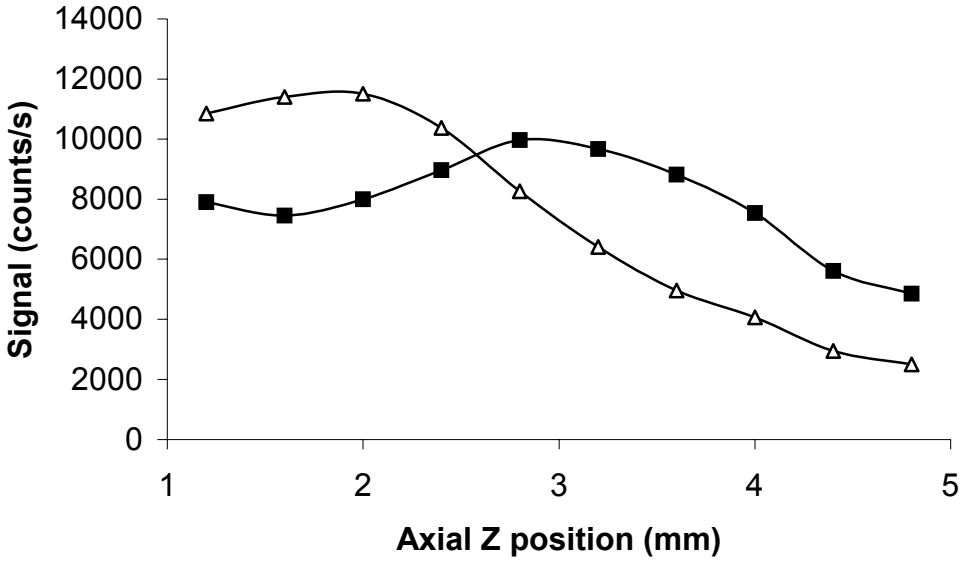

Figure 5.9 Axial profile of I in 0.01 M NaOH with unheated (full squares) and heated tube (open triangles) using 20 ug/L I solution.

5.4 Signal improvement vs the temperature of the heated tube

The pre-evaporation tube used in this project was made of borasilicate glass and could be heated up to 400°C (for fear of melting it). To assess the effect of temperature on the signal of analytes, signal intensities of representative analytes (Zn, Mo and As) were measured as a function of increasing temperature (Figure 5.10). Clearly, the higher the temperature, the greater the signal enhancement. This suggests that using quartz glass tubing along with an efficient heating tape to reach higher temperatures would likely result in significant improvements in analyte signal and, thus, in sensitivity and detection limits. Attempting this would be worthwhile for all applications

where the lowest possible detection limits are required. Future work on a higher temperature tube is thus warranted.

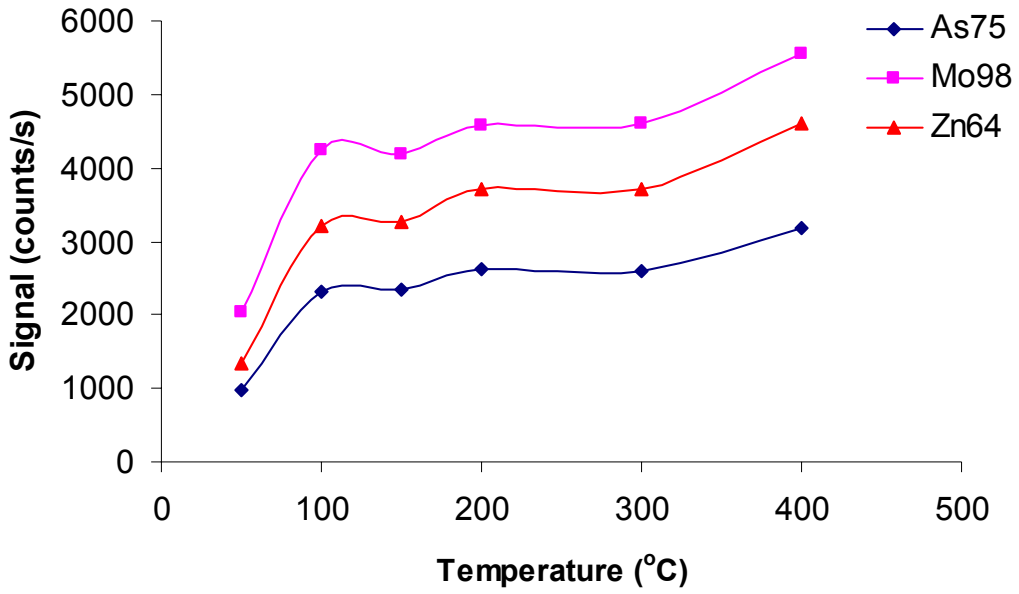

Figure 5.10 Analyte signal at different temperatures upon heating the pre-evaporation tube

5.5 Summary

A pre-evaporation tube is a simple way of improving sensitivity and detection limits in ICP-MS. By increasing evaporation, it can promote Coulomb fission events, which further reduces the droplet size distribution, hence producing more usable droplets i.e. that are ionised in the ICP. Since smaller ionic analytes have a greater charge density than larger ionic analytes of equal charge are more likely to undergo Coulomb fission. As a result, the enhancement in analyte signal upon using the pre-evaporation tube is

inversely dependent on analyte mass, except for neutral analytes, whose signal is suppressed when arising from a mono-elemental solution. Indeed, the number of Coulomb fission events is then reduced compared to that from an equi-concentrated multielemental solution where the concomitant analytes are ionic. Such suppression can thus easily be circumvented by adding concomitant ionic analytes or by changing the pH to make the analyte ionic. Because the Coulomb fission limit depends on the size and charge of droplets, as well as the identity and concentration of the matrix [114], a change in droplet size distribution is thus a more likely explanation than an increase in atom-electron collision [108] to explain signal enhancement in ICP-MS. It also explains the apparent earlier desolvation observed in presence of 0.02 M K or Cs [155], as these matrices likely promoted Coulomb fission and thereby resulted in smaller droplets that could then undergo desolvation, vaporisation, etc., lower in the plasma.

On the other hand, the pre-evaporation tube makes the system more sensitive to matrix effects, since the Coulomb fission processes depend strongly on the nature and concentration of concomitant elements as well as on the solution pH. However, adding a given amount of an ionic concomitant element to every solution could compensate these effects. In fact, when using this interface between HPLC and ICP-MS (which is the ultimate goal for the development of this pre-evaporation tube), the HPLC eluent or buffer might serve this purpose. If the buffer is too volatile, as the one selected for

As speciation in Chapter 6, then a concomitant analyte could be merged to the effluent from the analytical column, as is demonstrated in chapter 6. As well, using a quartz tube to achieve a higher temperature should greatly improve the sensitivity and detection limits for multi-elemental analysis by ICP-MS, and should thus be the subject of future work.

Chapter 6 Application of the pre-evaporation tube to As speciation analysis

The toxicological properties of arsenic depend on its chemical form and its oxidation state. The actual toxicity of As species (specific forms of an element defined as to molecular, complex, electronic or nuclear structure) [168] varies greatly. Inorganic arsenic is considered the most acutely toxic form. Arsenite (As^{III}) is the most toxic and water-soluble species among them, whereas arsenate (As^{V}) is also relatively toxic. They both have been classified as carcinogens. The methylated arsenic compounds MMA and DMA are much less toxic. On the other hand, arsenobetaine ($(CH_3)_3As^+CH_2COO^-$) is virtually non-toxic [34]. Therefore, a determination of the total arsenic concentration in real samples does not provide any information on toxicity. Chemical speciation is required to determine the types and the amounts of arsenic compounds present in a given sample, which has generated much interest in recent years. Different types of HPLC separations have been carried out to resolve different arsenic species from interferences, through their different affinity for the stationary and mobile phases [34]. The most extensively used HPLC system for arsenic speciation analysis is ion-exchange chromatography (IEC), along with ICP-MS as a detector, which has been proven to be a very sensitive method for multi-elemental analysis [33].

This work focused on four arsenic species (As(III), As(V), MMA and DMA, because they are considered to be the four major toxic arsenic species. These species have varying acidity constants and mostly exist in anionic form in water, which make them very amenable to separation by IEC using either a stationary phase containing a cationic functional group (anion exchange) or an anionic functional group (cation exchange). The IEC technique is also very suitable for separation of small charged organometallic ions. In this part of the thesis, anion exchange chromatography was used to separate the four arsenic species with ICP-TOFMS as detector.

The determination of As by ICP-MS is not as straightforward as that of several other elements. Its relatively high first IP results in a degree of ionisation of only 52% [115], which, in turn, translates in an ICP-MS sensitivity that is about half that achieved for elements, such as Co, that are fully ionised. Furthermore, because of its high IP, As is also more susceptible to matrix effects affecting the ionisation equilibrium in the plasma. Finally, As is mono-isotopic i.e. there is no alternative isotope that can be used for its determination when a spectroscopic interference arises. Several methods, such as the addition of organic modifiers [89, 92, 99, 157] or hydride generation [31, 32] have been used to improve sensitivity and overcome interferences. However, the introduction of organic modifiers causes carbon-related interferences, whereas a relatively complicated experimental setup is required for hydride generation.

The pre-evaporation tube is a simple setup that preserves plasma energy by pre-evaporating the solvent before it enters the plasma. This preserved plasma energy should allow an increase in the degree of ionization of analytes with high IP, such as As, and thus improve sensitivity. Furthermore, because the pre-evaporation tube decreases the aerosol droplet size distribution (see chapter 4), it should also improve the detection limit. Thus, the pre-evaporation tube was applied to As speciation by HPLC coupled to ICP-TOFMS.

The objectives of this chapter were to find a suitable mobile phase to separate the four As species with limited matrix effect (including minimal salt deposition on the cones) in ICP-MS and to determine the best separation and analysis conditions. Matrix effects arising from the mobile phase were evaluated by comparison to 1% HNO_3, which is the typical matrix in ICP-MS. The experiment was divided in three parts: 1) separation of four major arsenic species by ion-exchange HPLC; 2) assessment of the matrix effect of the mobile phase and 3) application of the pre-evaporation tube between HPLC and ICP-MS to As speciation analysis.

6.1 The chromatographic separation of four As compounds

A Dionex AG-7, AS-7 anion exchange column was used, which functions as a multi-mode ion exchanger. The four As compounds (As (III), As (V), MMA and DMA) contain acidic groups and their acidic dissociation constants (pK_a) are

listed in table 6.1 [169]. The degree of deprotonation of the compounds depends on pH and ionic strength of the mobile phase.

Table 6.1 Dissociation constants of arsenic compounds [169]

As compound	pK_{a1}	pK_{a2}	pK_{a3}
H_3AsO_4 (As^V)	2.22	6.98	11.52
CH_5AsO_3 ($MMAs^V$)	4.1		
$C_2H_7AsO_2$ ($DMAs^V$)	6.2		
H_3AsO_3 (As^{III})	9.23	12.13	13.4

6.1.1 Selection of the mobile phase

A non-volatile mobile phase of phosphate buffer (such as sodium and potassium phosphates) is very often utilized in reversed-phase HPLC when using a UV detector because of its UV transparent property. However, it is not suitable for ICP-MS detection since the phosphate buffer is non volatile and can deposit on the cones and ion lenses causing signal drift [34]. It can also cause spectroscopic interferences and non-spectroscopic interferences (matrix effects with signal suppression due to space charge effect). Thus, a volatile mobile phase that does not introduce additional spectroscopic interferences would be more appropriate for ICP-MS detection. For example, 1% v/v nitric acid is the most commonly used matrix in ICP-MS because it does not introduce extra spectroscopic interferences.

Ammonium nitrate, which has the same elemental composition as nitric acid, is considered an optimal eluent in IC-ICP-MS due to its following features [169]:

1. Thermal volatility, hence no significant salt deposition on the cones.
2. No extra background interferences compared to HNO_3 in ICP-MS.
3. High concentration tolerance by ICP-MS without space charge effect.
4. Possibility to adjust its pH value from acidic to slightly basic without impairing the ionic strength.
5. No complexing capacity of NH_4^+ with anions or NO_3^- with metals.
6. No potential precipitation of analytes (unlike a carbonate mobile phase, which can induce the precipitation of $CaCO_3$)

Other ammonium salts have been used as mobile phase in HPLC-ICP-MS as well, such as ammonium acetate and ammonium carbonate [34, 171]. However, these two mobile phases both introduce carbon into the plasma, which may result in carbon-related spectroscopic interferences and matrix effects (signal enhancement or suppression, see section 1.2.1). Thus, ammonium nitrate was selected for the mobile phase.

6.1.2 Selection of the separation conditions

The pH and the ionic strength of the mobile phase, as well as the solute concentration, the flow rate and the temperature can all influence the

separation and retention time of the analytes in IEC. In this work, the flow rate was kept at 1 mL/min, which is the typical sample uptake rate in ICP-MS, and all experiments were carried out at room temperature (i.e. 20ºC). A lower flow rate (such as 0.5 mL/min) led to a longer retention time and worsened the peak shape of the last eluting species (As^{V}). The mobile phase concentration should be kept as low as possible to avoid matrix effects while achieving an optimum separation. Thus, it was not greater than 0.025 M in this experiment. The pH of the mobile phase was then adjusted by adding nitric acid or ammonia solution in order to get the best separation.

Using 0.025 M NH_4NO_3 at different pH values for the separation of the four As compounds, only two or three peaks resulted when the pH was either under 7 or above 9, i.e. the four species could not be separated completely (the original pH of 0.025 M NH_4NO_3 is 5.65). However, at pH 8.6, three baseline-separated peaks were obtained (Figure 6.1). This chromatographic behavior is consistent with what can be predicted from the pK_a values. At pH 8.6, three arsenic species (As(V) , MMA and DMA, whose pK_{a1} range from 2.2 to 6.2, as shown in table 6.1) became anionic but As(III) (whose pK_{a1} is 9.23) remained neutral. Thus, the retention time should decrease with an increase in pK_a when using an anion exchange column. Therefore, the four arsenic species were expected to elute in the following order: As(III), DMA, MMA and As(V). This order was verified by simply injecting individual standard solutions of the four species and comparing the retention times. The first peak was due to

As(III) and DMA (which co-eluted), the second peak was from MMA and the third one from As(V) (Figure 6.1).

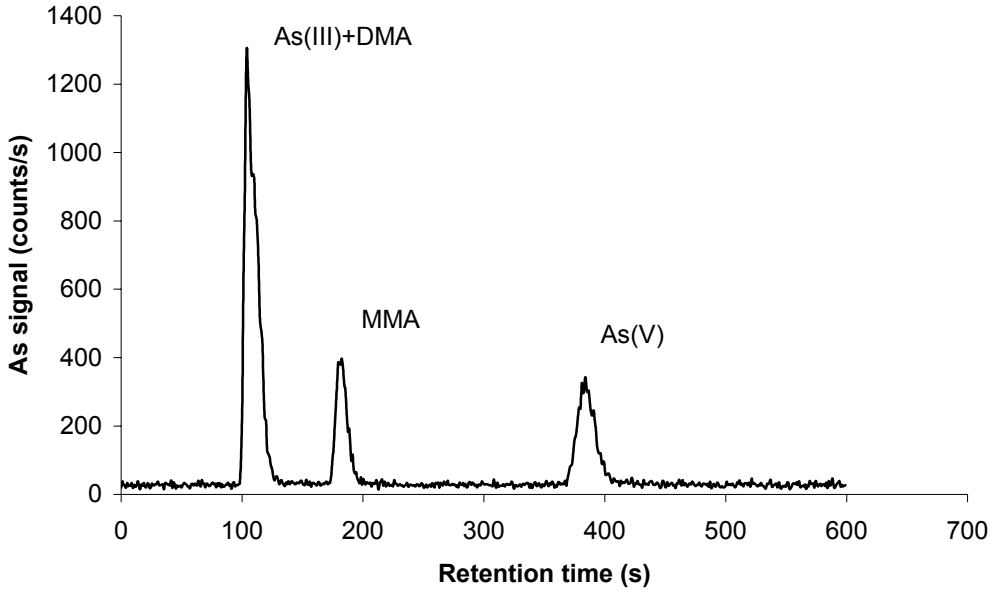

Figure 6.1 Chromatogram for four As species (As^{III}, As^{V}, MMA^{V} and DMA^{V}), each at a concentration of around 50 µg/L, using a mobile phase of 0.025 M NH_4NO_3 (pH 8.6) at 1 mL/min through a Dionex IonPac® Guard AG7 (4X50 mm) and Dionex IonPac® Analytical AS7 (4X250 mm). See table 2.1 for ICP-MS operating conditions.

A decrease in the mobile phase concentration (ionic strength) improved the resolution of As(III) and DMA (see Figures 6.2 and 6.3). However, As(V), which was the last one eluted, then interacted so strongly with the stationary phase that its elution time unduly increased and its peak shape degraded (in Figure 6.3, it lies completely outside the time scale). Although an isocratic separation mode is usually better for ICP-MS signal stability, a gradient elution program was needed to completely separate the four arsenic species. Nonetheless, a change in concentration of the mobile phase from 0.00625 M to 0.025 M was verified to not induce signal instability.

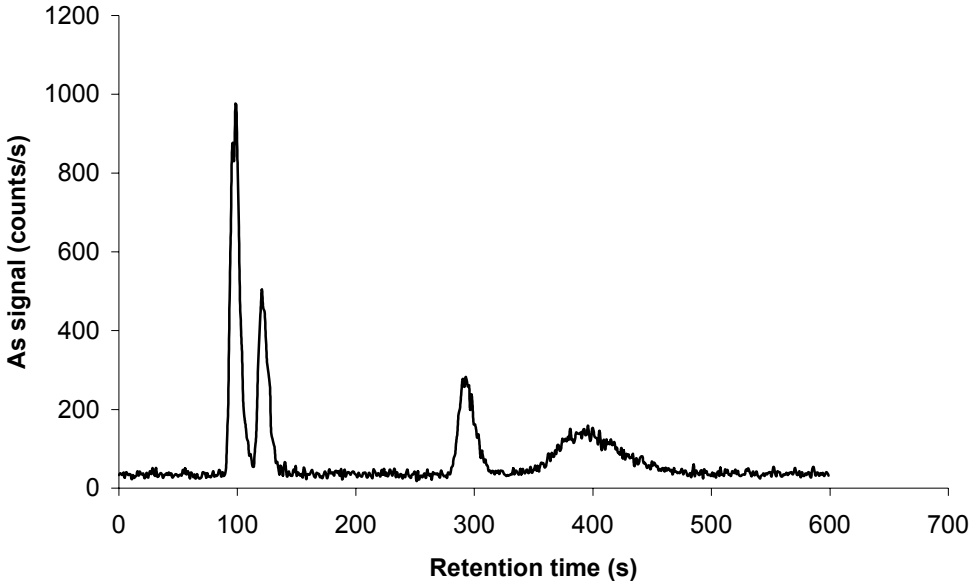

Figure 6.2 Chromatogram of four As species (As^{III}, As^{V}, MMA^{V} and DMA^{V}), each at a concentration of around 50 µg/L, using a 0.0125 M NH_4NO_3 mobile phase at pH 8.6. Other conditions were as in Figure 6.1

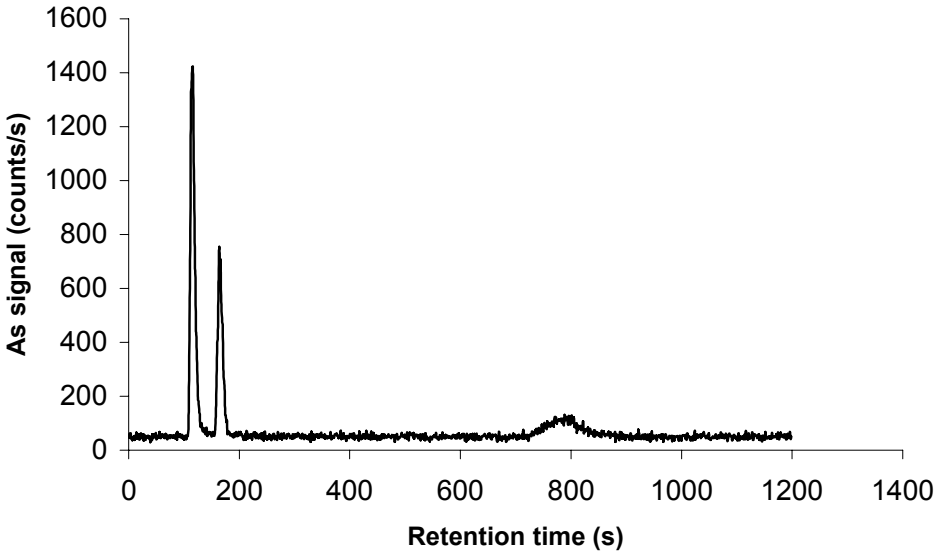

Figure 6.3 Chromatogram of four As species (As^{III}, As^{V}, MMA^{V} and DMA^{V}), each at a concentration of around 50 µg/L, using a 0.00625 M NH_4NO_3 mobile phase at pH 8.6. Other conditions were as in Figure 6.1. As(V) had a retention time greater than 1200 s.

Therefore, a gradient program (described in Table 2.3) from 0.00625 M to 0.025 M at pH 8.6 was chosen for the separation of four As species, and a baseline separation was achieved within 12 minutes (Figure 6.4). All subsequent separations were carried out under these gradient conditions.

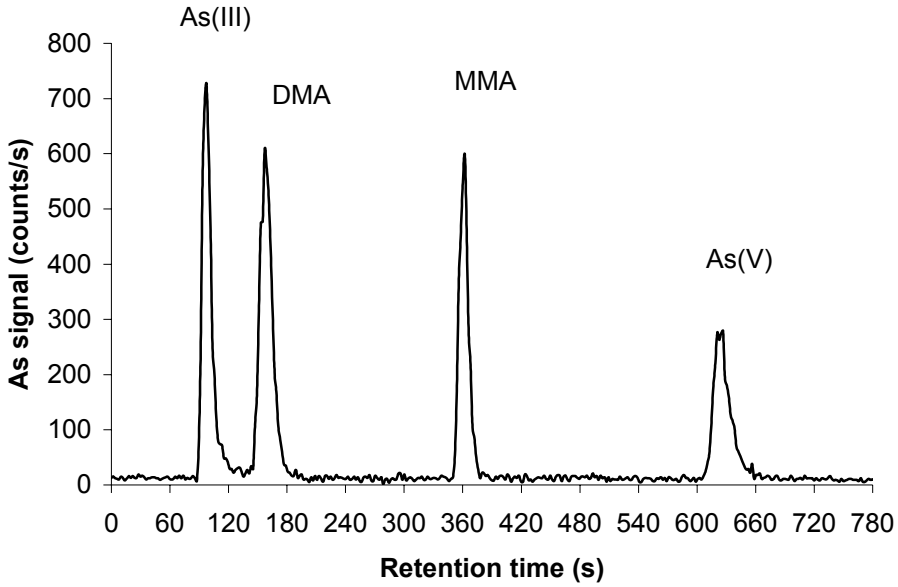

Figure 6.4 Chromatogram of four As species (As^{III}, As^{V}, MMA^{V} and DMA^{V}), each at a concentration of around 50 µg/L using the gradient program (see Table 2.3)

Table 6.2 Theoretical plate numbers* corresponding to Figure 6.2 and 6.4

	As(III)	DMA	MMA	As(V)
Figure 6.2	292	405	919	177
Figure 6.4	194	411	1636	1984

*Calculated using $N=16t_r^2/W^2$ (W= baseline peak width, t_r= retention time)

6.2 Matrix effect from NH_4NO_3

Ammonium nitrate is volatile and only introduces nitrogen, hydrogen and oxygen into the plasma, which is very similar to nitric acid. Its matrix effect was investigated by dissolving the analyte in 0.025 M NH_4NO_3, and measuring the resulting analyte signal by ICP-MS, which was then compared to that observed when the same analyte was in a 1% HNO_3 matrix. Spatial profiling was carried out for 14 analytes ($^{27}Al^+$, $^{51}V^+$, $^{52}Cr^+$, $^{58}Ni^+$, $^{60}Ni^+$, $^{63}Cu^+$, $^{55}Mn^+$, $^{66}Zn^+$, $^{75}As^+$, $^{78}Se^+$, $^{98}Mo^+$, $^{114}Cd^+$, $^{121}Sb^+$, $^{139}La^+$, $^{208}Pb^+$) as described in Chapter 4, with and without the pre-evaporation tube. Axial profiles of the 14 analytes under unheated and heated conditions were obtained. The optimum axial Z position for each analyte is shown in Figure 6.5. The resulting change in axial Z position upon heating the tube is similar to that observed in 1% HNO_3 (i.e. the optimum axial Z position of each analyte decreased or moved closer to the sampler cone with a heated tube; see Figure 4.2). The preserved plasma energy shortened the residence time needed in the plasma.

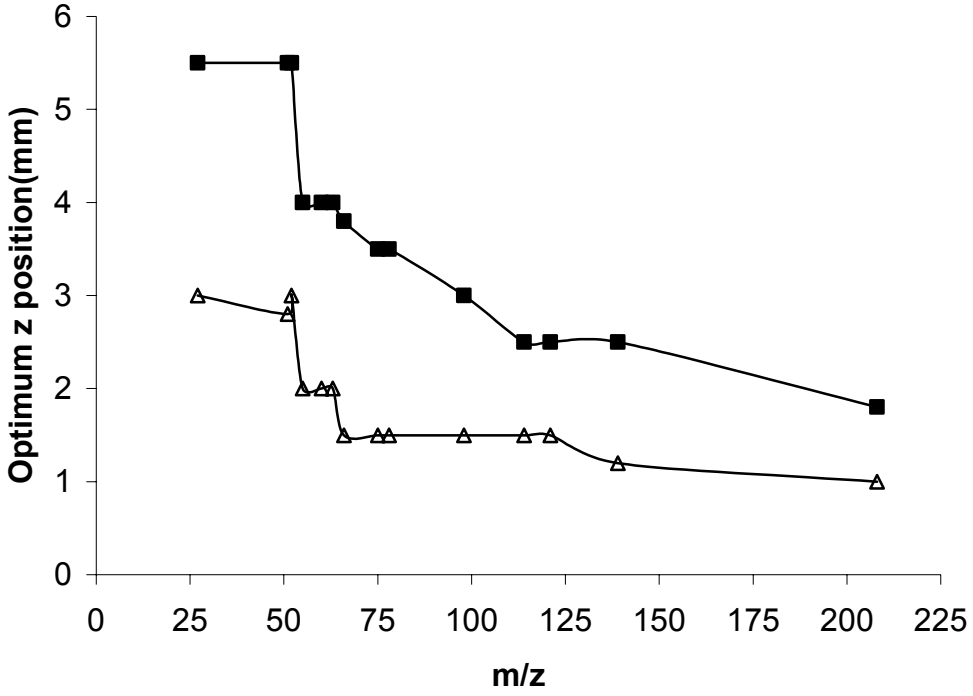

Figure 6.5 Optimum axial Z position in 0.025 M NH_4NO_3 with an unheated (full squares) and heated (open triangles) 5 mm i.d. tube

The radial profiles of the 14 analytes in NH_4NO_3 became narrower and more Gaussian (Figure 6.6), which is also in agreement with the previous radial profiles in 1% HNO_3. Moreover, Figure 6.7 shows that both matrices had a similar effect on analyte signal (identical radial profiles were similarly obtained for As in the two matrices with the pre-evaporation tube). Thus, switching from 1% HNO_3 to 0.025 M NH_4NO_3 had no apparent effect on the plasma, presumably because these matrices have a similar volatility.

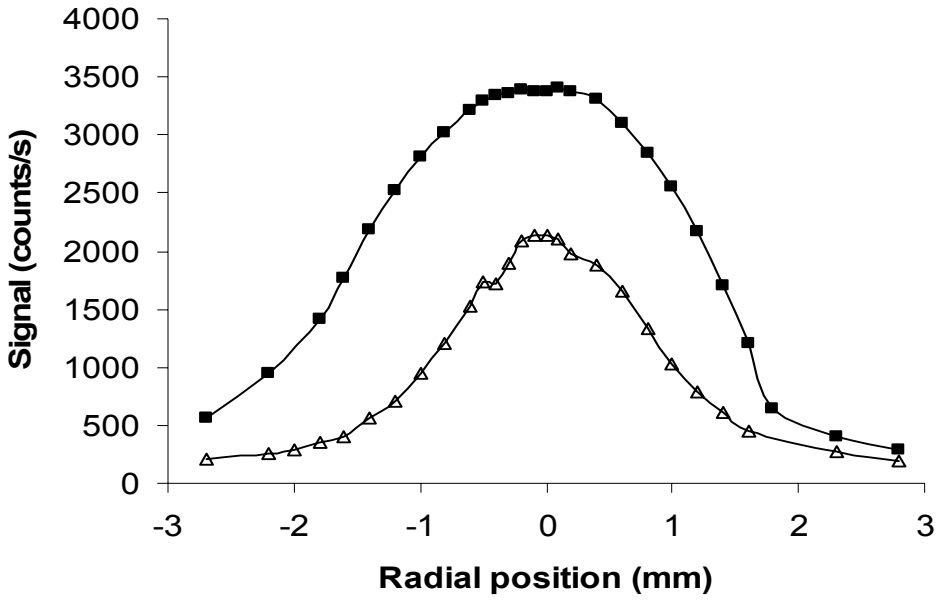

Figure 6.6 Radial profile of As in 0.025 M NH_4NO_3 without (full squares) and with a heated tube (open triangles, 11-cm long, 2-mm i.d) outside the torch box.

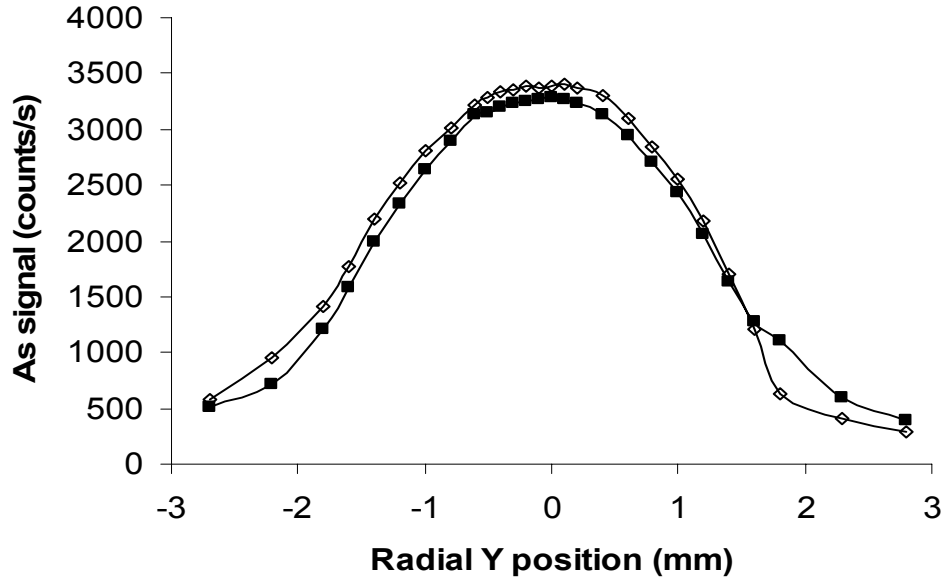

Figure 6.7 Radial profile of As in 1% HNO_3 (0.2 M, open diamonds) and 0.025 M NH_4NO_3 (full squares) under optimum unheated conditions.

The signals of each analyte in the two matrices (0.025 M NH_4NO_3 and 1% HNO_3) which were obtained under the same optimum condition, with and without a heated tube, on the same day are compared in figures 6.8 and 6.9. Evidently, no (or negligible) matrix effects exist since most analytes signal had the same intensity in both matrices, under either heated or unheated conditions (i.e. the As signal ratio in the two matrices was 1). Therefore, 0.025 M NH_4NO_3 (or a more dilute solution) can be used as a mobile phase for As speciation analysis by ICP-MS, both when using the pre-evaporation interface and in the standard configuration.

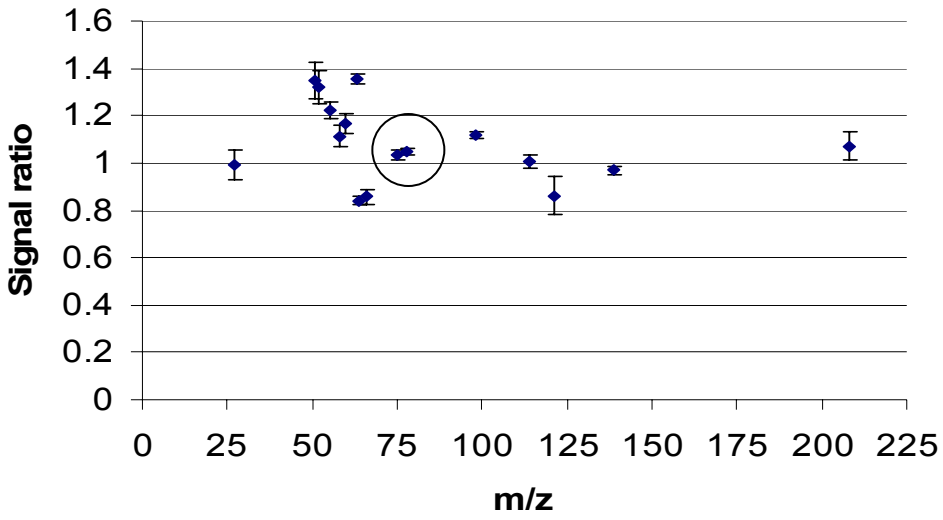

Figure 6.8 Signal ratio (signal in 0.025M NH_4NO_3/signal in 1% HNO_3, n=3) of 14 analytes (20 µg/L) under unheated condition (i.e. standard configuration).

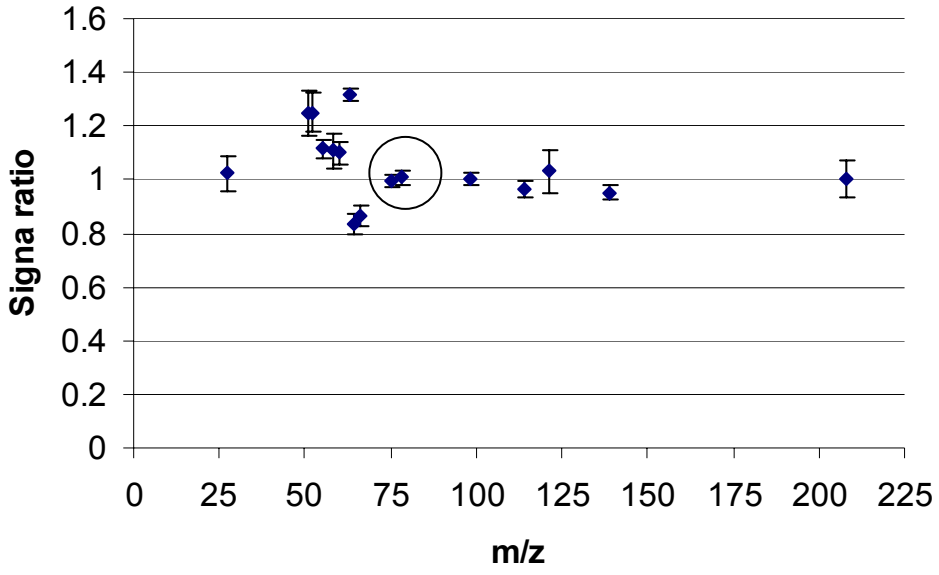

Figure 6.9 Signal ratio (signal in 0.025 M NH_4NO_3/signal in 1% HNO_3, n=3) of 14 analytes (20 µg/L) with a heated tube.

6.3 Application of the pre-evaporation tube to As speciation analysis

The effect of a pre-evaporation tube on As speciation analysis using the gradient separation program is shown in Figure 6.10. Upon heating the pre-evaporation tube, NH_4NO_3 (which has a similar volatility to HNO_3) was expected to evaporate, leaving the analytes to determine the extent of Coulomb fission events. So, the suppression of the As(III) and DMA signals that is observed compared to when the tube is not heated is commensurate with their chemical forms, as, for example, As(III) was mostly neutral under these conditions (pK_a 9.23, see table 6.1). On the other hand, the signal of As(V), which was completely ionic at a pH of 8.6, was enhanced as expected.

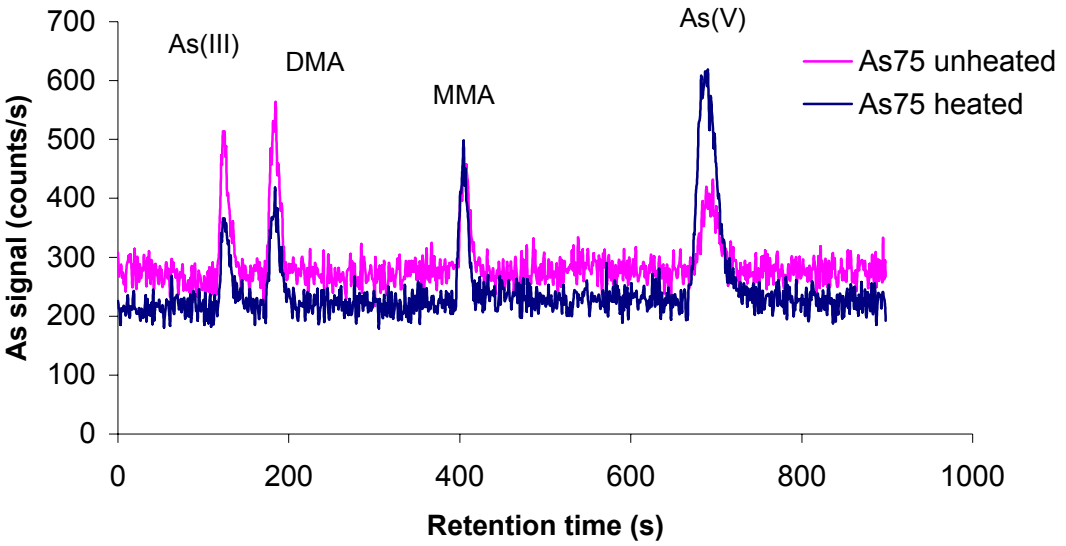

Figure 6.10 Chromatogram of four As species (As^{III}, As^{V}, MMA^{V} and DMA^{V}), each at a concentration of 25 µg/L using a gradient separation program (Table 2.3) and a pre-evaporation tube

A way to alviate this problem would be to switch to a non-vilotile ionic mobile phase. However, since this may introduce solid build-up on the interface, an alternate approach was taken. Indeed, adding concomitant ionic analytes to a solution containing neutral analyte can prevent analyte signal suppression upon heating the pre-evaporation tube (see chapter 5). Therefore, the experiment was repeated with a tee inserted between the HPLC and ICP-MS systems to allow the addition of concomitant ionic analytes, which would then promote Coulomb fission upon heating the pre-evaporation tube. The 50 µg/L concomitant ionic analytes solution (of Al, V, Cr, Mn, Cu, Ni, Zn, Mo, Cd, La, Pb, Sb) was pumped at the same rate as the HPLC system. Since this would cause a dilution of the effluent from the HPLC, this was compensated by

increasing the As species concentration to 50 µg/L. The results are shown in Figure 6.11. The signals of all 4 As species were enhanced significantly. Furthermore, the baseline with the heated tube was lower than that without heating. Again, this is commensurate with a decrease in noise level because of the decrease of droplet size that results from both pre-evaporation and the promotion of Coulomb fission. All these results clearly show that the promotion of Coulomb fission by pre-evaporation of the solvent is an important process that has been so far mostly overlooked but could nonetheless be used advantageously for enhanced multi-elemental analysis.

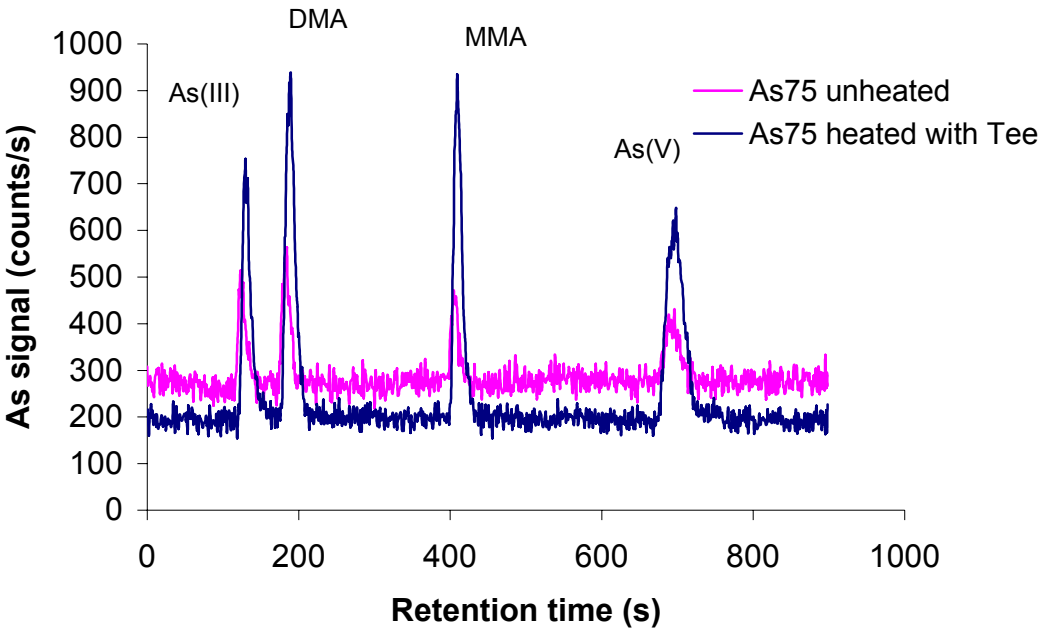

Figure 6.11 Chromatogram of four As species (As^{III}, As^{V}, MMA^{V} and DMA^{V}) each at a concentration of 25 µg/L using a gradient separation program (Table 2.3). Using a tee, the analyte concentration was 50 ug/L before 1:1 mixing with a 50 µg/L solution of concomitant ionic analytes.

6.4 Summary

In this chapter, NH_4NO_3 was investigated as a mobile phase for As speciation. This matrix up to a concentration of 0.025 M did not cause a significant matrix effect for As (as well as for most of 13 other analytes with different ionization potentials and mass) in comparison to a 1% HNO_3 matrix. Since NH_4NO_3 contains the same elements as HNO_3 and is similarly volatile, it did not introduce extra spectroscopic and non-spectroscopic interferences. This is very beneficial for arsenic speciation analysis by ICP-MS, as a solution of NH_4NO_3 is the ideal mobile phase for the separation of four major arsenic species under slightly basic condition (pH 8.6) by anion exchange chromatography. Baseline separation could be achieved using a gradient program of this mobile phase, which may be suitable for routine arsenic speciation analysis by IC-ICP-MS.

A pre-evaporation tube was also used to significantly enhance the sensitivity of ICP-MS for ionic As species. The enhancement could be generalised to all As species by adding concomitant analytes to the effluent from the IC system. This indeed ensured that Coulomb fission events would still occur even when non-ionic analytes were present in a volatile matrix. This simple approach, which should be applicable to all ICP-MS instruments should significantly enhance speciation analysis in general (i.e., not just for As).

Chapter 7 Conclusions and future work

In this thesis, effects arising from different matrices and the related mechanisms for signal enhancement or suppression were investigated. As well, two methods were used and characterized for improving the sensitivity of ICP-MS analysis. To investigate the matrix effects from organic modifiers, different organic compounds were added to 1% HNO_3. Radial profiles of ions distributions in the plasma were then used to investigate the analyte signal enhancement mechanism. To improve the sensitivity for multi-elemental analysis, a simple method of inserting a pre-evaporation tube between the spray chamber and the plasma torch was studied. The matrix effects caused by concomitant analytes with a heated and unheated pre-evaporation tube were also investigated. Furthermore, in order to apply this pre-evaporation tube to As speciation, the separation of four major As species using an NH_4NO_3 mobile phase at pH 8.6 was done by using IC-ICP-MS, following assessment of any matrix effect arising from the mobile phase (NH_4NO_3).

Spatial profiles could accurately represent the distribution of ions in the plasma as secondary discharge between the plasma and the sampler cone was shown to be minimal on the instrument. Therefore, radial profiles were used to investigate matrix effects arising from the addition of organic compounds (organic solvent and surfactant) to 1% HNO_3 and the possible mechanisms resulting in analyte signal enhancement or suppression. Different surfactants (ionic and non-ionic) and different organic solvents

(MeOH, acetone and ethylene glycol) were used for this investigation. The negative charge of the ionic SDS (0.2% m/v) preferentially attracted lighter cations, resulting in an increase in analyte transport efficiency that was inversely dependent on mass. However, the addition of 2% v/v MeOH induced a widening of the radial distribution of both analytes and polyatomic background ions because of a spread of MeOH in the plasma, which carried along ions, hence resulting in a suppression of analyte signal (that was inversely dependent on mass). On the other hand, the addition of 0.2% SDS had no significant effect on the plasma itself and the same bell-shaped radial analyte ion distribution as in 1% HNO_3 was observed.

However, a change in the analyte ions radial distribution from bell-shaped to bimodal resulted from an addition of 2% v/v MeOH, which matched those of carbon-containing polyatomic ions. This observation, in combination with the observation that Ar^+ was simultaneously suppressed in the central channel, increases the significance of charge transfer with C^+ as an ionisation mechanism in the plasma for analytes with a high ionization potential. The organic solvent volatility also affected ion radial distribution. The lower the BP of the solvent, the wider the radial peak. A study of the combined effect of SDS and MeOH is completed, to assess analyte signal enhancement across the mass range. This study demonstrated that spatial profiling of both analytes and background ions distribution in the plasma is an efficient way of investigating matrix effects.

To improve the sensitivity for multi-elemental analysis, a pre-evaporation tube was developed and characterized. Different sizes (diameter and length) as well as different configurations (inside and outside the torch box) were tested. Using a 5-mm i.d. (11-cm long) heated glass tube instead of the plastic connection tubing inside the torch box provided the best improvement in sensitivity and detection limits for multi-elemental analysis. Therefore, it is currently used inside the torch box of the Renaissance instrument.

The pre-evaporation tube changed the distribution of ions in the plasma. The radial profiles of analytes became narrower and more Gaussian, which then effectively increased the transmission of analyte ions through the sampler and skimmer cones. Furthermore, the analyte oxide ratio decreased while the doubly charged analyte ratio remained unchanged at the axial position used for multi-elemental analysis. The optimum axial position for all analytes moved closer to the coil (lower sampling depth) using the heated tube. However, the compromise optimum axial position for multi-elemental analysis with the heated tube was truly optimal for a greater number of elements compared to that without a heated tube. Moreover, slightly improved sensitivity and detection limits resulted across the mass range using a heating temperature of only 400°C (outside tube temperature). Since similar results were obtained with other torches and spray chambers as well as on a quadrupole-based instrument [143], this simple approach should be beneficial to all ICP-MS instruments. Furthermore, the sensitivity and detection limits

might be further improved by using another material than glass, which can bear higher temperatures (such as a quartz tube).

The pre-evaporation tube is a simple way of improving sensitivity and detection limits in ICP-MS since it changed the distribution of ions in the plasma, decreased noise level and preserved plasma energy. Furthermore, by increasing the evaporation of solvent (thereby decreasing droplet size), the pre-evaporation tube can promote Coulomb fission events, which further reduce the droplet size distribution, hence producing more and even smaller droplets, which can then more easily produce analyte ions in the ICP. The Coulomb fission event frequency depends on the size and charge density of droplets. Since smaller ionic analytes have a greater charge density than larger ionic analytes of equal charge, droplets containing them are more likely to undergo Coulomb fission. As a result, the enhancement in analyte signal upon using the pre-evaporation interface is inversely dependent on analyte mass when they are ionic in solution.

In contrast, no increase in the number of Coulomb fission events would be expected for neutral analytes in mono-elemental HNO_3 solutions. Thus, the number of Coulomb fission events would be smaller than that from an equi-concentrated multi-elemental solution containing ionic concomitant analytes. This apparent suppression (when compared to the signal observed in a multi-elemental solution) can be easily circumvented by adding concomitant ionic

analytes or by changing the pH to make the analyte ionic. Because the Coulomb fission limit depends on the size and charge of droplets, as well as the identity and concentration of the matrix [114], a change in droplet size distribution caused by Coulomb fission events is thus a better explanation for signal enhancement in ICP-MS than an increase in atom-electron collision [108] It also better explains the apparent earlier desolvation observed in presence of 0.02 M K or Cs [155], as these matrices likely promoted Coulomb fission and thereby resulted in smaller droplets that could then undergo desolvation, vaporisation, etc., lower in the plasma.

On the other hand, the pre-evaporation tube makes the system more susceptible to matrix effects, since the Coulomb fission processes depend strongly on the nature and concentration of concomitant elements as well as on the solution pH. However, adding a given amount of an ionic concomitant element to every solution was observed compensate these effects.

The ultimate goal of this work was to find a way to enhance the sensitivity of ICP-MS for As to then apply it to As speciation analysis. The two approaches considered had different benefits: the introduction of organic compounds only enhanced the signal of elements with a high IP, whereas the pre-evaporation tube enhanced all analyte signals, including that of As. Thus, the pre-evaporation tube is a more universal approach, since it improved sensitivity

for multi-elemental analysis, and should therefore be used in all applications requiring low detection limits.

For As speciation analysis, NH_4NO_3 was chosen as a mobile phase and provided baseline separation of four major As species. It should be an ideal matrix for ICP-MS since, at a concentration up to 0.025 M, it did not introduce extra spectroscopic interferences and non-spectroscopic interferences compared to HNO_3. Therefore, this mobile phase is very suitable for routine arsenic speciation analysis by IC-ICP-MS in the standard configuration (i.e. without a heated tube).

With the pre-evaporation tube, however, droplets containing As(III), which is neutral at pH 8.6 (pK_a 9.23), would unlikely undergo Coulomb fission because NH_4NO_3 is volatile (similarly to HNO_3). However, this could be remedied by adding concomitant ions or using a non-volatile ionic eluent or buffer, which would then promote Coulomb fission events and thus result in enhanced sensitivity for IC-ICP-MS.

Future work should investigate if this pre-evaporation tube has any drawback for sample analysis or speciation analysis by IC-ICP-MS. A quartz tube should also be compared to the glass tube as a higher temperature may further improve the sensitivity and detection limits for multi-elemental analysis by ICP-MS.

References

1. K. E. Jarvis, A. L. Gray and R. S. Houk, *Handbook of inductively coupled plasma mass spectrometry,* 1992, 59-66 (Chapman and Hall Inc. New York, USA).

2. R. S. Houk, V. A. Fassel, G. D. Flesch, H. J. Svec, A. L. Gray and C. E. Taylor, Inductively coupled argon plasma as an ion-source for mass spectrometric determination of trace elements, *Anal. chem*. 52 (1980) 2283-2289.

3. A. L. Gray, ICP as an ion source-origins, achievements and prospects, *Spectrochim. Acta. Part B* 40 (1985) 1525-1537.

4. N. Bradshaw, E. F. H. Hall and N. E. Sanderson, Inductively coupled plasma as an ion source for high-resolution mass spectrometry, *J. Anal. At. Spectrom. 4* (1989) 801-803.

5. L. Moens and N. Jakubowski, Double-focussing mass spectrometers in ICPMS, *Anal. Chem.* 70 (1998) 251A-256A.

6. G. M. Hieftje, Toward the next generation of plasma mass spectrometers. Plenary lecture, *J. Anal. At. Spectrom.* 7 (1992) 783-799.

7. G. M. Hieftje and G. H. Vickers, Development in plasma source/mass spectrometry, *Anal. Chim. Acta,* 216 (1989) 1-24.

8. D. Beauchemin, Inductively Coupled Plasma Mass Spectrometry, *Anal. Chem.* 76 (2004) 3395-3415.

9. G. M. Hieftje, D. P. Meyers, G. Li, P. P. Mahoney, T. W. Burgoyne, S. J. Ray and J. P. Guzowski, Toward the next generation of atomic mass spectrometers. *J. Anal. At. Spectrom.* 12 (1997) 287-292.

10. A. Montaser, J. A. McLean, H. Liu and J. M. Mermet, in *Inductively coupled plasma mass spectrometry*; Montaser, A., Ed., 1998, 1-31 (Wiley-VCH, New York).

11. R. Thomas, *A beginner's guide to ICP-MS, Part III:* the plasma source. *Spectroscopy,* 16(6) (2001) 26-30.

12. M. Resano, I. Gelaude, R. Dams, F. Vanhaecke, Solid sampling–electrothermal vaporization–inductively coupled plasma mass spectrometry for the direct determination of Hg in different materials using isotope dilution with a gaseous phase for calibration, *Spectrochim. Acta Part B* 60 (2005) 319– 326.

13. C. Pickhardt, A. V. Izmer, M. V. Zoriy, D. Schaumloffel, J. S. Becker , On-line isotope dilution in laser ablation inductively coupled plasma mass spectrometry using a microflow nebulizer inserted in the laser ablation chamber, *Int. J. Mass Spectrom.* 248 (2006) 136–141.

14. J. C. A. Wuilloud, R. G. Wuilloud, A. P. Vonderheide and J. A. Caruso, Gas chromatography/plasma spectrometry—an important analytical tool for elemental speciation studies, *Spectrochim. Acta Part B* 59 (2004) 755-792.

15. J. W. Olesik and J. C. Fisher, Incompletely desolvated droplets in argon inductively coupled plasmas: the number, original size and effect on emission intensities. *Spectrochim. Acta Part B* 46 (1991) 851-868.

16. J. A. McLean, H. Zhang and A. Montaser, A direct injection high-efficiency nebulizer for inductively coupled plasma mass spectrometry, *Anal. Chem.* 70 (1998) 1012-1020.

17. V. A. Fassel, and B. R.Bear, Ultrasonic nebulization of liquid samples for analytical inductively coupled plasma-atomic spectroscopy--an update. *Spectrochim. Acta Part B* 41 (1986) 1089-1113.

18. A. Montaser, H. Tan, I. Ishii, S. H. Nam and M. Cai, Argon Inductively Coupled Plasma Mass Spectrometry with Thermospray, Ultrasonic, and Pneumatic Nebulization, *Anal. Chem. 63 (1991)* 2660-2665.

19. J. A. McLean, M. G. Minnich, L. A. Iacone, H. Liu, and A, Montaser, Nebulizer diagnostics: fundamental parameters, challenges, and techniques on the horizon, *J. Anal. At. Spectrom.* 13 (1998) 829-842.

20. N. Jakubowski, I. Feldmann, D. Stuewer and H. Berndt, Hydraulic high pressure nebulization-application of a new nebulization system for inductively coupled plasma mass spectrometry, *Spectrochim. Acta Part B* 47 (1992) 119-129.

21. K. Luo and H. Berndt, Sample introduction in ICP spectrometry by hydraulic high-pressure nebulization, *Spectrochim. Acta Part B* 49 (1994) 485-492.

22. S. Saverwyns, X. Zhang, F. Vanhaecke, R. Cornelis, L. Moens and R. Dams, Speciation of six arsenic compounds using high- performance liquid chromatography-inductively coupled plasma mass spectrometry with sample introduction by thermospray nebulization *J. Anal. At. Spectrom.* 12 (1997) 1047-1052.

23. N. Fitzgerald, J. F. Tyson and D. A. Leighty, Reduction of water loading effects in inductively coupled plasma mass spectrometry by a Nafion membrane dryer device, *J. Anal. At. Spectrom.* 13 (1998) 13-16.

24. H. Liu, R. H. Clifford, S. P. Dolan, A. Montaser, Investigation of a high-efficiency nebulizer and a thimble glass frit nebulizer for elemental analysis of biological materials by inductively coupled plasma-atomic emission spectrometry, *Spectrochim. Acta Part B* 51 (1996) 27-40.

25. J. L. Todolí and J. M. Mermet, Sample introduction systems for the analysis of liquid microsamples by ICP-AES and ICP-MS*, Spectrochim. Acta Part B* 61 (2006) 239–283.

26. D. R. Wiederin, F. G. Smith, and R. S. Houk, Direct injection nebulization for inductively coupled plasma mass spectrometry. *Anal. Chem.* 63, (1991) 219-225.

27. C. S. Westphal, K. Kahen, W. F. Rutkowski, B. W. Acon and A. Montaser, Demountable direct injection high efficiency nebulizer for inductively coupled plasma mass spectrometry, *Spectrochim. Acta Part B* 59 (2004) 353-368.

28. X. C. Le, X. Lu and X-F. Li, Arsenic speciation, *Anal. Chem*. 76 (2004) 26A-33A.

29. Y. Liu, V. Lopez, J. J. Zhu, D. R. Wiederin and W. F. Beckert, Capillary electrophoresis coupled on-line with inductively coupled plasma mass spectrometry for elemental speciation, *Anal. Chem.* 67 (1995) 2020-2025.

30. M. S. Da Rocha, A. B. Soldado, E. Blanco-Gonzalez and A. Sanz-Medel, Speciation of mercury compounds by capillary electrophoresis coupled on-line with quadrupole and double focusing inductively coupled plasma mass spectrometry, *J. Anal. At. Spectrom.* 15 (2000) 513-518.

31. D. Beauchemin, Hydride generation interface for the determination of inorganic As and organoarsenic by ICP-MS using open-focused microwave digestion to enhance the pre-reduction process, *J. Anal. At. Spectrom.* 13 (1998) 1-5.

32. M. J. Maher, Ellwood, A. William, An automated hydride generation - cryogenic trapping- ICP - MS system for measuring inorganic and methylated Ge, Sb and As species in marine and fresh waters. *J. Anal. At. Spectrom.* 17 (2002) 197-203.

33. D. Beauchemin, K. W. M. Siu, J. W. McLaren and S. E. Berman, Determination of arsenic species by high-performance liquid chromatography- inductively coupled plasma mass spectrometry, *J. Anal. At. Spectrom.* 4 (1989) 285-289.

34. C. B. Hymer, J. A. Caruso, Arsenic and its speciation analysis using high-performance liquid chromatography and inductively coupled plasma mass spectrometry, *J. Chromatogr. A* 1045 (2004) 1-13.

35. M. Leermakers, W. Baeyens, M. De Gieter, B. Smedts, C. Meet, H. C. De Bisschop, R. Morabito, Ph. Quevauviller, Toxic arsenic compounds in environmental samples: Speciation and validation, *Trends Anal. Chem.* 25 (2006) 1-10.

36. S. H. Nam, H. Zhang, M. Cai, J.S. Lim and A. Montaser, A status report on helium inductively coupled plasma mass spectrometry. *Fresenius J. Anal. Chem.* 355 (1996) 510-520.

37. D. Beauchemin and J. M. Craig, Investigations on mixed-gas plasmas produced by adding nitrogen to the plasma gas in ICP-MS. *Spectrochim. Acta Part B* 46 (1991) 603-614.

38. A. E. Holliday and D. Beauchemin, Preliminary investigation of direct sea-water analysis by inductively coupled plasma mass spectrometry using a mixed-gas plasma, flow injection and external calibration, *J. Anal. At. Spectrom.* 18 (2003) 1109-1112.

39. H. Niu and R. S. Houk, Fundamental aspects of ion extraction in inductively coupled plasma mass spectrometry. *Spectrochim. Acta Part B* 51 (1996) 779-815.

40. S. E. Hobbs and J. W. Olesik, Inductively coupled plasma-spectrometry fluctuations due to individual aerosol droplets and vaporizing particles. *Ana. Chem*. 64 (1992), 274-283.

41. A. S. Al-Ammar, E. Reitznerova and R. M. Barnes, Feasibility of using beryllium as internal reference to reduce non-spectroscopic carbon species matrix effect in the inductively coupled plasma-mass spectrometry (ICP-MS) determination of boron in biological samples. *Spectrochim. Acta Part B* 54 (1999) 1813-1820.

42. Y. P. Hu and Z. X. Zhang, Further study of a rate model for inductively coupled plasma analyte spectra using a Monte Carlo technique. *Microchem. J.* 53 (1996) 260-272.

43. D. S. Hanselman, N. N. Sesi, M. Huang and G. M. Hieftje, The effect of sample matrix on electron density, electron temperature and gas temperature in argon inductively coupled plasma examined by Thomson and Rayleigh scattering. *Spectrochim. Acta Part B* 49 (1994) 495-526.

44. D. J. Douglas, and S. D. Tanner, in *Inductively coupled plasma mass spectrometry* (Montaser, A., Ed.), 1998, 615-679 (Wiley-VCH, New York)

45. D. J. Douglas and J.B. French, Gas dynamic of the inductively coupled plasma mass spectrometry interface. *J. Anal. At. Spectrom.* 3 (1988), 743-747.

46. K. Sakata and K. Kawabata, Reduction of fundamental polyatomic ions in inductively coupled plasma mass spectrometry, *Spectrochim. Acta Part B* 49 (1994) 1027-1038.

47. R. Thomas, *A beginner's guide to ICP-MS,* Part IV: the interface region. *Spectroscopy* 16(7) (2001) 26-30.

48. S. D. Tanner, Space charge in ICP-MS: calculation and implications. *Spectrochim. Acta Part B* 47 (1992) 809-823.

49. G. Li, Y. Duan, and G. M. Hieftje, Space charge effects and ion distribution in plasma source mass spectrometry. *J. Mass. Spectrom.* 30 (1995) 841-848.

50. P. P. Mahoney, S. J. Ray and G. M. Hieftje, Time-of-flight mass spectrometry for elemental analysis, *Appl. Spectrosc*. 51 (1997) 16A-28A

51. K. G. Heumann, S. M. Gallus, G. Radlinger and J. Vogl, Precision and accuracy in isotope ratio measurements by plasma source mass spectrometry. *J. Anal. At. Spectrom.* 13 (1998) 1001-1008.

52. S. J. Ray, G. M. Hieftje, Mass analyzers for inductively coupled plasma time-of-light mass spectrometry. *J. Anal. Atom Spectrom.* 16 (2001) 1206-1216.

53. M. Guilhaus, Essential elements of time-of-flight mass spectrometry in combination with the inductively coupled plasma ion source *Spectrochim. Acta Part B* 55 (2000) 1511-1525.

54. M. Guilhaus, V. Mlynski and D. Selby, Perfect timing: time of flight mass spectrometry, *Rapid Commun. Mass Spectrom*. 11 (1997) 951-962.

55. D. P. Myers, G. Li, P.P. Mahoney and G.M. Hieftje, An inductively coupled plasma- time of flight mass spectrometer for elemental analysis. Part II: direct current quadrupole lens system for improved performance, *J. Am. Soc. Mass Spectrom.* 6 (1995) 400-410.

56. X. D. Tian, H. Emteborg and F. C. Adams, Analytical performance of axial inductively coupled plasma time of flight mass spectrometry (ICP-TOFMS), *J. Anal. At. Spectrom.* 14 (1999) 1807-1814.

57. M. Balcerzak, An Overview of Analytical Applications of Time of Flight-Mass Spectrometric (TOF-MS) Analyzers and an Inductively Coupled Plasma-TOF-MS Technique, *Anal. Sci*., 19 (7) (2003) 979-989.

58. R. E. Sturgeon, J. W. H. Lam and A. Saint, Analytical characteristics of a commercial ICP orthogonal acceleration time-of-flight mass spectrometer (ICP-TOFMS), *J. Anal. At. Spectrom.* 15 (2000) 607-616.

59. E. Hoffmann and V. Stroobant, *Mass Spectrometry: principles and application* (second edition, John Wiley & Sons, Ltd, 2002), 92.

60. H. Emteborg, X. Tian and F. C. Adams, Quality assurance of arsenic, lead, tin and zinc in copper alloys using axial inductively coupled plasma time-of-flight (ICP-TOF-MS). *J. Anal. At. Spectrom*. 14 (1999) 1567-1572.

61. S. Luan, H. Pang, S. C. K. Shum and R. S. Houk, Noise characteristics of aerosols produced by inductively coupled plasma nebulizers, *J. anal. At. Spectrom.* 7(1992) 799-805.

62. D. J. Douglas and L. A. Kerr, Study of solids deposition on inductively coupled plasma mass spectrometry samplers and skimmers, *J. Anal. At. Spectrom.* 3 (1988) 749-752.

63. E. H. Evans and J. J. Giglio, Interferences in inductively coupled plasma mass spectrometry, *J. Anal. At. Spectrom*. 8 (1993) 1-18.

64. J. W. Ferguson, R. S. Houk, High resolution studies of the origins of polyatomic ions in inductively coupled plasma-mass spectrometry, Part I. Identification methods and effects of neutral gas density assumptions, extraction voltage, and cone material, *Spectrochim.Acta Part B* 61 (2006) 905-915.

65. M. Guihaus, Principles and instrumentation in time of flight mass spectrometry, *J. Mass Spectrom*. 30 (1995) 1519-1532.

66. R.Thomas, *A beginner's guide to ICP-MS,* Part VII: Mass separation device-double focusing magnetic sector technology 16(11) (2001) 22-26.

67. D. Beauchemin, Inductively Coupled Plasma Mass Spectrometry, *Anal. Chem.* 78 (2006) 4111-4135.

68. S. D Tanner, V. I. Baranov and D. R. Bandura, Reaction cells and collision cells for ICP-MS: a tutorial review. *Spectrochim.Acta Part B* 57 (2002) 1361-1452.

69. A. E. Holliday, The reduction of spectroscopic and non-spectroscopic interferences in inductively coupled plasma mass spectrometry, Thesis (2005), 29.

70. F. Vanhaecke and L. Moen, Overcoming spectral overlap in isotopic analysis via single- and multi-collector ICP–mass spectrometry, *Anal. Bioanal. Chem*. 378 (2004) 232-240.

71. J. Mora, S. Maestre, V. Hernandis and J. L. Todoli, Liquid sample introduction in plasma spectrometry. *Trends Anal. Chem*. 22 (2003) 123-132.

72. M. G. Minnich and R. S. Houk, Comparison of cryogenic and membrane desolvation for attenuation of oxide, hydride and hydroxide ions and ions containing chlorine in inductively coupled plasma spectrometry. *J. Anal. At. Spectrom.* 13 (1998) 167-174.

73. M. Krachler, C. Mohl, H. Emons and W. Shotyk. Influence of digestion procedures on the determination of rare earth elements in peat and plant samples by USN-ICP-MS. *J. Anal. At. Spectrom*. 17 (2002) 844-851.

74. R. E. Russo, X. L. Mao, H. C. Liu, J. Gonzalez and S. S. Mao, Laser ablation in analytical chemistry – a review. *Talanta* 57 (2002), 425-451.

75. F. Vanhaecke, M. Resano and L. Moens, Electrothermal vaporisation ICP-mass spectrometry (ETV-ICP-MS) for the determination and speciation of trace elements in solid samples—a review of a real-life application from the author's lab. *Anal. Bioanal. Chem.* 374 (2002) 188-195.

76. Z. F. Zhang, S. Y. Chen, H. M. Yu, M. Sun and W. Q. Liu. Simultaneous determination of arsenic, selenium, and mercury by ion exchange vapor generation inductively coupled plasma mass spectrometry. *Anal. Chim. Acta.* 513 (2004) 417-423.

77. X. D Cao, M. Yin and X. R. Yang, Elimination of the spectral interferences from polyatomic ions with rare earth elements in inductively coupled plasma mass spectrometry by combining algebraic correction with chromatographic separation. *Spectrochim. Acta Part B* 56 (2001) 431-441.

78. R. Garcia-Sanchez, J. Bettmer and L. Ebdon, Development a new method for the separation of vanadium species and chloride interference removal using modified silica capillaries-DIN-ICP-MS, *Microchem. J.* 76 (2004) 161-171.

79. E. H. Evans and L. Ebdon. Simple approach to reducing polyatomic ion interferences on arsenic and selenium in inductively coupled plasma mass spectrometry. *J. Anal. At. Spectrom.* 4 (1989), 299-300.

80. F. Laborda, M. J. Baxter, H.M. Crews and J. Dennis. Reduction of polyatomic interferences in inductively coupled plasma mass

spectrometry by selection of instrument parameters and using an argon-nitrogen plasma: effect on multi-element analyses, *J. Anal. At. Spectrom.* 9 (1994) 727-736.

81. C. W. McLeod, A. R. Date and Y. Y. Cheung, Metal oxide ions in inductively coupled plasma-mass spectrometric analysis of nickel base alloy. *Spectrochim. Acta Part B* 41 (1986) 169-174.

82. J. G. Williams and A. L. Gray, High dissolved solids and ICP-MS: are they compatible? *Anal. Proc*. 25 (1988) 385-388.

83. S. H Tan and G. Horlick, Matrix effect observations in inductively coupled plasma mass spectrometry. *J. Anal. At. Spectrom*. 2 (1987) 745-763.

84. G. Xiao and D. Beauchemin, Reduction of matrix effects and mass discrimination in inductively coupled plasma mass spectrometry with optimised argon-nitrogen plasma. *J. Anal. At. Spectrochim*. 9 (1994) 509-518.

85. M. M. Fraser and D. Beauchemin, Effect of concomitant elements on the distribution of ions in inductively coupled plasma mass spectrometry Part 1. Elemental ions. *Spectrochim. Acta* Part B 55 (2000) 1705-1731.

86. B. Gammelgard and O. Jons, Determination of selenium in urine by inductively coupled plasma mass spectrometry: interferences and optimization. *J. Anal. At. Spectrom*. 14 (1999) 867-874.

87. J. M. Craig, and D. Beauchemin, Reduction of the effects of concomitant elements in inductively coupled plasma mass spectrometry by adding nitrogen to the plasma gas. *J. Anal. At. Spectrom.* 7 (1992) 937-942.

88. A. W. Boorn, M.S. Cresser, R.F. Browner, Evaporation characteristics of organic solvent aerosols used in analytical atomic spectrometry**,** *Spectrochim. Acta Part B* 35 (1980) 823-832.

89. E. H. Larsen, S. Stürup, Carbon-enhanced inductively coupled plasma mass speciation, spectrometric detection of arsenic and selenium and its application to arsenic speciation, *J. Anal. At. Spectrom*. 9 (1994) 1099-1105.

90. S. Wangkarn, S. A. Pergantis, Determination of arsenic in organic solvents and wines using microscale flow injection inductively coupled plasma mass spectrometry, *J. Anal. At. Spectrom*. 14 (1999) 657-662.

91. M. J. Campbell, C. Demesmay and M. Ollé, Determination of total arsenic concentrations in biological matrices by inductively coupled plasma mass spectrometry, J. Anal. At. Spectrom. 9 (1994) 1379-1384

92. Z. Hu, S. Hu, S. Gao, Y. Liu, S. Lin, Volatile organic solvent-induced signal enhancements in inductively coupled plasma-mass spectrometry: a case of study of methanol and acetone, *Spectrochim. Acta Part B* 59 (2004) 1463–1470.

93. M. Kovacevic, W. Goessler, Direct introduction of volatile carbon compounds into the spray chamber of an inductively coupled plasma mass spectrometer: Sensitivity enhancement for selenium, *Spectrochim. Acta Part B* 60 (2005) 1357-1362.

94. F. Abou-Shakra, M. P. Rayman, N. I. Ward, V. Hotton, G. Bastian, Enzymatic digestion for the determination of trace elements in blood serum by inductively coupled plasma mass spectrometry, *J. Anal. At. Spectrom.* 12 (1997) 429-433.

95. I. Liorente, M. Gómez, C. Cámara, Improvement of selenium determination in water by inductively coupled plasma mass spectrometry through use of organic compounds as matrix modifiers, *Spectrochim. Acta Part B* 52 (1997) 1825-1838.

96. D. Schaumloffel, J. Ruiz Encinar and R. £obinski, Development of a Sheathless Interface between Reversed-Phase Capillary HPLC and ICPMS via a Microflow Total Consumption Nebulizer for Selenopeptide Mapping, *Anal. Chem*. 75 (2003) 6837-6842.

97. S. Cao, H. Chen, X. Zeng, Determination of mercury in biological samples using organic compounds as matrix modifiers by inductively coupled plasma mass spectrometry, *J. Anal. At. Spectrom*. 14 (1999) 1193-1186.

98. P. Kralj, M. Veber, Investigations into nonspectroscopic effects of organic compounds in inductively coupled plasma mass spectrometry, *Acta Chim. Slov*. 50 (2003) 633-644.

99. P. Allain, L. Jaunault, Y. Mauras, J.-M. Mermet and T. Delaporte, Signal enhancement of elements due to the presence of carbon-containing compounds in inductively coupled plasma mass spectrometry, *Anal. Chem*. 63 (1991) 1497-1498.

100. J. Borkowska-Burnecka, U. Jankowiak, W. Zyrnicki, K. A. Wilk, Effect of surfactant addition on ultrasonic leaching of trace elements from plant samples in inductively coupled plasma-atomic emission spectrometry, *Spectrochim. Acta Part B* 59 (2004) 585-590.

101. M. A. M. da Silva, V. L. A. Frescura, A. J. Curtius, Determination of trace elements in water samples by ultrasonic nebulization inductively coupled plasma mass spectrometry after cloud point extraction, *Spectrochim. Acta Part B* 55 (2000) 801-811.

102. E. K. Paleologos, C. D. Stalikas, M. I. Karayannis, An optimised single-reagent method for the speciation of chromium by flame atomic absorption spectrometry based on surfactant micelle-mediated methodology, *Analyst* 126 (2001) 389-393.

103. M. Murillo, Z. Benzo, E. Marcano, C. Gomez, A. Garaboto, C. Marin, Determination of copper, iron and nickel in edible oils using emulsified solutions by ICP-AES, *J. Anal. At. Spectrom.* 14 (1999) 815-820.

104. M. R. Fernández de la Campa, E. Segovia García, M. C. Valdés-Hevia y Temprano, B. Aizpún Fernández, J. M. Marchante Gayón, A. Sanz-Medel, Effects of organized media on the generation of volatile species for atomic spectrometry, *Spectrochim. Acta Part B* 50 (1995) 377–391.

105. R. I. Ellis, J. F. Tyson, Use of a surfactant in the determination of arsenic by flow injection hydride generation atomic absorption spectrometry, *Spectrochim. Acta Part B* 51 (1996) 1859-1866.

106. H. G. Infante, M. L. Fernández Sánchez, A. Sanz-Medel, Vesicle-assisted determination of ultratrace amounts of cadmium in urine by electrothermal atomic absorption spectrometry and inductively coupled plasma mass spectrometry, *J. Anal. At. Spectrom.* 13 (1998) 899-903.

107. D. C. Gregoire, The effect of easily ionisable concomitant elements on non-spectroscopic interferences in inductively coupled plasma mass spectrometry, *Spectrochim.Acta* Part B 42 (1987) 895-907.

108. D. Beauchemin, J. W. McLaren and S.S Berman, Study of the effects of concomitant elements in inductively coupled plasma mass spectrometry, *Spectrochim. Acta Part B* 42 (1987) 467-490.

109. S. E. Hobbs and J. W. Olesik, Laser- excited fluorescence studies of matrix-induced errors in inductively coupled plasma spectrometry—implication for ICP-MS, *Appl. Spectrosc*. 45 (1991) 1395-1407.

110. K. O'Hanlon, L. Ebdon and M. Foulkes, Effect of easily ionisable elements on the mass transport efficiency of solutions and slurries used in plasma emission spectrometry, *J. Anal. At. Spectrom*. 12 (1997) 329-331.

111. I. I. Stewart, J. W. Olesik, The effect of nitric acid concentration and nebulizer gas flow rates on aerosol properties and transport rates in inductively coupled plasma sample introduction, *J. Anal. At. Spectrom.* 13 (1998) 1249-1256.

112. C. Pan, G. Zhu, R. F. Browner, Comparison of desolvation effects with aqueous and organic (carbon tetrachloride) sample introduction for

inductively coupled plasma atomic emission spectrometry, *J. Anal. At. Spectrom.* 5 (1990) 537-542.

113. J. W. Olesik and A. W. Moore, Influence of small amount of organic solvents in aqueous samples on argon inductively coupled plasma spectrometry, *Anal. Chem*. 62 (1990) 840-845.

114. J. Q. Xu, D. Balik, G. R. Agnes, Aerosol static electrification and its effects in inductively coupled plasma spectroscopy, *J. Anal. At. Spectrom.* 16 (2001) 715-123.

115. R. S. Houk, Mass spectrometry of inductively coupled plasmas, *Anal. Chem*. 58 (1986) 97A-98A, 100A-105A.

116. A. E. Holliday, D. Beauchemin, Spatial profiling of analyte signal intensities in ICP-MS, *Spectrochim. Acta Part B* 59 (2004) 291–311.

117. G. Horlick, S. H. Tan, M. A. Vaughan and C. A. Rose, The effect of plasma operating parameters on analyte signals in inductively coupled plasm mass spectrometry, *Spectrochim. Acta Part B* 40 (1985) 1555-1572.

118. H. P. Longerich, B. J. Fryer, D. F. Strong and C. J. Kantipuly, Effect of operating conditions on the determination of the rare earth elements by inductively coupled plasma mass spectrometry (ICP-MS), *Spectrochim. Acta Part B* 42 (1987) 75-92.

119. N. Jakubowski, I. Feldmann and D. Stuewer, Analytical improvement of pneumatic nebulization in ICP-MS by desolvation, *Spectrochim. Acta Part B* 47 (1992) 107-118.

120. G. H. Vickers, D. A. Wilson, G. M. Hieftje, Spatial dependence of ion concentrations in inductively coupled plasma mass spectrometry, *Spectrochim. Acta Part B* 45 (1990) 499–506.

121. E. D. Salin, M. Antler and G. Bort, Evaluation of the simultaneous use of standard additions and internal standards calibration techniques for inductively coupled plasma mass spectrometry, *J. Anal. At. Spectrom.* 19 (2004) 1498-1500.

122. C. K. Sekhar, S. N. Chary, K. C. Tirumala and V. Aparna, Determination of trace metals in sea water by ICP-MS after matrix separation, *Acta. Chim. Slov.* 50 (2003) 409-418.

123. E. M. Heithmar, T. A. Hinner, J. T. Rowan and J. M. Riviello, Minimization of interferences in inductively coupled plasma mass spectrometry using on-line preconcentration, *Anal. Chem*. 62 (1990) 857-864.

124. M. Nicolai, C. Rosin, N. Tousset and Y. Nicolai, Trace metal analysis in estuarine and sea water by ICP-MS using on-line preconcentration and matrix elimination with chelating resin, *Talanta* 50 (1999) 433-444.

125. N. Praphairaksit and R. S. Houk, Attenuation of matrix effects in inductively coupled plasma mass spectrometry with a supplemental electron source inside the skimmer, *Anal. Chem*. 72 (2000) 2351-2355.

126. N. Praphairaksit and R.S. Houk, Reduction of mass bias and matrix effects in inductively coupled plasma mass spectrometry with supplemental electron source in a negative extraction lens, *Anal. Chem.* 72 (2000) 4435-4440.

127. X. Chen and R. S. Houk, Spatially resolved measurements of ion density behind the skimmer of an inductively coupled plasma mass spectrometer, *Spectrochim. Acta Part B* 51 (1996) 41-54.

128. X. S. Chen and R. S. Houk, Polyatomic ions as internal standards for matrix corrections in inductively coupled plasma mass spectrometry, *J. Anal. At. Spectrom.* 10 (1995) 837-841.

129. P. Krystek and K. G. Heumann, Development of accurate mass spectrometric routine and reference methods for the determination of trace amounts of iridium and rhodium in photographic emulsions, *J. Anal. At. Spectrom*. 14 (1999) 1443-1447.

130. N. G. Beck, R. P. Franks and k. W. Bruland, Analysis for Cd, Cu, Ni, Zn and Mn in estuarine water by inductively coupled plasma mass spectrometry coupled with an automated flow injection system, *Anal. Chim. Acta* 455 (2002) 11-22.

131. D. Beauchemin and A. A. Specht, On-line isotope dilution analysis with ICPMS using reverse flow injection, *Anal. Chem*. 69 (1997) 3183-3187.

132. J. D. Fasset and P. J. Paulsen, Isotope dilution mass spectrometry for accurate elemental analysis, *Anal. Chem*. 61 (1989) 643A-647A.

133. J. Ruzicka and E. H. Hansen, Flow injection analysis Part I. A new concept of fast continuous flow analysis. *Anal. Chim. Acta*, 78 (1975) 145-157.

134. Z. Y. Huang, F. R. Chen, Z. Zhuang, X. Wang F. S.C. Lee, Trace lead measurement and on-line removal of matrix interference in seawater by isotope dilution coupled with flow injection and ICP-MS, *Anal. Chim. Acta* 508 (2004) 239–245.

135. V. N. Epov, K. Benkheddaa and R. D. Evansa, Determination of Pu isotopes in vegetation using a new on-line FIICP-DRC-MS protocol after microwave digestion, *J. Anal. At. Spectrom*. 20 (2005), 990-992.

136. A. A. Specht and D. Beauchemin, Automated on-line isotope dilution analysis with ICP-MS using sandwich flow injection, *Anal. Chem*. 70 (1998) 1036-1040.

137. J. Wang, E. H. Evans and J.A. Caruso, Minimization of non-spectroscopic matrix interferences for the determination of trace elements in fusion samples by flow injection inductively coupled plasma mass spectrometry, *J. Anal. At. Spectrom*. 6 (1991) 605-608.

138. Y. C. Sun, C. Y. Lin, S. F. Wu, Y.T. Chung, Evaluation of on-line desalter-inductively coupled plasma-mass spectrometry system for determination of Cr(III), Cr(VI), and total chromium concentrations in natural water and urine samples, *Spectrochim. Acta Part B* 61 (2006) 230–234.

139. H. H. Chen and D. Beauchemin, Determination of trace metals in saline water using flow injection on-line precipitation coupled with inductively coupled plasma mass spectrometry, *J. Anal. At. Spectrom*. 16 (2001) 1356-1363

140. J. Wang and E. H. Hansen, On-line sample-pre-treatment schemes for trace-level determinations of metals by coupling flow injection or sequential injection with ICP-MS, *Trends Anal. Chem*. 22 (2003) 836-846.

141. N. Jakubowski, I. Feldmann and D. Stuewer, Diagnostic investigation of aerosol with varying water content in inductively coupled plasma mass spectrometry, *J. Anal. At. Spectrom*. 8 (1993) 969-977.

142. S. E. Long, R. F. Browner, Influence of water on conditions in the inductively coupled argon plasma, *Spectrochim. Acta Part B* 43 (1988) 1461– 1471.

143. G. R. Peters, D. Beauchemin, Effect of pre-evaporating the solvent on the analytical performance of inductively coupled plasma mass spectrometry, *Spectrochim. Acta Part B* 48 (1993) 1481–1494

144. J. W. Olesik, Investigating the fate of individual sample droplets in inductively coupled plasmas, *Appl. Spectrosc*. 51 (1997) 158A–175A.

145. R. Thomas, A beginner's guide to ICP-MS part II: the sample introduction system. *Spectroscopy* 16(5) (2001) 58.

146. A. L. Gray, Influence of load coil geometry on oxide and double charged ion response in inductively coupled plasma source mass spectrometry, *J. Anal. At. Spectrom.* 1 (1986) 247-249.

147. D. R. Lide, *CRC handbook of chemistry and physics,* D. R. Lide ed., 1993 (CRC Press, Boca Raton, FL).

148. J. W. Olesik, Fundamental research in ICP-OES and ICP-MS, *Anal. Chem.* 68 (1996) 469A-474A.

149. L. Ebdon, E. H. Evans, N. W. Barnett, Simplex optimization of experimental conditions in inductively coupled plasma atomic emission spectrometry with organic solvent introduction, J. Anal. At. Spectrom. 4 (1989) 505-508.

150. A. E. Holliday, D. Beauchemin, Spatial profiling of ion distributions in a nitrogen-argon plasma in inductively coupled plasma mass spectrometry, *J. Anal. At. Spectrom.* 18(2003) 289–295.

151. F. Vanhaecke, R. Dam, C. Vandecasteele, 'zone model' as an explanation for signal behaviour and non-spectrol interferences in inductively coupled plasma mass spectrometry, *J. Anal. At. Spectrom.* 8 (1993) 433-438.

152. S. D. Lofthouse, G. M. Greenway, S. C. Stephen, Microconcentric nebuliser for the analysis of small sample volumes by inductively coupled plasma mass spectrometry, *J. Anal. At. Spectrom.* 12 (1997) 1373-1376.

153. CRC Handbook of Chemistry and Physics, 58th ed, CRC Press Inc., cleveland Ohio (1977)

154. D. C. Harris, *Quantitative Chemical Analysis*, 6th ed, W. H. Freeman and Company, New York, 2003, 67-73.

155. M. M. Fraser and D. Beauchemin, Effect of concomitant elements on the distribution of ions in inductively coupled plasma mass spectrometry: part 2. Polyatomic ions, *Spectrochim. Acta Part B* 56 (2001) 2479-2495.

156. S. Liu, D. Beauchemin, The effect of pre-evaporation on ion distributions in inductively coupled plasma mass spectrometry, *Spectrochim. Acta B*, 61 (2006) 157-163

157. S. Liu, D. Beauchemin, Effect of methanol and sodium dodecylsulfate on radial profiles of ion abundance in inductively coupled plasma mass spectrometry, *Spectrochim. Acta B,* 61 (2006) 319-325

158. B. A. Thomson, J. V. Iribarne, Field induced ion evaporation from liquid surface at atmospheric pressure, *J. Chem. Phys.*, 71 (1979), 71, 4451-4463.

159. D. C. Grégoire, Chapter 3 in *Wilson & Wilson's Comprehensive Analytical Chemistry*, Vol. XXXIV, Discrete sample introduction techniques for inductively coupled plasma mass spectrometry, 2000, pp.347-444 (D. Barceló, Ed., Elsevier, Amsterdam, The Netherlands).

160. P. W. J. M. Boumans, F. J. de Boer, Studies of a radio frequency inductively coupled argon plasma for optical emission spectrometry—III. Interference effects under compromise conditions for simultaneous multi-element analysis, *Spectrochim. Acta Part B* 31 (1976) 355-375.

161. J. A. Borowiec, A. W. Boorn, J. H. Dillard, M. S. Cresser, R. F. Browner and M. J. Matteson, Interference Effects from Aerosol Ionic Redistribution in Analytical Atomic Spectrometry, *Anal. Chem.* 52 (1980) 1054-1059.

162. C. C. Tseng, R. Viskanta, Enhancement of water droplet evaporation by radiation absorption, *Fire Saf*. J. 41 (2006) 236–247.

163. T. P. Fischer, S. Shuttleworth and P. A. O'Day, Determination of trace and platinum-elements in high ionic-strength vocanic fluids by sector-field inductively coupled plasma mass spectrometry (ICP-MS), *Fresenius J. Anal. Chem*. 362 (1998) 457-464.

164. S. E. Hobbs, J. W. Olesik, The effect of desolvating droplets and vaporizing particles on ionization and excitation in Ar inductively coupled plasmas, *Spectrochim. Acta Part B* 48B (1993) 817-833.

165. J. A. Nóbrega, M. C. Santos, R. A. de Sousa, S. Cadore, R. M. Barnes, M. Tatro, Sample preparation in alkaline media, *Spectrochim. Acta B* 61 (2006) 465-495.

166. C. Kahakachchi, P. C. Uden, J. F. Tyson, Extraction of arsenic from spiked soil and standard reference materials, *Analyst* 129 (2004) 714–718.

167. E. H. Larsen, J. Engman, J.J. Sloth, M. Hansen, L. Jorhem, Determination of inorganic arsenic in white fish using microwave-assisted alkaline alcoholic sample dissolution and HPLC-ICP-MS, *Anal. Bioanal. Chem.* 381 (2005) 339–346.

168. J. Szpunar, Trace element speciation analysis of biomaterial by high performance liquid chromatography with inductively coupled plasma mass spectrometric detection, *Trends Anal. Chem.* 19 (2000) 127-137.

169. Q. Xie, R. Kerrich, E.Irving, K. Liber and F. Abou-Shakra, Determination of five arsenic species in aqueous samples by HPLC coupled with a hexapole cell ICP-MS, *J. At. Anal. Spectrom.* 17 (2002) 1037-1041.

170. A. A. Ammann, Determination of strong binding chelators and their metal complexes by anion-exchange chromatography and inductively coupled plasma mass spectrometry, *J. Chromatogr. A* 947 (2002) 205-216

171. B. S. Sheppard and J. A. Caruso, Arsenic speciation by ion chromatography with inductively coupled plasma mass spectrometric detection, *Analyst*, 117 (1992) 971-975.